

8-2010

CHARACTERIZING A NOVEL GENETIC LOCUS ASSOCIATED WITH FAMILIAL CO- OCCURRENCE OF THORACIC AORTIC ANEURYSMS AND INTRACRANIAL ANEURYSMS

Alexander H. Li

Follow this and additional works at: http://digitalcommons.library.tmc.edu/utgsbs_dissertations

 Part of the [Genetics Commons](#), and the [Other Genetics and Genomics Commons](#)

Recommended Citation

Li, Alexander H., "CHARACTERIZING A NOVEL GENETIC LOCUS ASSOCIATED WITH FAMILIAL CO-OCCURRENCE OF THORACIC AORTIC ANEURYSMS AND INTRACRANIAL ANEURYSMS" (2010). *UT GSBS Dissertations and Theses (Open Access)*. Paper 73.

This Thesis (MS) is brought to you for free and open access by the Graduate School of Biomedical Sciences at DigitalCommons@The Texas Medical Center. It has been accepted for inclusion in UT GSBS Dissertations and Theses (Open Access) by an authorized administrator of DigitalCommons@The Texas Medical Center. For more information, please contact laurel.sanders@library.tmc.edu.

CHARACTERIZING A NOVEL GENETIC LOCUS ASSOCIATED WITH FAMILIAL
CO-OCCURRENCE OF THORACIC AORTIC ANEURYSMS AND INTRACRANIAL
ANEURYSMS

by
Alexander Li, BS

APPROVED:

Dianna M. Milewicz, M.D., Ph.D., Supervisor

Gilbert Cote, Ph.D.

Jacqueline Hecht, Ph.D.

Joseph McCarty, Ph.D.

Sanjay Shete, Ph.D.

APPROVED:

Dean, The University of Texas
Graduate School of Biomedical Sciences at Houston

CHARACTERIZING A NOVEL GENETIC LOCUS ASSOCIATED WITH FAMILIAL
CO-OCCURRENCE OF THORACIC AORTIC ANEURYSMS AND INTRACRANIAL
ANEURYSMS

A
DISSERTATION
Presented to the Faculty of
The University of Texas
Health Science Center at Houston
and
The University of Texas
M. D. Anderson Cancer Center
Graduate School of Biomedical Sciences
in Partial Fulfillment
of the Requirements
for the Degree of
MASTER OF SCIENCE

by
Alexander Li, BS.

Houston, Texas
August, 2010

DEDICATION

This dissertation is dedicated to the many families suffering from inherited vascular disease who have volunteered their time and information to help researchers understand the biological basis of this affliction. None of the work in this dissertation would be possible without their contributions.

ACKNOWLEDGEMENTS

I would like to first thank my advisor, Dr. Dianna Milewicz for giving me the opportunity to progress in my continued education at the University of Texas Health Science Center in Houston. I would also like to thank the members of my committee for their guidance with this project: Dr. Gilbert Cote, Dr. Jacqueline Hecht, Dr. Joseph McCarty, and Dr. Sanjay Shete. Many thanks also go to the past and present members of the Milewicz Lab, who have all provided valuable support for the completion of this project: Dongchuan Guo, Jiumei Cao, Ellen Regalado, Van Tran-Fadulu, Ellen Regalado, Alicia Carlson, Callie S. Kwartler, Amy J. Reid, Christina L. Papke, Zhao Ren, Ling Li, Himabindu Pappu, and Carmen Elliott. I would also like to thank Tommy Reese, Siddharth Prakash, and Robert Yu of the Texas Medical Center for their direct contributions to this project.

CHARACTERIZING A NOVEL GENETIC LOCUS ASSOCIATED WITH FAMILIAL
CO-OCCURRENCE OF THORACIC AORTIC ANEURYSMS AND INTRACRANIAL
ANEURYSMS

Publication No. _____

Alexander Li, BS

Supervisory Professor: Dianna M Milewicz, M. D., Ph.D.

The Mendelian inheritance of genetic mutations can lead to adult-onset cardiovascular disease. Several genetic loci have been mapped for the familial form of Thoracic Aortic Aneurysms (TAA), and many causal mutations have been identified for this disease. Intracranial Aneurysms (ICA) also show linkage heterogeneity, but no mutations have been identified causing familial ICA alone.

Here, we characterized a large family (TAA288) with an autosomal dominant pattern of inherited aneurysms. It is intriguing that female patients predominantly present with ICA and male patients predominantly with TAA in this family. To identify a causal mutation in this family, a genome-wide linkage analysis was previously performed on nine members of this family using the 50k GenChips Hind array from Affymetrix. This analysis eventually identified a single disease-segregating locus, on chromosome 5p15. We build upon this previous analysis in this study, hypothesizing that a genetic mutation inherited in this locus leads to the sex-specific phenotype of TAA and ICA in this family

First we refined the boundaries of the 5p15 disease linked locus down to the genomic coordinates 5p15: 3,424,465- 6,312,925 (GRCh37/hg19 Assembly). This locus was named the TAA288 critical interval. Next, we sequenced candidate genes within the TAA288

critical interval. The selection of genes was simplified by the relatively small number of well-characterized genetic elements within the region. Seeking novel or rare disease-segregating variants, we initially observed a single point alteration in the metalloproteinase gene *ADAMTS16* fulfilling this criteria. This variant was later classified as a low-frequency population polymorphism (rs72647757), but we continued to explore the potential role of the *ADAMTS16* as the cause of disease in TAA288. We observed that fibroblasts cultured from TAA288 patients consistently upregulated the expression of this gene more strongly compared to matched control fibroblasts when treated with the cytokine TGF- β 1, though there was some variation in the exact nature of this expression. We also observed evidence that this protein is expressed at elevated levels in aortic aneurysm tissue from patients with mutations in the gene *TGFBR2* and Marfan syndrome, shown by immunohistochemical detection of this protein.

TABLE OF CONTENTS

APPROVAL PAGE	i
TITLE PAGE	ii
DEDICATION	iii
ACKNOWLEDGEMENTS	iv
ABSTRACT	v
TABLE OF CONTENTS	vii
LIST OF FIGURES	ix
LIST OF TABLES	xi
ABBREVIATIONS	xii
CHAPTER 1: INTRODUCTION AND LITERATURE REVIEW	1
1.1 Description of Aneurysms	2
1.2 Disease Genetics	6
1.3 Extracellular Matrix and Aneurysm Pathology	10
1.4 Study Proposal	17
CHAPTER 2: METHODS	26
2.1 Linkage Analysis Methods	27
2.2 Mutation Detection Methods	30
2.3 Transcript and Protein Level Detection Methods	34
CHAPTER 3: RESULTS	41
3.1 Linkage Analysis Results	42
3.2 Mutation Detection Results	52
3.3 Transcript and Protein Level Detection Results	65

CHAPTER 4: DISCUSSION	77
4.1 Selection of ADAMTS16 Candidate Gene	78
4.2 ADAMTS16 in Aneurysm Tissues	79
4.3 Possible Function of ADAMTS16	81
4.4 Future Work	84
REFERENCES	88
VITA	103

LIST OF FIGURES

CHAPTER 1

Figure 1.1: Basic Aneurysm Morphology	6
Figure 1.2: Pathology of Aortic Aneurysms	11
Figure 1.3: Pathology of Cerebral Aneurysms	12
Figure 1.4: Protein Domains of the ADAMTS Family	14
Figure 1.5: The TAA288 Family	21

CHAPTER 2

CHAPTER 3

Figure 3.1: Genomic Regions Linked to the TAA288 Disease Phenotype	43
Figure 3.2: TAA288 1q32 Microsatellite Phasing	44
Figure 3.3: TAA288 5p15 Microsatellite Phasing	45
Figure 3.4: Other Pedigrees with Evidence of Linkage to 5p15.	50
Figure 3.5: Comparison of 5p15 Linked Regions of Pedigrees with Inherited...	51
Figure 3.6: Segregation of ADAMTS16 Intron 13 Variant rs72647757 within...	57
Figure 3.7: Segregation of rs72647757 Minor Allele within Pedigrees having...	62
Figure 3.8: Immunohistochemical detection of ADAMTS16 in Aortic Media	66
Figure 3.9: Immunohistochemical detection of ADAMTS16 in Aortic Adventitia	67
Figure 3.10: Amplification of ADAMTS16 Transcript from Patient and Control...	69
Figure 3.11: ADAMTS16 Transcript Levels in Control Fibroblasts Treated with...	71
Figure 3.12: ADAMTS16 Transcript Levels in TAA288 Patient and Control...	72
Figure 3.13: Immunoblot of Cultured Control Lysates Compared to Surridge et al.	75
Figure 3.14: Immunoblot of Cultured Control and TAA288 Patient Fb Lysates	76

CHAPTER 4:

Figure 4.1: Schema of ADAMTS16 Dysregulation in TAA288 Family

51

LIST OF TABLES

CHAPTER 1

Table 1.1: TAA288 Clinical Data	22
---------------------------------	----

CHAPTER 2

CHAPTER 3

Table 3.1: Two-Point LOD Scores of TAA288 5p15 Microsatellite Genotypes	49
---	----

Table 3.2: Sequencing Targets in the 5p15 Disease-Linked Region of TAA288	54
---	----

Table 3.3: Novel Sequence Alterations Observed in TAA288	56
--	----

Table 3.4: Rare rs72647757 Allele Compared in Aneurysm and Control Populations	59
--	----

Table 3.5: Occurrence rs72647757 Minor Allele within Pedigrees having Inherited...	61
--	----

Table 3.6: CNV Events in TAA288 Detected by Both PennCNV and CNVP...	64
--	----

CHAPTER 4

ABBREVIATIONS

ACTA2	α - smooth muscle actin
ADAMTS	a disintegrin and metalloproteinase with thrombospondin type-1 motif
CNV	copy number variation
CT	computed tomography
DMEM	Dulbecco's Modified Eagle Medium
ECM	extracellular matrix
ICA	intracranial aneurysms
IRX	Iroquois homeobox
LOD	logarithm of odds
MB	mega base, 1 million basepairs
MFS	Marfan syndrome
MYH11	β -myosin heavy chain, smooth muscle isoform
PBS	phosphate-buffered saline
PCR	polymerase chain reaction
SAH	subarachnoid hemorrhage
SMC	smooth muscle cell
SNP	single nucleotide polymorphism
TAAD	thoracic aortic aneurysms and dissections
TGF- β 1	transforming growth factor β 1
TGFBR2	transforming growth factor beta receptor II
VSMC	vascular smooth muscle cell

CHAPTER 1: INTRODUCTION AND LITERATURE REVIEW

1.1. Description of Aneurysms

The Aorta and Intracranial Arteries

The aorta is the largest blood vessel in the human body, directing the flow of oxygenated blood away from the heart into the progressively smaller branches of the systemic arterial circulation. The ascending aorta originates from the left ventricle of the heart and briefly extends upward before arching down through the thoracic and abdominal cavities, where it terminally branches into the two common iliac arteries. Thus, the aorta is divided into three anatomically and developmentally distinct segments: the ascending aorta, the aortic arch, and the descending aorta. Of the smaller vessels that branch from the body of the aorta, the carotid arteries emerge superiorly from the aortic arch and are the primary suppliers of oxygenated blood to the neck and head [1]. Blood supply to the brain is provided through the cerebral arteries, which originate from the internal carotid and vertebral arteries.

As an elastic artery bearing the force of pulsatile blood flow from the heart, the walls of the aorta are comprised of three specialized tissue layers: the intima, media and adventitia. The intima is a monolayer of endothelial cells that directly interface with the blood and are separated from the rest of the wall by an elastic sheet called the internal elastic lamina. The middle layer, or media, is a relatively thick layer of concentric lamellae, alternating layers of vascular smooth muscle cells (VSMCs) and organized elastic fibers, which function respectively to contract and distribute wall stress in order to provide much of the strength and elastic properties of this vessel [2]. The outer adventitial layer of the aorta is largely comprised of collagen fibers and fibroblast cells (Fb). The walls of the aorta are thick

enough to require their own blood supply, the *vasa vasorum* (latin for “vessels of the vessels”), as blood nutrients from the arterial lumen are unable to reach the cells comprising the outer portions of the media and adventitia.

The large elastic aorta differs from smaller arteries such as the intracranial arteries, also called muscular arteries, in several ways [1]. Compared to the aorta, the intracranial arteries have reduced medial thickness relative to their diameters. The media of these vessels also lack concentric layers of elastic fibers separating smooth muscle cell layers. *Vasa vasorum* are only observed in regions of intracranial arteries located within 1.5 cm of extracranial segments of the same vessel, and are otherwise absent in intracranial vessels [3].

Description and Classification of Aneurysm

An aneurysm is defined as an abnormal and localized dilation of an artery, exceeding 1.5 times the normal vessel diameter [4]. These enlargements can exist asymptotically in patients for long periods of time, remaining undetected until an acute dissection occurs. A dissection is defined as a tear in the intimal layer of the artery wall, including the internal elastic lamina, allowing blood to flood into the medial layer, creating a false lumen between the medial and intimal layers. The layers can continue to separate along the plane of the vessel anterograde or retrograde from the dissection site, increasing the length of the aneurysm. In severe cases, a dissection can lead to vessel rupture, where the outer adventitial layer tears and blood hemorrhages into the cavities of the body. A larger aneurysm diameter generally increases risk of a dissection or rupture, but rare exceptions apply; vessel rupture can even occur in the absence of an aneurysm [5]. Complications from these dilations are the

most prevalent form of aortic disease, responsible for over 16,000 deaths annually in the United States [6].

There are several classification systems for aneurysms. One classification is according to the general morphological shape of the event. A fusiform aneurysm is “spindle” shaped, having tapered ends and the widest point occurring in the middle. In contrast, a saccular aneurysm is “berry” shaped, taking the form of a round asymmetrical protrusion from the vessel (Figure 1.1). Aneurysms are also classified by their anatomical location within the body. Under this classification, the most common form of aortic aneurysms are abdominal aortic aneurysms (AAA), followed by the thoracic aortic aneurysms (TAA). Aneurysms occurring in the cranial arteries are termed intracranial aneurysms (ICA). ICA and TAA will remain the focus of this dissertation for two reasons. The first is that recent studies have observed ICA at a higher prevalence in TAAD patients compared to the general population [7;8], and screening for ICA in patients with TAAD is now recommended. The second reason is that we will later discuss a single-family linkage analysis of a pedigree afflicted with the inherited forms of both TAAD and ICA.

Aneurysm Subtypes: TAAD and ICA

Overall incidence of thoracic aortic aneurysms and dissections (TAAD) in Caucasians is 5.9/100,000 people per year [9], with an average age of 65 and slightly higher prevalence in males than females. However, risk of rupture does not differ between genders [10;11]. Aneurysms of the ascending aorta tend to be fusiform in shape, and dissections at this site lead to high rates of morbidity and mortality [12].

TAAD can manifest in patients with genetic syndromes such as Marfan and Ehlers-Danlos type IV [13-15], but is more commonly observed as an isolated, non-syndromic disease. Eighty percent of non-syndromic TAAD patients do not have a first-degree relative with this disease, and are classified as sporadic cases. The remaining 20% of non-syndromic TAAD patients have a family history of the disease, and are classified as having inherited or familial TAAD [16].

ICAs are a prevalent form of aneurysm not involving the aorta, occurring most commonly at major bifurcations of the cranial arteries. ICAs affect between 5-10% of the general population [17], with an estimated 2.3% of the population carrying undetected ICAs [18]. Estimates of ICA rupture rates are as high as 6.5% in the general population, with a risk of rupture that is proportional to aneurysm size [19]. ICA rupture can cause subarachnoid hemorrhage (SAH), which confers an overall risk of 12.4% for sudden death [20]. Risk factors for developing ICA include female gender, smoking, hypertension, and excessive alcohol consumption [21].

Like TAAD, ICA can occur in an inherited or sporadic form, with 5-12% of ICA patients having first degree relative with this disease [22;23]. The inherited form of ICAs tend to rupture at an earlier age than sporadic cases [24], and there is a 7-fold increased risk of rupture among affected first degree relatives compared to second degree relatives [25].

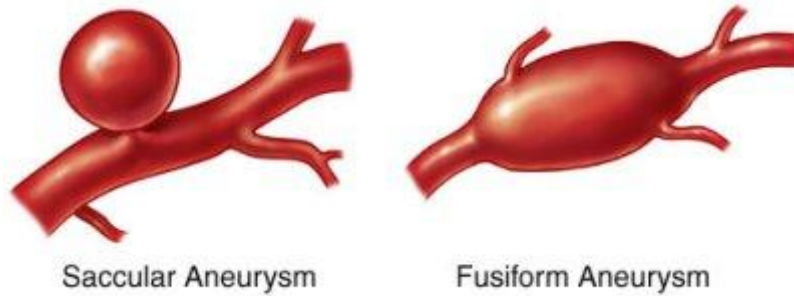


Figure 1.1: Basic Aneurysm Morphology. This image depicts the distinct morphological difference between saccular and fusiform aneurysms. ICA tend to have a saccular shape, while TAAD tend to be fusiform. (This image used with permission from <http://www.daviddarling.info/encyclopedia/A/aneurysm.html>)

1.2. Disease Genetics

Genetic Basis of TAAD

Familial TAAD is a genetically heterogeneous disease. The familial form of TAAD is often inherited as an autosomal dominant trait, with a decreased penetrance and variable age of onset [26]. Genetic linkage studies of families having the inherited form of this disease have identified a number of disease-linked genetic loci, including the TAAD1 locus on chromosome 5q13-14 [27], the TAAD2 locus on chromosome 3p-24-25 [28], and the FAA1 (Familial Aortic Aneurysms) locus on chromosome 11q23-24 [29]. Another locus was identified in a family with inherited TAAD and patient ductus arteriosus (PDA), termed the TAAD/PDA locus located on chromosome 16p12.2-13.13 [30].

Mutations causing the familial form of TAAD have been identified in several genes, using the candidate gene sequencing approach. Some of these gene products are directly integrated into the VSMC intracellular contractile machinery, such as *MYH11* (smooth muscle β -myosin heavy chain 11) located at 16p12 within the TAAD/PDA locus [31], and *ACTA2* (actin, α 2, smooth muscle, aorta) located at 10q21.31 [32]. Causal mutations for Marfan syndrome have also been observed at 15q21 in the gene *FBNI* (fibrillin-1) [33], which is involved with the extracellular scaffolding that provides a source of contractile force for VSMC functions. Mutations causing familial non-syndromic TAAD have also been observed in the gene *TGFBR2* (transforming growth factor, beta receptor II) located at 3p22 [34], which encodes the transmembrane receptor for TGF- β and is involved with VSMC differentiation. Mutations in *FBNI* cause Marfan syndrome and non-syndromic TAAD, reflecting the close relationship between this syndrome and TAAD [35]. Mutations in *TGFBR2* have been observed in patients with Loeys-Dietz Syndrome, a syndromic cause of TAAD [36;37]. However, a number of families with inherited TAAD do not map to any known loci and lack mutations in any of the genes known to cause TAAD. Thus, there are still undiscovered genetic causes of familial TAAD.

Intriguingly, three of the genes known to cause inherited TAAD (*FBN*, *TGFBR1*, and *TGFBR2*) encode protein products implicated in signaling of the cytokine TGF- β 1. This multifunctional cytokine is secreted by cells as part of a biologically inactive complex known as the large latency complex (LLC) which binds to ECM components such as Fibrillin (*FBN*). Fibrils of this gene product normally bind and sequester the inactive LLC within the ECM. However, mutations in this gene are thought to alter the ability of fibrillin to sequester the LLC, causing excessive release of bioactive TGF- β 1 to nearby cells[38]. The *TGFBR1*

and *TGFBR2* genes encode transmembrane receptors for TGF- β 1 ligand, which can bind these receptors after release from the LLC. These receptors propagate the cellular signal initiated by TGF- β 1 ligand binding their extracellular domain through cytoplasmic serine-threonine kinase domains. Strangely, an increase of downstream TGF- β signaling is observed in patients with mutations in these genes [39].

It is also important to note from studies of inherited TAAD that a single gene mutation can cause multiple forms of vascular disease. *ACTA2* mutations have been observed in multiple families having a diversity of vascular disease within the same pedigree [40]. In a large family with inherited TAAD, a mutation (R149C) in *ACTA2* was observed in affected members having TAAD as well as livedo reticularis, a rash caused by occlusion of the dermal capillaries [41]. In a separate family study, a woman with a heterozygous mutation in *ACTA2* (T326N) had an ascending aortic aneurysm at age 59, while her son carrying this same alteration had a stroke at age 25 [42]. Similarly, mutations in *MYH11* are also associated with both inherited TAAD and PDA [43]. These observations suggest that common molecular mechanisms underlie certain distinct forms of vascular disease, and thus a single mutation can have pleiotropic clinical manifestations with distinct disease phenotypes.

Genetic Basis of ICA

There is considerable genetic heterogeneity of inherited ICA, indicated by the number of disease-linked loci in families with inherited ICA. Linkage studies in these families have identified major disease-linked loci on chromosome 1p34.3-36.13 in a North American and

Dutch family [44; 45], chromosome 5p15.2-14.3 in a large French Canadian family [46], chromosome 7q11 in Japanese and Caucasian cohorts [47], chromosome 19q13.3 in Japanese and Finnish families [48; 49], and Xp22.2-22.32 in Japanese and Dutch families [50; 51]. There are also many additional loci mapped with less suggestive evidence for linkage [52]. ICA have also been observed in patients with Marfan syndrome [53], though there is not strong support for an association between these two diseases [54].

Associations between genetic population polymorphisms and the ICA phenotype have been observed in several studies of Japanese populations. Alleles of three SNPs in *COLIA2* are more prevalent in ICA affected individuals compared to controls [55]. Recently, associations have been verified in Japanese populations between ICA and the genotypes of several single nucleotide polymorphisms (SNPs) located on chromosome 9p21, in both the inherited and sporadic forms of this disease [56;57].

Despite the number of genetic loci linked to ICA, no novel causal mutations have been identified within any of the linked loci [58]. Sequencing of candidate genes for ICA involved with the TGF- β signaling pathway identified novel variants in the co-receptors endoglin (*ENG*) and betaglycan (*TGFBR3*) with some association between these variants and the aneurysm phenotype [59]. The ICA linked region on 7q11 contains the genes for elastin (*ELN*) and collagen type 1 alpha2 (*COLIA2*), which both encode products found in arterial walls. However, no novel disease-causing alterations have been identified in the protein coding regions of these genes. This suggests that mutations causing this disease may not reside in gene regions directly encoding a protein product, and may instead lie in noncoding regions such as introns and distal regulatory regions.

1.3. Extracellular Matrix and Aneurysm Pathology

Aneurysm Pathology

The most common pathological observation in aortic aneurysms and dissections is fragmentation of the medial elastic layers [60] (Figure 1.2). Other pathological characteristics include loss of VSMCs, proteoglycan accumulation, and inflammation [61;62]. Although the muscular cranial arteries lack the medial elastic layers found in the aorta, abrupt disruption of the internal elastic lamina and disorder of the media is also observed in ICA [63]. Histopathological examination of ruptured ICA often reveals disorganized VSMCs and hypocellular walls at the site of enlargement [64] (Figure 1.3).

Matrix metalloproteinases (MMPs) target and degrade components of the extracellular matrix (ECM), and have been observed at elevated levels in both TAAD and ICA [65-67]. Specifically, MMP2 and MMP9 target and degrade elastic fibers and are observed at elevated levels in the medial layers of ascending aortic aneurysms, with MMP9 protein detected at especially abundant levels in thoracic aortic dissections [68;69]. Genetic variants of MMP9 are also associated with an increased risk for developing ICA [70].

Similar to MMPs, members of the ADAMTS gene family (A Disintegrin and Metalloproteinase with Thrombospondin type-1 motif) are extracellular matrix proteases. Identified target substrates of this gene family, such as versican and procollagens, have the potential to play a role in the development of vascular disease. In addition, members of this gene family have been implicated in TGF- β signaling, such as ADAMTS10 which may bind Fibrillin in the ECM [71]. A member of this gene family (ADAMTS16) is located within a genomic interval shared among all affected members of a family with inherited aneurysms,

which we later describe in chapter 1.4. In addition, we observed a rare genetic variant of the ADAMTS16 gene which was enriched in the inherited aneurysm population (Chapter 3.2). These observations led to us investigate the potential role of this gene family in the development of aneurysms.

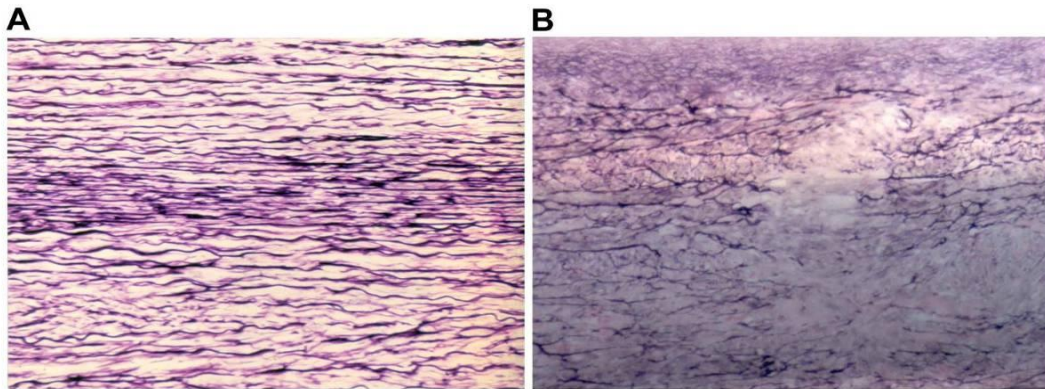


Figure 1.2: Pathology of Aortic Aneurysms. This figure shows a cross section of human aorta samples stained for elastin. (A) The figure on the left shows a normal healthy aorta, with elastin fibers of the media arranged in parallel. (B) The image on the right is taken from a TAAD patient, showing disruption of these fibers. (Image used with permission from Dr. Maximilian Buja, University of Texas)

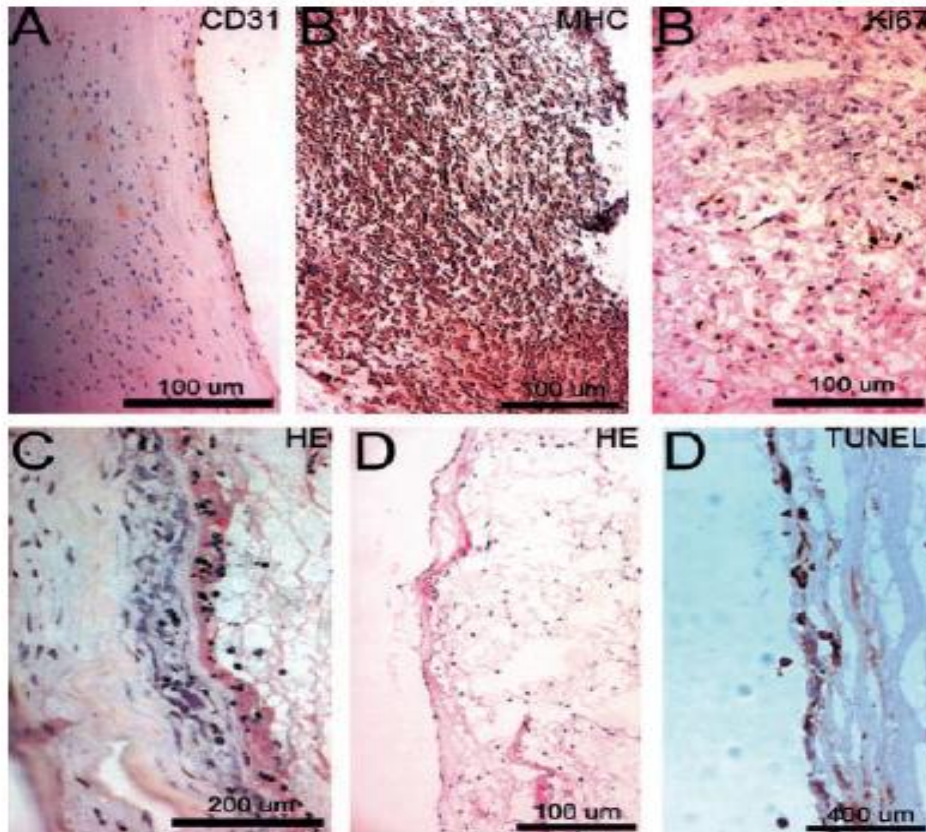


Figure 1.3: Pathology of Cerebral Aneurysms. This figure shows various cross sections of a human cerebral aneurysms, with staining types indicated in the upper right of each image. (A) Organized VMSCs are sometimes observed in these aneurysms, but (B) a thickened wall with disorganized VSMCs is more common. (C) Initial hypoplasia is observed in some of these aneurysms as well as a (D) hypocellular wall, sometimes lined with luminal thrombosis. (Image used with permission from Stroke. Frosen J, et al: Remodeling of saccular cerebral artery aneurysm wall is associated with rupture: histological analysis of 24 unruptured and 42 ruptured cases. Stroke 2004; 35:2287-2293)

The ADAMTS Gene Family

The first member of the ADAMTS metalloproteinase family was characterized in 1997 [72]. Metalloproteinases are proteolytic enzymes requiring a metal ion in order to perform their catalytic activity; members of this specific family utilize zinc. The ADAMTS proteins are large multidomain proteins, which are synthesized inside of cells and secreted into the extracellular matrix (ECM), where they reside in their mature form. Members of this gene family share a number of common domains, including a propeptide domain, a zinc-activated protease domain, and a disintegrin domain (Figure: 1.4). Each member also has a unique C-terminal ancillary domain, containing at least one thrombospondin (TSP) type-1 repeat, which is involved in the localization of the ADAMTS protein to its target substrate in the ECM.

Several post-translational modifications of ADAMTS proteins may occur, presenting opportunities for regulation of protein levels and activity. All members of this family are modified by the addition of an N-linked carbohydrate, which affects the secretion of these proteins into the ECM [73-75]; the only exception is ADAMTS4. Disruption of this process prevents the secretion of the protein, so this modification is thought to serve as a check for proper protein folding prior to secretion [76;77]. Members of the ADAMTS family must also be activated within the ECM by post-translational removal of their propeptide domain, which is thought to mechanically inhibit the adjacent protease domain. The calcium-dependant serine endopeptidase furin performs this excision extracellularly on several ADAMTS family members [78-82]. However, a notable exception to this mechanism is ADAMTS9, whose proteolytic activity decreases after furin processing [83].

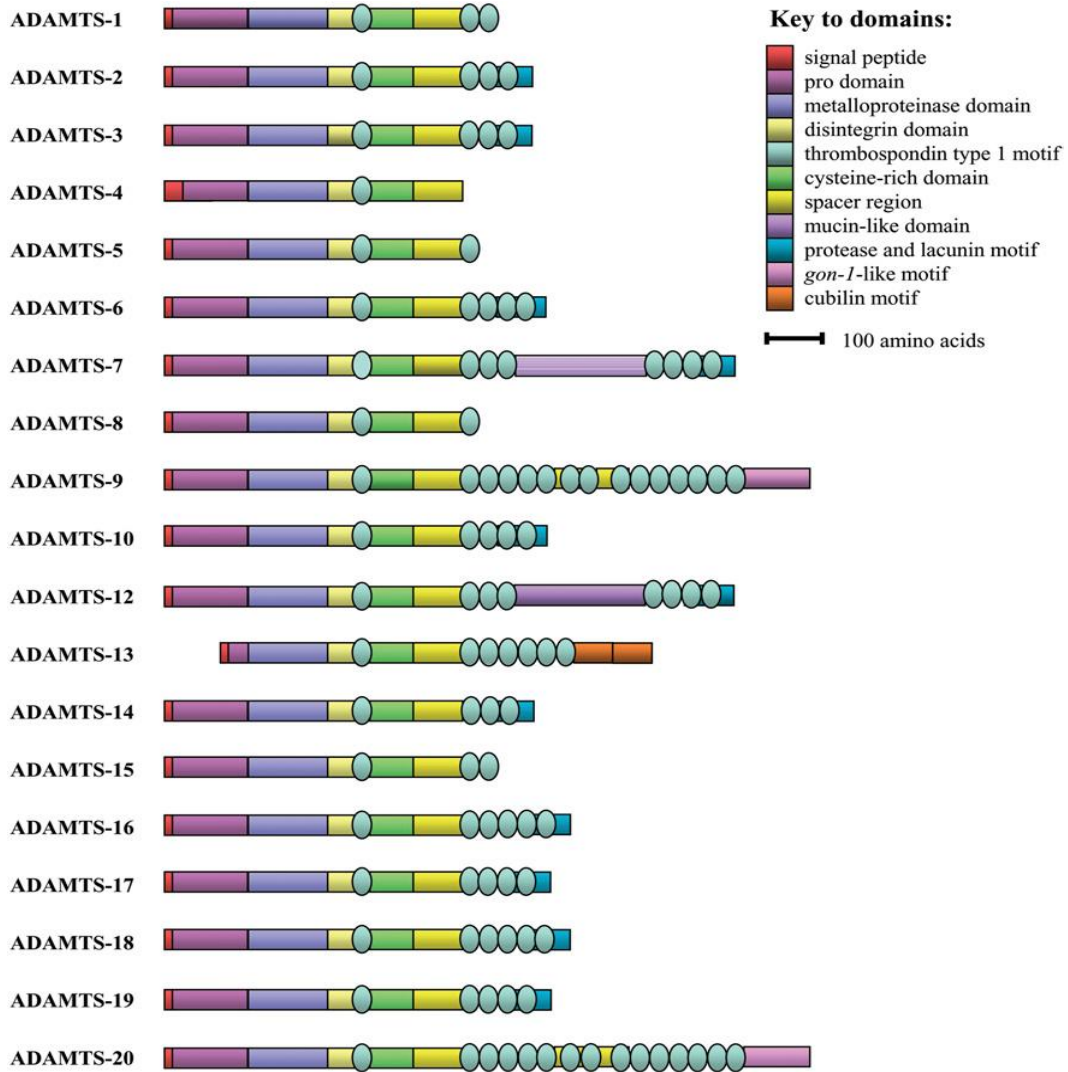


Figure 1.4: Protein Domains of the ADAMTS Family. The image above depicts the location and function, within the linear peptide, of the protein domains of each member of the ADAMTS gene family. (This research was originally published in Biochem J. Porter et al. The ADAMTS Metalloproteinases. *Biochem J.* 2005; 15; 386:15-27. © the American Society for Biochemistry and Molecular Biology.)

Generation of ADAMTS Isoforms

Many ADAMTS proteins have multiple isoforms. These isoforms can be generated from post-translational cleavage or via alternative splicing events during gene transcription. Post-translational modification has been well studied in ADAMTS4, and several isoforms of this protein have been observed in culture. Inhibiting matrix metalloproteinases (MMPs) reduces the prevalence of the smaller isoforms *in vitro* [84], presumably because a subset of these proteins target ADAMTS proteins. Many of these ADAMTS4 isoforms are truncated at the C-terminus and vary not only by proteolytic efficacy, but also by their specific cleavage target sequence within the same substrate [85]. Similar observations have been reported in other members of this gene, including ADAMTS12 [86;87].

Alternative splicing events have also been observed in ADAMTS transcripts, usually resulting in a smaller form of the protein due to specific exons being omitted from the full-length transcripts [88-90]. However, alternative splicing events in *ADAMTS6* can generate transcripts that are longer or shorter than the canonical transcript of this gene, and the levels of these two alternative transcripts relative to each other vary in response to the cytokine TNF- α [91]. However, many of these alternative splicing events have only been observed at the transcriptional level, and it is not clear whether all alternative transcripts of these genes are translated into protein products.

ADAMTS Genes and Human Disease

Mutations in members of the ADAMTS gene family have been implicated in a number of human diseases. *ADAMTS13* is the best characterized member of this gene family, and mutations in this gene cause inherited thrombotic thrombocytopenic purpura (TTP), a thrombotic microangiopathy resulting the excess accumulation of blood clots in small vessels [92;93]. This protein cleaves large multimers of the plasma glycoprotein Von Willebrand Factor (vWF) into smaller units at the Y842-M843 peptide bond *in vivo*, and without this cleavage red blood cells experience excess shear stress in smaller vessels leading to hemolysis and anemia. Multiple disease-causing *ADAMTS13* mutations have been observed in patients with this disease, including some splice-site mutations. Mutations in *ADAMTS2* have been shown to cause the recessively inherited disorder Type VIIC Ehlers-Danlos Syndrome (EDS) [94], characterized by extreme skin fragility, due to decreased processing and maturation of procollagen, the target of this metalloproteinase. Another connective tissue disorder, recessive Weill-Marchesani syndrome (WMS), is caused by mutations affecting the catalytic domain and at splicing sites of *ADAMTS10* [95;96]. WMS is characterized by lens dislocation (ectopia lentis), unusually short fingers (brachydactyly), a short broad head (brachycephaly), and short stature. Mutations causing truncated *ADAMTS17* transcripts have also been observed in WMS patients, including a 1bp insertion at exon 18 and a mutation abolishing the donor sequence of intron 12 [97]. *In vivo* substrates for *ADAMTS10* and *-17* are not known.

There is emerging evidence for the role of the ADAMTS proteins in vascular disease. *ADAMTS1* is normally observed at very low levels in the vasculature, but is dramatically upregulated in the VSMCs and foam cells of atherosclerotic plaques [98]. Similarly, *ADAMTS7* levels have been positively associated with VSMC migration of balloon-injured

rat carotid arteries, and is thought to have a role in the development of atherosclerotic lesions [99]. Elevated expression of ADAMTS4 is observed in baboon aorto-iliac grafts exposed to high blood flow, and in VSMC cultures undergoing Fas ligand-induced cell death [100]. Other groups have reported unpublished evidence suggesting that ADAMTS10 binds fibrillin-1, a protein with implications in TAAD and MFS [101]. Here, we investigated the potential of one member of this gene family, ADAMTS16, to cause inherited aneurysms (see below).

1.4. Study Proposal

Our study focuses on family TAA288, a large Caucasian family living in the United States with an autosomal dominant pattern of non-syndromic aneurysms. Female patients in this family predominantly present with saccular ICA, while male patients predominantly present with TAA (Figure 1.4). DNA sequencing of affected members of this family did not detect any mutations in the known TAAD-causing genes. This family was also subjected to a genome-wide linkage on the 50k GenChips Hind array from Affymetrix. Evidence of linkage was observed on only two chromosomes: 1q32 and 5p15. This presents us with the opportunity to characterize a novel genetic locus associated with inherited aneurysms.

The clinical criterion for diagnosis of TAAD in this study was an aortic root exceeding 4 cm in diameter, as determined by clinical imaging. Imaging was either performed using 2D echocardiography or measurements were taken from medical records. The presence of ICA was similarly diagnosed by cerebrovascular imaging using MRA or CT angiography. Clinical information on members of the TAA288 family is provided in Table 1.1.

TAA288 Clinical Information

The proband of TAA288 (III:8) is a female who was ascertained at age 29, with medical imaging revealing a dilation of the extracranial portion of her internal carotid arteries. Subsequent imaging revealed more abnormal structures of her carotid arteries, including small infundibula at the origins of each of her posterior communicating arteries. Though her ascending aortic diameter at the sinus of Valsalva was normal (2.7 cm), all three of her brothers were observed with aortic aneurysms at this location. Patient III:5 was ascertained at age 36 with a 4.6 cm aortic aneurysm at the sinus of Valsalva, III:7 at age 32 measuring 4.6 cm, and III:6 underwent surgery at age 35 with an aortic root measuring 5.5 cm. The father of these individuals died suddenly of unknown causes at age 59. Though no autopsy was performed, sudden death is characteristic of TAAD. There is also significant occurrence of other cardiovascular disease in the extended family of these siblings.

A paternal aunt of the proband (II:1) died at age 54, with a CT scan revealing a left frontal hematoma with SAH. Her son (III:3) died at age 42 from an acute type A aortic dissection. His aortic root measured 8.9 cm at autopsy, but an echocardiogram three years prior had measured his aortic root merely 3.3 cm; a total increase of 5.6 cm in three years. His sister (III:2) has undergone echocardiogram and cerebrovascular imaging, showing no signs of cardiovascular disease herself. However, her son (IV:1) had borderline measurements at age 15 (3.75 cm), but quickly developed an enlarged aortic root of 4.19 cm by age 18. Thus, III:2 was scored as an obligate carrier for the genetic disposition for vascular disease in this family.

Another paternal aunt of the proband died suddenly at age 57 from a cerebral dissection. Her son (III:9) underwent echocardiogram imaging at age 41, to reveal a TAA measuring 4.5cm in diameter. Individual III:4 underwent thoracic imaging and did not meet our criteria for TAA, but has not yet undergone cranial imaging. Two other members of this pedigree (III:10, and III:11) have not undergone cranial imaging. Thus, the disease status of members III:4, III:10, and III:11 is currently unknown. According to our genome-wide analysis, the genomic region most strongly linked to the disease phenotype of this family is located on chromosome 5p15.

ADAMTS16 in TAA288

The *ADAMTS16* gene lies within the 5p15 genomic interval linked to the TAA288 disease phenotype, and was first described in 2002 [102]. The target substrate of *ADAMTS16* *in vivo* is unknown, but the full length protein product has been shown capable of cleaving alpha-macroglobulin, a large blood protein inhibiting coagulation, *in vitro* [103]. Also, an artificial isoform of this protein truncated after TSP-1 was shown to have weak aggrecanase activity [104]. Initial expression profiling of this gene in human tissues revealed high levels of *ADAMTS16* mRNA in adult brain and ovaries, and fetal lungs and kidneys [105].

Several isoforms of ADAMTS16 have been reported. The full length transcript for this protein or ADAMTS16-001 (ENST00000274181) contains 23 exons encoding a polypeptide 1224 amino acids in length. The Ensembl database reports three alternative transcripts for this protein, one of which is protein coding isoform: ADAMTS16-002 is a transcript truncated after exon 11 and encodes a 570 aa product. The alternative transcript ADAMTS16-003 (ENST00000433402) retains an intron and does not encode a protein

product. The last alternative transcript of this gene is ADAMTS16-005 (ENST00000513709) (there is no -004), which is a 189 bp fragment comprised of contiguous sequence from exon 13 and 15 combined, excluding exon 14.

Recent studies have found an association between SNP variants of ADAMTS16 and hypertension [106]. This is intriguing since hypertension is a major risk factor for the development of aneurysms, as well as many other vascular diseases. Another study showed that ADAMTS16 expression can be induced in cultured fibroblast cells treated with TGF- β 1 [107]. This cytokine treatment induces transformation of cultured fibroblasts into myofibroblasts, which express smooth muscle-specific proteins and have been suggested to play a role in the role of atherosclerotic lesion formation [108]. This observation also implicates *ADAMTS16* as a downstream target of TGF- β 1 signaling, which is a cytokine dysregulated in aneurysm patients with TGFBR2 mutations and Marfan syndrome. We were interested in utilizing the fibroblast model in our own studies, as dermal fibroblasts are easily cultured from skin biopsies taken from patients in clinic. In this interest, we successfully cultured dermal fibroblast samples from two members of the TAA288 family (III:5, IV:1).

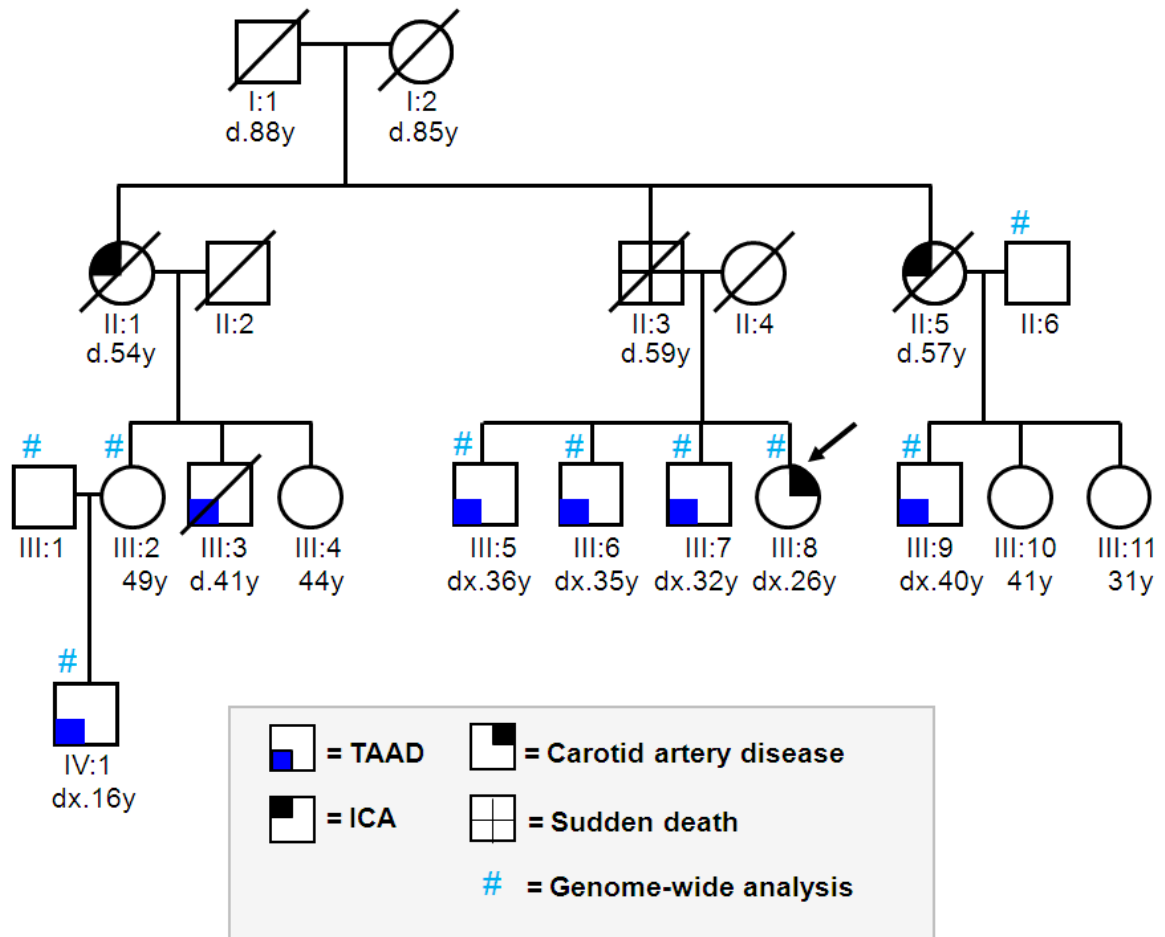


Figure 1.5: The TAA288 Family. This pedigree shows the family structure for TAA288, with the proband indicated with an arrow. Ages provided are age at death (d), age of diagnosis (dx) or current age. The nine samples indicated by “#” were genotyped on the Affymetrix 50k SNP platform for genome-wide linkage analysis. Note the prevalence of TAAD in males, and cranial aneurysms in females. See section 1.4 for clinical details.

Pedigree ID	Age at enrollment	Disease Status	Gender	TAAD, age at dx	Aortic measurements			ICA type, age at dx	CAD	HTN	HLD	DM	Smoking
					AN	SV	STJ						
III:2	43	Unknown/Carrier	F	-	3.2			1.79	46	-	-	-	-
III:3	41	Affected	M	Ao root aneurysm, 41	8.0				41	-	-	-	-
III:4	39	Unknown	F	-	2.4				?	unk	-	-	-
III:5	37	Affected	M	Ao root aneurysm, 36	4.6		3.3		36	unk	-	-	-
III:6	35	Affected	M	Ao root aneurysm, 35	5.5				35	unk	-	-	-
III:7	32	Affected	M	Asc aneurysm (unsp location)	4.3				26	unk	-	-	-
III:8	26	Affected	F	-	3.3	3.3	2.9	1.6	26	unk	-	-	-
III:9	41	Affected	M	Ao root aneurysm, 40	4.5			1.84	41	unk	-	+	-
III:10	36	Unknown	F	unk						unk	-	-	-
III:11	27	Unknown	F	unk						unk	-	-	-
IV:1	16	Affected	M	Ao root aneurysm, 19	4.2		2.4		19	-	-	-	-

Figure 1.1: TAA288 Clinical Details.

+ = Present
- = Absent
AN = Aortic Annulus
SV = Sinus of Valsalva
STJ = Sinotubular junction
DM = diabetes mellitus
Asc = Ascending aorta
BSA = body surface area (m²)
CAD = coronary artery disease
HTN = hypertension
HLD = hyperlipidemia

Myofibroblast Model in TAA288

Myofibroblast cells have been implicated in wound healing in a number of human tissues, including the vasculature [109]. *In vivo*, myofibroblasts commonly arise from the differentiation of local fibroblast cells at an injury site in response to mechanical stress or cytokines such as TGF- β 1 [110-112]. *In vitro* treatment of fibroblasts with TGF- β 1 also induces these cells to upregulate integrins and other ECM components [113;114]. In addition, these cells turn on a number of SMC contractile genes, like *ACTA2* which encodes SM α -actin as is a marker for the differentiation of fibroblasts into myofibroblasts [115].

This is a convenient model for our disease, as a simple skin biopsy can yield dermal fibroblast cells for our use in cell culture experiments. Fibroblast cultures made from affected patients from TAA288 will carry the genetic alteration responsible for this phenotype. This allows the direct observation of aberrant gene expression in patient cell lines, by comparing gene expression in cells derived from TAA288 patients to those derived from control subjects without disease. Several members of TAA288 (discussed below) agreed to provide us with skin biopsies for our gene expression studies.

Hypothesis & Specific Aims

Here, we hypothesize that the disease phenotype in family TAA288 is inherited as a single gene autosomal dominant disorder, with a gender influenced phenotype: TAAD in males and ICA in females. A previously performed genome-wide linkage analysis of this family implicated only two loci, with neither one previously reported to be linked to either

aneurysm subtype. This analysis is discussed in chapter 2. Our objective is to identify the causal mutation in this family, in order to better understand the molecular mechanisms causing this disease and to identify the individuals in this family at risk of developing vascular disease.

Two important observations support our hypothesis. First, a single mutation causing TAAD can also be associated with other forms of vascular disease. Mutations in the gene *ACTA2* have already been described, where a single mutation causing inherited TAAD is also observed in family members with other early onset vascular diseases such as livedo reticularis [116;117]. Thus a single pleotropic mutation in the TAA288 family could be responsible for both the inherited form of TAAD and ICA observed in this family. The second observation is that there are common pathological features shared by these two aneurysm types. Degeneration of the medial layer is observed in both TAAD and ICA [118]. This common pathology is suggestive of a common biological mechanism that can cause this inherited subtype of disease: concurrence of TAAD and ICA.

There are three specific aims of this study. First, we will verify and refine the disease linked genomic loci associated with the TAA/ICA phenotype in family TAA288, as indicated by a previously performed genome-wide analysis. This will be performed by genotyping microsatellite markers within and adjacent to the 1q32 and 5p15 loci, in order to confirm and fine map linkage to each region. The next aim is to identify rare and novel DNA sequences found within the disease-linked loci. Online references will be used to identify candidate genes within this locus, and DNA Sanger sequencing methods will be used to detect genetic alterations. The third and final aim will be to explore the effects of said variants, and characterize their potential to cause the disease phenotype in TAA288. This will be

performed in fibroblast cultures available from patients in this family. Potential roles for any novel candidate genes in the development of aneurysm phenotypes will also be discussed.

CHAPTER 2: METHODS

2.1 Linkage Analysis Methods

Sample Collection

Collection of all samples used in this study was approved by the Institutional Review Committee at the University of Texas Health Science Center Houston. After obtaining the appropriate consent, biological samples were collected from members of the TAA288 family; these samples included buccal swabs, blood samples, autopsy samples and skin biopsies.

DNA Extraction

Genomic DNA was isolated from blood and buccal samples according to the PureGene genomic DNA isolation kit protocol (Gentra Systems). Two notable exceptions were patients II:2 and III:3, with their respective genomic DNA extracted from autopsy samples and fibroblast cultures.

DNA extraction from paraffin-embedded prostate from the autopsy of patient II:2 was performed using the AgencourtTM FormaPure Kit: Nucleic Acid Isolation from Formalin-Fixed, Paraffin-Embedded Tissue manufacturer's protocol. Five attempts were made in parallel, with each consisting of five sections (10 μm) made from paraffin-embedded slides. Each sample containing tissue sections was incubated with 200 μl Lysis Buffer at 72°C for 1 hour. 20 μl of Buffer PK containing isopropanol was added, and the samples were incubated at 55°C for an additional hour. The sample was cooled on ice and treated with 150 μL of Bind I Buffer and 320 μl of Bind II Buffer containing DNA-affinity magnetic beads. The sample was briefly incubated at 55°C for 5 minutes, and then allowed to separate

by magnetic force on the provided SPRIStand for tubes. The supernatant was discarded and samples were washed with Wash Buffer and separated by magnetic force again. The sample was then washed twice with 70% EtOH, once with 90% isopropanol, and then once more with 70% EtOH, separated each time by magnetic force. Total nucleic acid was eluted in 80 μ l of nuclease-free H₂O by incubation at 65°C for 30 seconds, and quantified on a Nanodrop™ ND-1000 spectrophotometer using the nucleic acid setting at wavelength 260 nm.

DNA extraction was performed on perished fibroblast cultures from patient III:3, received from a cryo-storage facility in New Orleans. While originally containing frozen fibroblast cultures from this patient, the facility lost electrical power in the wake of hurricane Katrina and samples were no longer viable upon arrival in Houston in the fall of 2008. Genomic DNA was purified from the received tissue sample from patient III:3, using the QIAamp DNA Mini and Blood Mini Handbook protocol: DNA purification from Blood or Body Fluids (Spin Protocol, 11/2007).

Microsatellite Marker Selection and Genotyping

Microsatellite markers were selected for fine-mapping of TAA288 disease-linked regions indicated by genome-wide SNP linkage analysis. Marker selection criteria included a genomic physical position within a TAA288 disease-linked linked region, an inter-marker spacing of less than 5 MB, and preferably a >0.7 heterozygosity score. Primer sequences and map location were obtained from the MAP-O-MAT (<http://compgen.rutgers.edu/mapomat/>) and NCBI UniSTS databases (<http://www.ncbi.nlm.nih.gov/sites/entrez?db=unists>) [119].

All oligonucleotide primers were synthesized by Integrated DNA Technologies (Coralville, IA).

Genotyping of microsatellite markers was achieved through Polymerase Chain Reaction (PCR) amplification of genomic DNA. Universal primer tags (FAM, HEX, NED) were added to one member of each oligonucleotide pair, to allow fluorescent end-labeling of PCR products [120]. Amplification was then performed using HotStar Taq DNA Polymerase in a 10 μ l amplification reaction. Each reaction contained 10 ng genomic DNA, 1x PCR buffer, 1x Q Buffer, 2.5 mM dNTP, 25 mM MgCl₂, 5 pM primers (forward, reverse, and universal) and 0.25 units of Taq (5 units/ μ l). Generating fluorescently-labeled PCR products required a two-step amplification reaction as follows: initial activation at 95°C for 15 minutes, followed by 10 cycles of fluorescent labeling (denaturing at 95°C for 30s, annealing at 60°C for 30s, elongation at 72°C for 30s) and 35 cycles of genomic amplification (denaturing at 95°C for 30s, annealing at 60°C for 30s, elongation at 72°C for 1 min).

Amplification products were diluted 1:100 in Formamide HiDi and combined with Genescan™ 400HD or 600HD Rox Size Standard. After denaturing samples at 95°C for 5 minutes, fragment sizes were analyzed on the ABI 3130 platform using GeneMapper v4.0 software (Applied Biosystems).

Microsatellite fragment size alleles were analyzed for Mendelian consistency and disease-segregation within each pedigree. Manual phasing was performed by observing for Mendelian inheritance consistency in parents and offspring within the TAA288 pedigree, and then inferring allele positions on individual chromosomes. The results of manual genotyping and phasing were then verified for Mendelian consistencies using Pedcheck software [121].

Linkage Statistical Analysis

Statistical tests of linkage on our acquired genotype data was performed using the affected-pedigree-member method [122]. Pairwise and Multipoint Logarithm of Odds (LOD) scores were calculated using FASTLINK software v3p, specifically the MLINK and LINKMAP programs [123;124]. An age-dependant penetrance model was used, based off known allele frequencies and observations from previous linkage studies of familial TAAD [125;126]. Specific penetrance values used for genome-wide SNP-based linkage were 10% for individuals <30 years of age, 30% for ages 30-40, 70% for ages 40-60, and 90% for ages > 60.

2.2 Mutation Detection Methods

Copy Number Variation Detection

Genomic DNA from patient III:5 was analyzed on the Illumina 610-Quad BeadChip assay. Genotyping results were analyzed under two algorithms, PennCNV [127] and CNV partition (Illumina) with events detected by both algorithms considered for further analysis. Results were compared to The Children's Hospital of Philadelphia (CHOP) CNV project (<http://cnv.chop.edu/>) as a control reference database. Genotyping analysis was performed by Dr. Siddharth Prakash of the Baylor College of Medicine.

Target Gene Selection

Genes were selected based on their genomic physical position within the TAA288 critical interval. Gene locations were ascertained through the NCBI website located at <http://www.ncbi.nlm.nih.gov>; specific NCBI genomic coordinates used were *homo sapiens* chromosome 5p15: 3,424,465- 6,312,925 bp (GRCh37/hg19 Assembly). The exons of verified genes within these genomic coordinates were selected as the primary targets for DNA sequencing.

Primer Design

Intron-based, exon-flanking oligonucleotide primer sequences were manually selected for sequencing of target genes. Primers were designed to anneal to genomic sequences of forward and reverse DNA strands, based off the Ensembl reference sequence available at <http://uswest.ensembl.org/index.html>. General selection criteria for primers included a length of approximately 20 base pairs, a GC content of 40-60%, the absence of any known polymorphic nucleotide sites and an intronic position flanking target exon sequence by at least 100 bp. Optimal amplicon size was 500 bp, and primers were designed to anneal at least 100 bp upstream of the target exon sequence. Oligonucleotide primers were ordered from Integrated DNA Technologies (Coralville, IA).

PCR & DNA Sequencing

PCR amplification of genomic DNA was performed using the selected primers. Each PCR was carried out as a 10 microliter reaction containing 5 μ M forward and reverse primers, 10ng genomic DNA, 2mM dNTPs, 25mM MgCl₂, and 0.125 units of HotStar DNA polymerase (Qiagen, Valencia CA). PCR conditions were as follows: initial denature at 95°C for 15 minutes, followed by 35 cycles of 95°C denature for 30 seconds, annealing at 60°C for 30 seconds, and extension at 70°C for one minute. A final hold of 72°C for 3 minutes was used to ensure enzyme inactivation, and then samples were stored at 4°C until further use. PCR products were then treated with 1 μ l of ExoSAP (GE Healthcare) to remove unused primers and dNTPs, and treated to the following incubations: 37°C for 45 minutes, followed by enzyme inactivation at 80°C for 15 minutes.

Sequencing of ExoSAP-cleaned PCR product was performed using BigDye™ reagents (ABI, CA, USA). Each 10 μ l reaction contained 5 μ l of cleaned PCR product, 5 μ M either forward or reverse primer, 2.5 μ l of 5x Sequence Buffer, and 0.5 μ l of BigDye™ terminator V3.1. Sequencing condition included 35 cycles of denaturing at 95°C for 15 seconds, annealing at 60°C for 15 seconds, and extension for 90 seconds at 80°C. Sequence products were then cleaned with 7 μ l of XTerminator™ and 31 μ l of SAM™ solution (ABI, CA, USA). Sequences were read on the ABI 3730 platform using the BDX_Rapid36_POP7V3_96 module.

Initial sequencing was performed on only a few affected patients in TAA288 and one unaffected spouse as a disease control, for efficient use of time and reagents. Genotypes in these individuals at known population polymorphisms and novel alterations were documented. Novel genetic alterations were then sequenced in the remaining affected members of TAA288 to investigate co-segregation with the disease phenotype.

Genotyping Analysis

Mutation detection was only performed on high quality chromatograms generated by the ABI3730 platform. DNA chromatograms were first manually checked for quality using Chromas Lite freeware (www.technelysium.com.au/chromas_lite.html) to verify successful digestion of primer fragments and excess dNTPs. Forward and reverse chromatograms were aligned and compared using Mutation Surveyor 3.01 software (SoftGenetics, State College, PA). Bidirectional sequencing and mutational analysis of amplicons containing novel variants was repeated at least twice to verify authenticity. Known genetic variants were also observed and documented.

Statistical Test of Association

Rare or novel alleles ascertained by DNA sequencing were tested for association to the aneurysm phenotype within three general population strata: patients with sporadic aneurysms, patients with inherited aneurysms, and controls with no aneurysms. Criteria for distinguishing inherited and sporadic disease were discussed in chapter 1. We tested each strata for allelic association separately using a 2x2 contingency table for this analysis, arbitrarily assigning allele states (genotypes) to columns and disease states (affected or unaffected) to rows. A one-tailed Fisher's exact test was used to calculate significant associations, with $\alpha = 0.05$ as the threshold for statistical significance.

2.3 Transcript and Protein Level Detection Methods

Immunodetection of ADAMTS16 in Aortic Tissues

Immunohistochemical detection of protein in human tissues was performed by Tommy Reese at St, Luke's hospital in Houston, TX. Paraffin-embedded tissue sections were de-paraffinized with xylenes and hydrated in distilled H₂O. Antigen retrieval was performed by submersion of slides in warmed EDTA buffer for 35 minutes, and quenched using 30% H₂O₂. Slides were then blocked for 20 minutes, and incubated in sc-50490 antibody 1:50 for one hour at room temperature. Secondary antibody was applied for 30 minutes at room temperature, and slides were developed with DAB chromogen solution until antigen sites turned a distinct brown color. Slides were then counterstained for 45 seconds using Richard-Allan hematoxylin, and mounted with Permount reagent.

Dermal Fibroblast Explants and Cultures

We successfully explanted dermal fibroblasts from skin biopsies provided by two members of the TAA288 family (III:5 and IV:1). Three millimeter dermal biopsies were obtained and stored in Dulbecco's Modified Essential Medium (DMEM) containing 10% fetal bovine serum (FBS) and an antibiotic/antimycotic supplement for transportation to our facilities. The tissue was washed in 70% EtOH, rinsed with 1xPBS, and then placed in DMEM. Here, the epidermal and adipose layers were manually removed and discarded, isolating the dermal layer. The dermal layer was transported to a 60 mm cell culture dish, minced, and covered with a glass coverslip. Complete media (DMEM containing 10% FBS

and antibiotic) was added to this dish to create a primary fibroblast culture, which was allowed to grow at 37°C with 5% CO₂; media was changed twice weekly.

Fibroblast cultures created from successful explants were maintained in a sterile incubator under similar conditions (37°C with 5% CO₂) at all times, except when being directly manipulated. As with explants, we replaced complete media twice a week in fibroblast cultures. Fibroblast cultures passage 2-5 were used for experiments.

Myofibroblast Protocol, TGF-β1 Treatment

Dermal fibroblasts were allowed to grow in T75 flasks containing complete media as described above. Cells having reached confluence were trypsinized from their T75 flasks and plated onto replicate dishes, either 60 mm or 35 mm diameter, at 80-100% confluence in complete DMEM. These plates sat undisturbed for 24 hours, allowing cells to settle, and then serum-starved for additional 24 hrs in 0.2% FBS DMEM. Low serum media was then replaced with DMEM containing 0.2% FBS ± 10 ng/mL TGF-β1(R&D Systems, inc). Cells were harvested at pre-determined time points after receiving TGF-β1 by removing media and freezing at -80°C for future use of RNA or protein.

Previous experiments have shown that fibroblasts treated with TGF-β1 express high levels of SM α –actin, used as a marker for myofibroblast differentiation [128]. For this reason we did not choose to harvest any time points beyond 72 hrs.

VSMC Cultures

Vascular smooth muscle cells previously explanted from the aortas of control individuals were also used, taken from frozen aliquots stored at -80°C . SMCs were grown in T75 flasks containing SmBm (Lonza) supplemented with 15% FBS, 0.5 mL insulin, 1.0 mL rhEGF, and 0.5 mL rhFGF, and an antibiotic/antimycotic reagent and housed in a sterile incubator at 37°C with 5% CO_2 ; SmBm media was changed twice weekly. Once confluent, SMCs were plated at 70 cells/mm^2 in culture dishes, allowed to settle for 24 hours, then treated for 24 hours with SmBm (Lonza) supplemented with 0.2% FBS and an antibiotic/antimycotic reagent. Media was then removed and plates were frozen at -80°C at predetermined time points for future use of RNA and protein.

RNA Extraction

RNA was extracted from total cell lysate using Tri ReagentTM (Sigma), according to the manufacturer protocol. One mL of Tri ReagentTM was added directly to frozen cells immediately after removing from -80°C . Plates with Tri ReagentTM were incubated with slow agitation at room temperature for 15 minutes, and then mechanically scraped with Fisherbrand Disposable Cell Lifters. Lysate was then passed through a 1 mL pipette tip 20 times to ensure homogenization, and then transferred into a 1.7 mL Denville Posi-ClickTM Tube (C-2170). 200 μL of Chloroform was added to the tube containing lysate, shaken by hand for 15 sec and incubated at RT for 5 minutes. Samples were centrifuged at 13,000 rpm for 15 minutes at 4°C , and 400 μL of the clear supernatant layer was transferred to a fresh 1.7 mL tube; only a small amount of supernatant was transferred to avoid genomic DNA

contamination. 500 mL of isopropanol was added to the supernatant, and tubes were inverted 20x and incubated at RT for 5 mins to ensure efficient precipitation of RNA. Tubes were again centrifuged at 10,000 rpm for 15 mins at 4°C to create an RNA pellet. Excess isopropanol was removed by vacuum suction, and the pellet was then washed with 1 ml of 75% EtOH. After light mixing, the tubes were centrifuged one final time at 13,000 rpm for 5 minutes at 4°C. Excess EtOH was removed by suction down to a volume of ~100 µl, and the remaining liquid was carefully removed by pipette. Samples were allowed to air dry for no more than 20 minutes, and then resuspended in 30µl of RNase-Free H₂O.

Quantification of RNA concentration was performed by analysis of optical density. After blanking with H₂O, 1 µl of RNA samples was added to a Nanodrop ND-1000 spectrophotometer using the nucleic acid setting. Nucleic acid content was quantified at wavelength 260 nm, and samples with a 260/280 ratio greater than 1.7 were used for further analysis.

cDNA Synthesis

cDNA was synthesized from isolated RNA using the High-Capacity cDNA Reverse Transcription Kit (ABI) using manufacturer's recommendations. Each reaction contained 200-500 ng of total RNA, 1x Reverse Transcription buffer, 1x dNTPs, 1x random primers and 50 units/uL of MultiScribe™ Reverse Transcriptase. Reactions were then incubated at 25°C for 10 min, 37°C for 120 min, 85°C for 5 min and stored at 4°C until later use.

DNA Gels

We performed PCR amplification of certain cDNA templates using the same reactions described in chapter III. We visualized our PCR product on either 0.8% agarose gel or 8% polyacrylamide gels. Gels were stained with EtBr and PCR products were visualized under ultraviolet light (UV).

Quantitative RT-PCR

Analysis of gene expression was performed using the TaqMan Gene Expression Assay system (ABI, CA). Each reaction was performed as a 10.5 μ L reaction, containing 1x target assay mix, 1x Taqman Universal PCR Master Mix, and 5 μ L of cDNA synthesized as previously described. Fluorescent signals from target assays were detected on the ABI Prism 7000 SeqDet system under the relative quantification settings. Specific cycling parameters used were 95°C for 10 minutes, followed by 40 cycles of: 95°C for 15 seconds and 60°C for 1 minute. We performed each reaction in triplicate on the same 96 well plate, along with reactions run in parallel containing GAPDH target assay mix as an endogenous control.

Relative expression of target genes was normalized to GAPDH expression using the $\Delta\Delta$ CT method, and tested for significance using Student's T-Test.

Protein Isolation

Plates containing cells intended for protein harvest were placed on ice after removal from -80°C freezers. Samples remained on ice throughout the isolation procedure. Protein isolation buffer was added to each dish, consisting of RIPA buffer (50 mM Tris-HCl at pH 7.4, 50 mM Tris-HCl pH 7.4, 150 mM NaCl, 1 mM EDTA, 1% NP-40, 0.25% Na-deoxycholate), phosphatase inhibitors (10 mM NaF, 1 mM Na₃VO₄) and 30 µl/mL protease inhibitor (PMSF and P8340 cocktail, Sigma). Cells were mechanically scraped from plates with Fisherbrand^R cell lifters and transferred to 1.7 mL Denville Posi-ClickTM Tubes. Samples were passed through a 22G needle 15x, then briefly vortexed every 5 minutes for a total of 30 minutes. Samples were then centrifuged for 30 minutes at 13,000 rpm at 4°C. Supernatant was collected and quantified by Bradford assay using Bio-Rad protein reagents.

Immunoblotting

Aliquots of 10 µg were taken from each protein sample, mixed with sample buffer, and incubated at 95°C in boiling water for 5 minutes. Boiled protein samples were then loaded into 8% Acrylamide gels made by diluting 12.5% EZ-RunTM Protein Gel Solution (cat no: BP7712-500, Fisher) with water, and adding crosslinking reagents (10% Ammonium Persulfate and N,N,N',N'-Tetra-methylethlenediamine (TEMED, cat no: 161-0801, Bio-Rad)). Gels were run in 1x EZ-RunTM Running Buffer at no more than 120V, and transferred to PVDF membranes in 20% MeOH transfer buffer at 80V for 60 min. Membranes were blocked in 1x Tris Buffered Saline containing 1% Tween-20 (TBST) and 5% immunograde nonfat milk for 1 hour at room temperature.

PVDF membranes containing protein were incubated with primary antibody detecting ADAMTS16 (sc-67440) or GAPDH (10R-G109a) for 8-12 hrs at 4°C. Membranes were then rinsed with TBST and incubated with HRP-conjugated secondary antibodies for 2 hours at room temperature. Proteins were visualized with Pierce ECL Western Blotting Substrate (Thermo Scientific) and exposed to Blue X-Ray Film (Phenix). Films were processed on a SRX-101a Medical Film Processor (Konica).

CHAPTER 3: RESULTS

3.1 Linkage Analysis Results

Microsatellite Fine-Mapping of Candidate Loci

We first examined the TAA288 disease-linked genomic regions on chromosomes 1q32 and 5p15. From this linkage analysis, a small region on chromosome 1q32 (202-212MB) displayed a Max LOD score of approximately 0.8 (Figure 3.1). In order to verify this observation, six microsatellite markers (D1S1725, D1S249, D1S2692, D1S205, D1S425, and D1S237) were selected with an intermarker spacing ~2.5 MB for genotyping over the 1q32 interval. Upon genotyping, we did not observe any alleles of these markers shared among affected family members of TAA288 (Figure 3.2) As a result, chromosome 1 was not considered for further linkage analysis.

We performed a similar analysis on chromosome 5p15, initially selecting four microsatellite markers with an intermarker spacing ~2.5 MB (D5S2005, D5S2505, D5S1953, D5S2004). Of these four markers, shared genotypes were observed among all affected members of TAA288 at one location (Figure 3.3). A single allele of the marker of D5S2505 was observed in all affected members of TAA288, as well as some members scored with unknown and unaffected disease status (D5S2505: allele “6”, Figure 3.3). As a result, additional markers in proximity to D5S2505 were selected for genotyping, in order to improve the mapping resolution of this area.

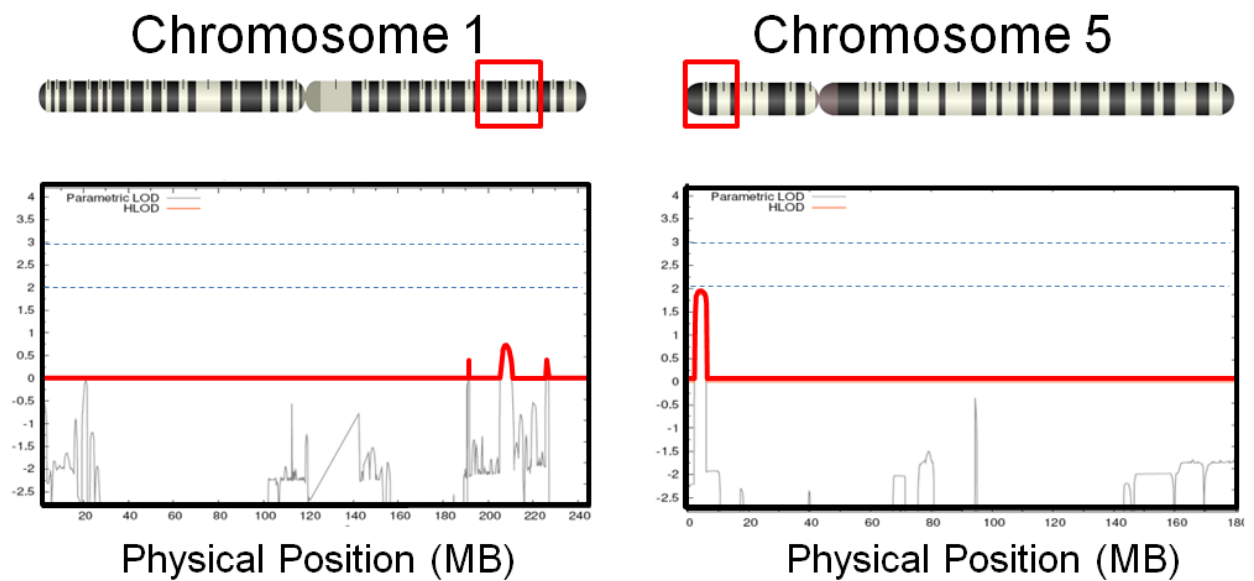


Figure 3.1: Genomic Regions Linked to the TAA288 Disease Phenotype. Two genomic regions had evidence of linkage within the TAA288 family. These two regions are located on chromosomes 1q32 and 5p15. Details of the analysis performed are described in chapter 2.2.

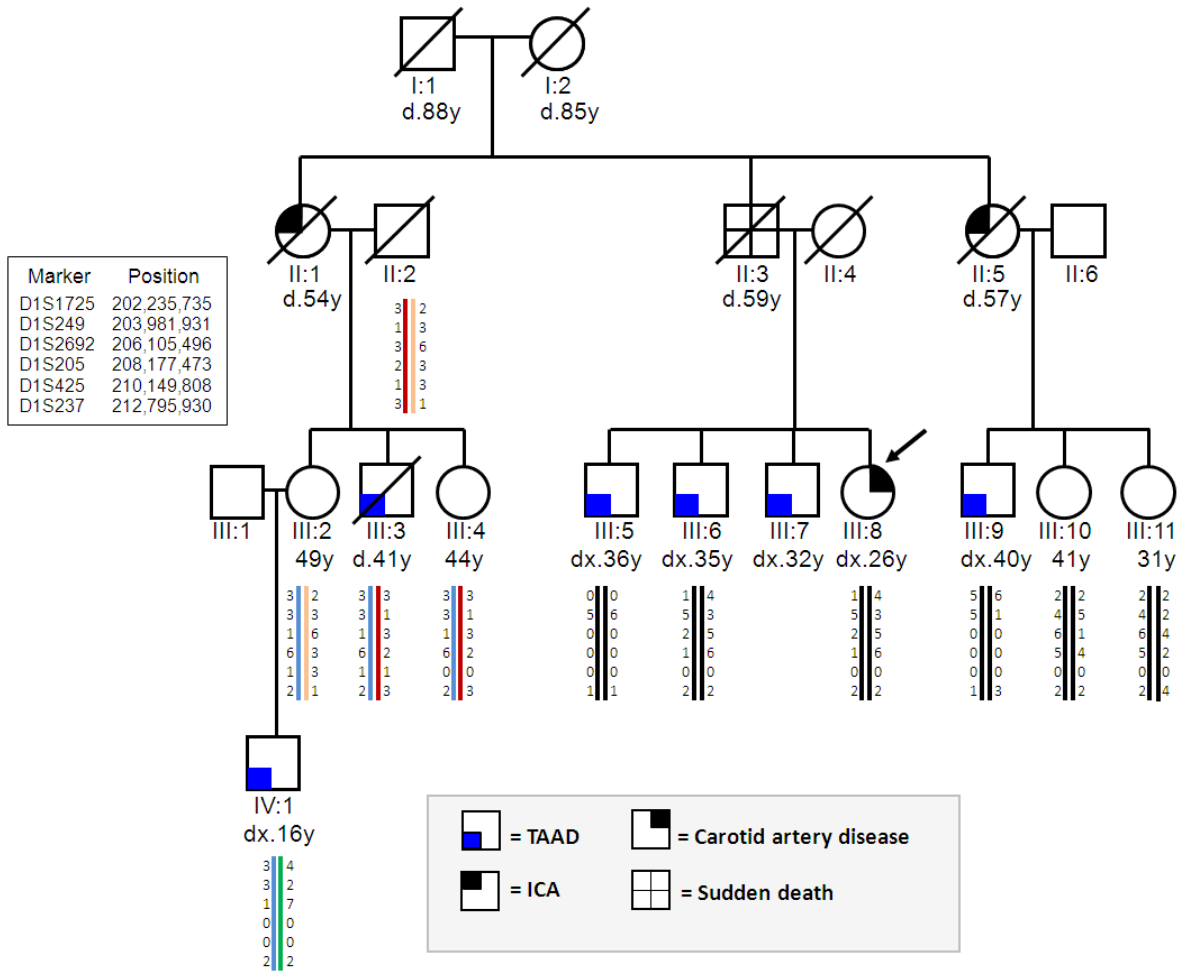


Figure 3.2: TAA288 1q32 Microsatellite Phasing. The pedigree above shows the genotypes of microsatellite markers, given as recoded allele, located within the chromosome 1q genomic region with evidence for linkage. Genotypes given as “0” did not successfully amplify. Colored bars were added to highlight the movement of marker haplotypes across generations; black bars are not phased. Genotyping and phasing of this region stopped when it was observed that no markers of these six alleles are shared between all affected members of this family. This region was not characterized further due to this lack of a shared haplotype among all disease-affected members of TAA288.

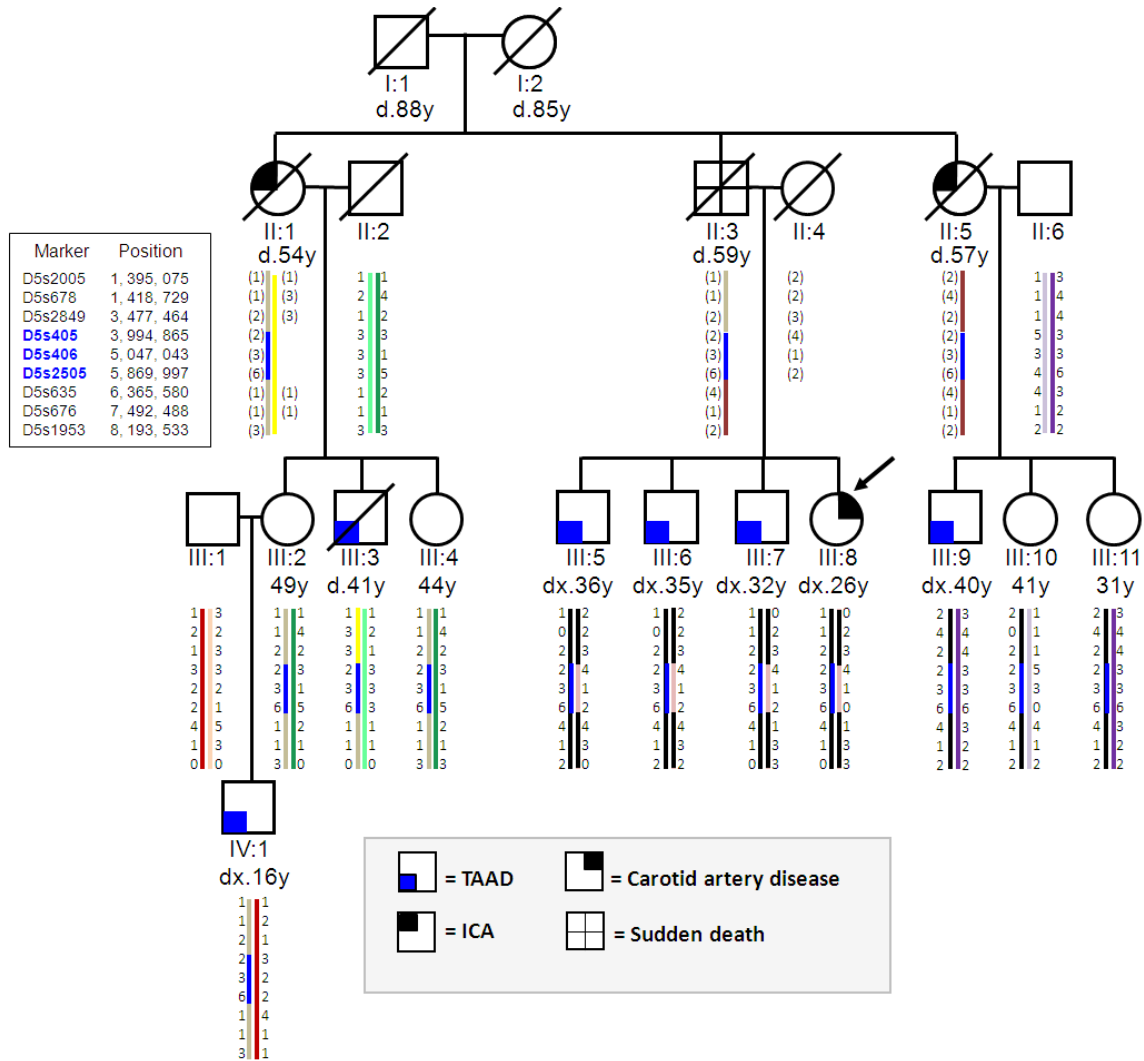


Figure 3.3: TAA288 5p15 Microsatellite Phasing. The pedigree above shows the results of manual phasing of 5p15 microsatellite markers, given as recoded alleles, in the TAA288 family. Genotypes given as “0” did not successfully amplify. Genotypes in parenthesis are inferred genotypes. Not all markers genotyped within this region are shown, for easier viewing. Note the blue bar adjacent to the alleles 2, 3, 6 for markers D5S405, 406 and 2505, respectively. These markers denote the TAA288 critical interval, which is the genomic region with the strongest evidence for linkage in this family. Also note the single recombination event observed in patient III:3 defining the telomeric boundary of this region (the “3” allele of marker D5S2849, on the yellow bar).

Critical Interval Containing the Defective Gene in Family TAA288

Further genotyping of microsatellite markers with proximity to D5S2505 revealed a subset of markers with alleles shared among all affected members of TAA288. Preliminary manual genotype phasing was performed on microsatellite marker genotypes within this region, with results suggesting that certain alleles of three adjacent microsatellite markers (D6S405, D5S406, D5S2505) lay on the same chromosomal fragment and segregated with the TAA288 phenotype (Figure 3.3). To confirm these observations, pairwise LOD scores were calculated for markers within the region. The pairwise LOD scores for these three adjacent markers was 0.83 for D5S405, 0.48 for D5S406, and 0.57 at D5S2505 observed at $\theta = 0$ (Table 3.1). Under this analysis, these three markers have the strongest evidence for linkage in the 5p15 genomic region. In contrast to this, many other markers in this region (D5S392, D5S2005, D5S678, D5S1970, D5S2849, D5S635, and D5S580) have LOD scores below -2.0 which is evidence for exclusion from linkage. This observed evidence of linkage at three adjacent markers in this region led to still further selection and genotyping of microsatellite markers, in an attempt to refine genotyping resolution of this interval.

Two crucial recombination events defined the boundaries TAA288 critical interval. The first defined the centromeric boundary at the marker D5S635, which we observed in the offspring of affected patient II:1. The children of II:1 (III:2, III:3, and III:4) share the “1” allele at this marker on their diseased chromosome, while other affected members of TAA288 share a “4” allele (Figure 3.3). It cannot be determined in which individual this recombination event occurred, due to insufficient DNA samples in generations I and II.

The second recombination event is observed in a single individual, III:3, and defines the telomeric boundary of the TAA288 critical interval. This affected patient has a “3” allele at the marker D5S2849, which is not observed in either of his siblings (III:2, III:4) or his unaffected father (II:2) (Figure 3.3). Therefore, we can infer that III:3 must have inherited the unique “3” allele from his affected mother (II:1) since his father does not carry this allele. Meanwhile, II:1 passed on her “2” allele to her other two children (III:2, III:4). Since all three siblings in generation III share the remaining disease haplotype (critical linkage interval) on the same chromosome adjacent to D5S2849, a recombination event must have occurred during a meiosis event within individual II:1. Our data suggest that this recombination occurred between markers D5S2849 and D5S405, on the chromosome passed on to III:3.

To define the boundaries of this region we observed the physical position of the two markers with the nearest outside-flanking positions relative to the five contiguous markers comprising the critical linkage interval. Thus, the genomic coordinates 5p: 3,424,465 - 6,312,925 (GRCh37/hg19) currently define the largest genomic region strongly linked to the disease phenotype in the TAA288 family.

Linkage of Other TAA288/ICA Families to 5p15

Two other families having multiple members with TAA288 and ICA inherited in an autosomal dominant pattern were selected for linkage analysis to the TAA288 critical interval, using the same microsatellite genotyping methods described. TAA395 is a Caucasian family also having a dominant pattern of aneurysms. Several men in this family

have TAA, and women in this pedigree have been observed with both TAA and ICA (Figure 3.4). DNA samples were only available for three affected members, but we observed shared alleles in these members at 4 markers: D5S2505, D5S635, D5S676, and D5S580. This same marker D5S2505 was previously used to define the TAA288 critical interval and is linked to the disease phenotype in that family (Figure 3.3). While DNA is not available from the deceased father of these three individuals in TAA395, the lack of these alleles in their unaffected mother allows us to infer that these alleles originated from their deceased father, who had aneurysms in his lifetime.

TAA480 is a small pedigree where we observed three brothers with TAAD, including the proband. The mother of the proband had an ICA, and two of her brothers also had TAAD (Figure 3.4). Three affected brothers (generation II) in TAA480 share a large chromosomal haplotype with undefined boundaries, possibly over 40 MB in size, which completely encompasses the TAA288 critical interval (Figure 3.5). Though TAA480 and TAA395 are fairly small, the evidence of linkage in these two pedigrees can be combined with the TAA288 data to strengthen the evidence of linkage between aneurysms and the 5p15 locus. We can also combine our studies with previously published data.

In 2006, a large French Canadian family with ICA inherited in an autosomal dominant pattern was observed with linkage to Chromosome 5p15.2-14.3 by Verlaan et al [129]. This observation was replicated by the same researchers in a second French Canadian family, implicating this genomic region in inherited ICA. The genomic interval reported by this group overlaps with the genomic regions shared by affected members of TAA480, and may also overlap with TAA395 (border not yet defined). However, the TAA288 critical interval does not directly overlap with this region (Figure 3.5).

MARKER	$\theta = 0$	$\theta = 0.1$	$\theta = 0.2$	$\theta = 0.3$	$\theta = 0.4$	$\theta = 0.5$
D5S392	-2.26	-0.57	-0.24	-0.09	-0.02	0
D5S2005	-2.62	-0.67	-0.33	-0.13	-0.03	0
D5S678	-6.13	-0.17	0.13	0.16	0.09	0
D5S1970	-6.4	-0.66	-0.26	-0.09	-0.02	0
D5S2849	-2.8	-0.29	-0.09	-0.03	0	0
D5S405	0.83 *	0.61	0.42	0.24	0.1	0
D5S406	0.48 *	0.37	0.27	0.17	0.08	0
D5S2505	0.57 *	0.41	0.28	0.18	0.09	0
D5S635	-2.28	-0.26	-0.04	0.04	0.05	0
D5S676	0.09	0.09	0.07	0.03	0.01	0
D5S580	-6.35	-1.13	-0.5	-0.2	-0.05	0

Table 3.1: Two-Point LOD Scores of TAA288 5p15 Microsatellite Genotypes. The table above contains two-point LOD scores calculated using microsatellite genotypes obtained from members of TAA288. The highest scores with the best evidence of linkage are indicated with an asterisk, and occur at the three markers D5S405, D5S406, and D5S2505 when $\theta = 0$. Affected members of TAA288 share one common allele at each of these three markers, as indicated in figure 2.6. LOD scores below -2.0 is evidence for exclusion from linkage. This statistical analysis was performed by Robert Yu of the MD Anderson Cancer Center.

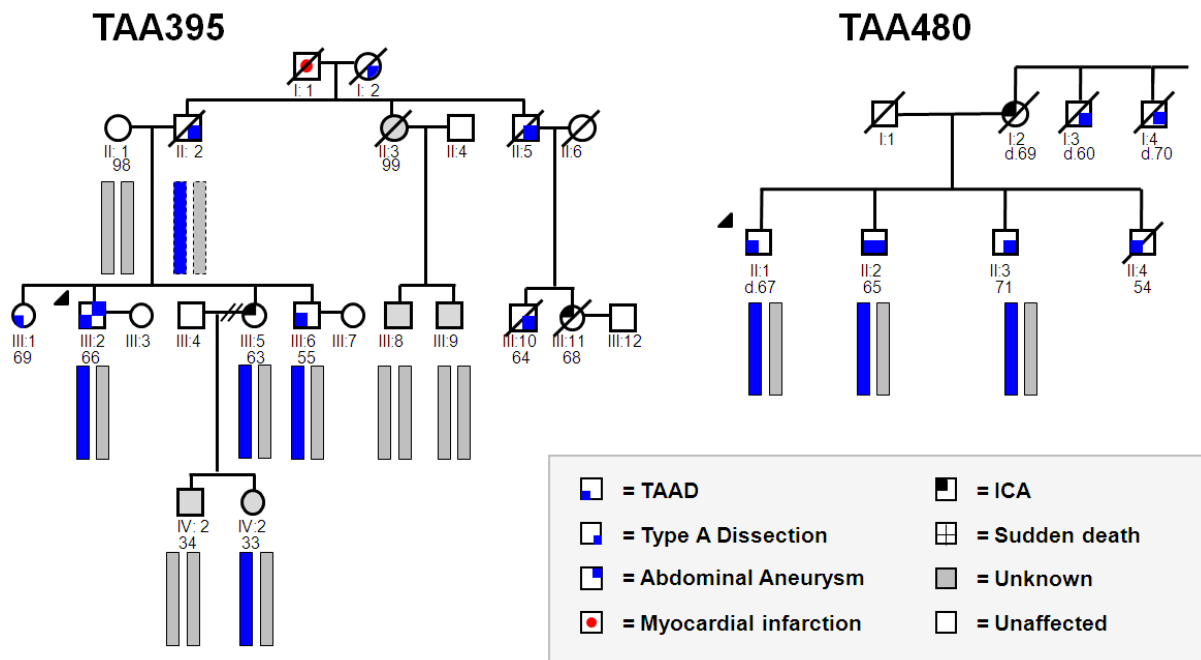


Figure 3.4: Other pedigrees with Evidence of Linkage to 5p15. Here we show two other pedigrees having a set of microsatellite alleles shared among affected members over this genomic interval. The specific alleles shared between these two families and TAA288 were not the same, and the genomic position of these intervals is shown in figure 3.5. The specific marker genotypes in these families are not depicted, and bars with a dotted outline were inferred.

Overlapping Familial Aneurysm Linkage to 5p15

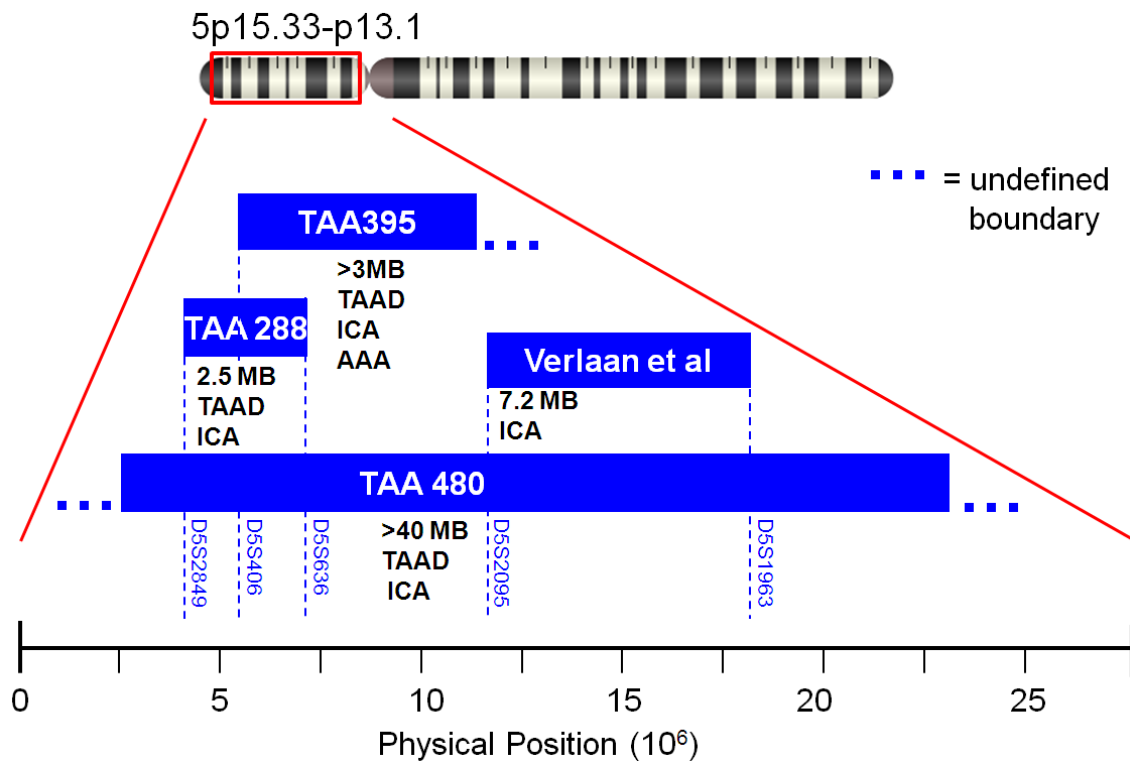


Figure 3.5: Comparison of 5p15 Linked Regions of Pedigrees with Inherited TAAD/ICA. This image depicts the relative position of possibly linked regions of chromosome five, compared between four different families from the Milewicz lab and the French Canadian families of Verlaan et al having inherited ICA. The red box indicated genomic coordinates: 5p15.33-13.1. Blue boxes show the relative positions of genomic linked regions for each family, and the positions of selected microsatellite markers in this genomic region. Borders of linkage regions indicated by “...” are not yet defined by recombinant alleles.

3.2. Mutation Detection Results

Target Gene Selection

The NCBI Reference Sequence (RefSeq) collection currently indicates six transcripts within the 5p15 TAA288 critical interval: *IRX1*, *LOC340094*, *ADAMTS16*, *LOC442131*, *KIAA0947*, and *FLJ33360* (Table 3.2). Of these transcripts, only *ADAMTS16* and *IRX1* are also described in the NCBI Online Mendelian Inheritance in Man (OMIM) database as having well characterized protein products. NCBI Entrez classifies *KIAA0947* as a protein coding gene with low complexity. The biological functions of *LOC340094* and *FLJ33360* mRNA transcripts are not known. *FLJ33360* was previously classified as a protein coding gene (NM_001001702.1), but this status was changed to non-coding as a significant portion of this transcript was found to be repetitive sequence. *LOC442131* is a predicted pseudogene with homology to the *S.Cerivisae* asparagine-linked glycosylation 3, alpha-1,3-mannosyltransferase (*ALG3*) gene.

We considered the possible role of the only two well-characterized genes in this region, *ADAMTS16* and *IRX1*, in the TAA288 disease phenotype. Iroquois Homeobox 1 (*IRX1*) belongs to a highly conserved family of transcription factors involved with complex pattern formation during embryonic development. In vertebrates, it has been implicated in neural development [130], which is intriguing given the observance of ICA in TAA288. Another member of this gene family, *IRX4*, has been implicated in the expression of myosin isoforms in the developing chicken heart [131], and *IRX4*-deficient mice develop cardiomyopathy [132]. *IRX1* has been studied in human carcinomas, and is regarded as a tumor-suppressing gene [133]. A Disintegrin and Metalloproteinase 16 (*ADAMTS16*) belongs to a family of matrix metalloproteinases with varied function. Three members of

this gene family, *ADAMTS2*, -3, and -14 process procollagen type I-III, with type III being the major isoform observed in the aorta [134]. Mutations in *ADAMTS2* also cause type VIIC Ehlers-Danlos syndrome [135;136]. *ADAMTS16* itself has unknown function.

Since there were so few genes within this region, all were selected for DNA sequencing with the exception of *LOC442131*, which was not listed in the NCBI database during the summer of 2008 when initial gene sequencing of this family commenced. Additionally, no protein product or RNA transcript has been observed for this predicted gene, lowering our confidence in its ability to cause human disease.

Two other genes were selected for sequencing with positions outside the TAA288 microsatellite-defined critical interval. *SEMA5A* and *PDCD6* have physical positions within the 5p15 SNP-defined linkage interval, but outside the microsatellite-refined linkage interval; both were selected for sequencing prior to fine-mapping of this region using microsatellite genotypes. *SEMA5A* was selected for its implication in cranial vascular defects [137], and *PDCD6* (also known as apoptosis-linked gene 2 (*ALG-2*)) plays a role in apoptosis [138], which could have implications in the arterial media degeneration observed in aneurysm pathology. Sequencing of the *SEMA5A* gene was performed by Dr. Dongchuan Guo.

Name	Description	Physical Position	Type	Exons	Longest Transcript (bp)
D5s2849		3,477,464	STR marker		
IRX1	Iroquois Homeobox 1	3,649,168 – 3,654,904	Protein Coding	4	1858
LOC340094	Hypothetical LOC340094	5,087,470 – 5,133,758	miscRNA		
ADAMTS16	ADAM metalloproteinase with thrombospondin type 1 motif, 16	5,193,443 – 5,373,417	Protein Coding	23	4979
LOC442131	Asparagine-linked glycosylation 3, alpha-1,3-mannosyltransferase homolog (<i>S. cerevisiae</i>) pseudogene	5,375,744 – 5,376,956	Pseudo / predicted	1	1213
KIAA0947	KIAA0947 protein	5,422,507 – 5,490,338	STR marker	19	7927
FLJ33360	FLJ33360 protein	6,363,554-6,390,405	miscRNA	2	2419
D5s635		6,365,580	STR marker		

Table 3.2: Sequencing Targets in the 5p15 Disease-Linked Region of TAA288. The table above lists all genes of interest in the 5p15 genomic interval, according to the NCBI database. The location of two microsatellite markers flanking this region is also shown to clarify genomic context.

Targeted Gene Sequencing of TAA288

We observed no novel alterations in the DNA sequences obtained from affected TAA288 members within the genes *SEMA5A*, *IRX1*, *PDCD6* or *LOC340094*. We documented known population variants observed from these efforts but no variants within these four genes were considered for further analysis. Further sequencing of *PDCD6* and *SEMA5A* was discontinued when the TAA288 critical interval, defined by microsatellite genotyping, was observed to exclude the genomic regions encompassing these genes.

We observed novel genetic alterations in three genes; *KIAA0947*, *FLJ33360*, and *ADAMTS16* (Table 3.3). Of these novel variants, we chose to further characterize novel alterations meeting two criteria: complete segregation with the disease phenotype of TAA288 to confirm the variant on the haplotype associated with disease, and low frequency of the variant in controls. Several novel point alterations were observed in *KIAA0947*, but were also observed in unaffected spouses of TAA288 and thus not characterized further. A novel alteration in *FLJ33360* was observed in one affected member of this family, but was not in any other affected members; it was not characterized further. We observed three novel point alterations in *ADAMTS16* located in intron 13, intron 20, and in the 3'UTR of this gene. The 3'UTR alteration was observed in an unaffected spouse of this family and not characterized further. The intron 20 variant of this gene we observed was novel at the time of sequencing but did not fully segregate with the disease phenotype of TAA288, thus this variant was not located on the affected haplotype. This point alteration was later characterized as the population variant rs57416330 in subsequent updates to reference databases.

Gene Name	Gene Context	Physical Coordinates	Population Allele	Type	Genotyping Results		
					Patient 1	Patient 2	Control
KIAA0947	Intron 12	5: 5,510,392	C	Indel	-/C	-/C	-/C
	Intron 12	5: 5,510,393	T	Indel	-/T	-/T	-/T
	Intron 18	5: 5,540,037	T	SNP	TA	TA	TA
ADAMTS16	Intron 13	5: 5,237,001	G	SNP	GA	GA	GG
	Intron 20	5: 5,306,548	A	SNP	AG	AA	AA
	3' UTR	5: 5319983	T	SNP	TA	TA	TA
FLJ33360	3' UTR	5: 6,312,606	C	SNP	CT	CC	CC

Table 3.3: Novel Sequence Alterations Observed in TAA288. The table above briefly summarizes the location of novel genetic alterations detected within the TAA288 family, with altered alleles marked in red. All novel alterations were point-alterations, and found in three genes. No alterations were found the amino acid coding sequences. The novel alterations in KIAA0947 and the ADAMTS16 3'UTR were immediately detected in control DNA samples. The novel alteration in FLJ33360 did not segregate with the disease phenotype, as it was not found in patient 2; the pattern was observed for the intron 21 alteration of ADAMTS16. Only the ADAMTS16 intron 13 alteration was observed in both patient samples, and not the control sample sequenced.

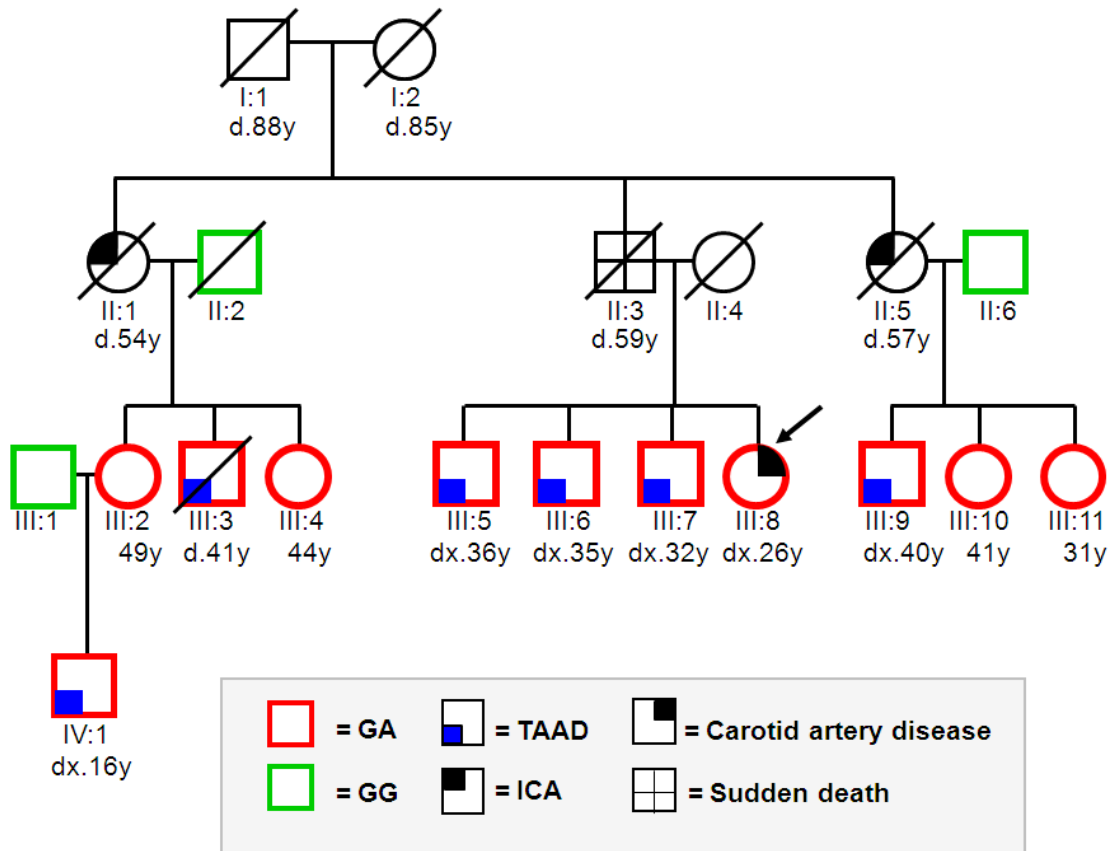


Figure 3.6: Segregation of ADAMTS16 Intron 13 Variant rs72647757 within TAA288.

Individuals denoted in green carry the heterozygous altered allele located in intron 13 of ADAMTS16 (rs72647757). This alteration is found in all affected individuals, and some unknown status individuals. Note that individuals III:14 and III:12 have not undergone thoracic or cranial imaging, and may carry undetected aneurysms. This alteration was initially investigated a possibly disease causing genetic variant due to the observed pattern of inheritance in this family. It was later added to the dbSNP online database, described as a rare population variant.

The intron 13 alteration we observed in *ADAMTS16* (initially novel) segregated with the disease phenotype of this family, and was not observed in the unaffected spouses of this pedigree (Figure 3.6); this was the only sequence alteration we observed to fulfill both of our criteria. The common allele of this point alteration is a single guanine residue, which is changed to an adenine in the rare form (wildtype genotype: GG; altered genotype: GA). Like the intron 20 alteration, this variant was not found in any population polymorphism databases during initial sequencing efforts, but was later reported as the population variant rs72647757. However, given the novel status of this variant at the time of discovery, we proceeded to characterize this variant (rs72646657) in other disease population strata.

Population Strata Analysis of rs72647757

We first characterized the frequency of the rare allele of rs72647757 in our own Caucasian control cohort, observing 5/916 altered chromosomes in this population. Later, the NCBI dbSNP reported a frequency of 3/184 altered chromosome in a separate Caucasian population cohort. A distinction was made between these two control groups when comparing to disease populations, and they were also analyzed as a combined control cohort (Table 3.4).

We sequenced rs72647757 in several disease cohorts: sporadic TAAD, sporadic ICA, familial TAAD, familial ICA, and familial TAAD/ ICA (Table 3.4). The rare allele of this variant was detected in 2/152 chromosomes from patients having sporadic ICA, and 3/308 chromosomes from patients having sporadic TAAD. We also pooled these two sporadic disease strata to form a Total Sporadic group (5/460), for separate analysis. The rare form of

Disease	Altered Chromosomes	Percent Altered	Fisher's Exact Test (p value)		
			vs Milewicz Controls	vs NCBI Controls	vs Total Controls
Sporadic ICA	2/152	1.31 %	0.2644	0.5907	0.3497
Sporadic TAAD	3/308	0.97 %	0.3273	0.4047	0.4463
(Total Sporadic)	5/460	1.09 %	0.2168	0.4146	0.3321
Familial ICA	2/90	2.22 %	0.1269	0.5331	0.1752
Familial TAAD	3/110	2.73 %	0.0472*	0.4070	0.0735
Familial TAAD & ICA (co-occurrence)	2/36	5.56 %	0.0283*	0.1991	0.0407 *
(Total Familial)	7/236	2.97 %	0.0048*	0.2966	0.0097 *
Milewicz Controls	5/916	0.55 %			
NCBI Controls	3/184	1.63 %			
(Total Controls)	8/1100	0.73 %			

Table 3.4: Rare rs72647757 Allele Compared in Aneurysm and Control Populations.

Sporadic patients were defined as having no other first degree relatives with vascular disease; only one member of each pedigree (proband) was sequenced to represent the inherited disease population. It should be noted that clinical information was not available for the NCBI controls. Sporadic aneurysm populations were subdivided into ICA and TAAD occurrence and analyzed separately. A similar analysis was performed on the inherited form of disease. Statistically significant p-values are denoted with an asterisk.

this variant was also observed in probands from families with inherited TAA (3/110), ICA (2/90), and co-occurrence of TAA/ICA (2/36); as with sporadic disease, we also pooled familial strata into a Total Familial group (7/236). Statistical analysis of allelic association revealed a significant association between the rare allele of rs72647757 in the familial TAA strata compared to the Milewicz-only control group ($p=0.0427$) (Table 3.3). Significant association of this allele was also observed in the combined familial disease strata compared to both the Milewicz-only ($p=0.0048$) and NCBI-Milewicz pooled control groups ($p=0.0097$). For sporadic aneurysms, no significant association of this allele was observed compared to either control group.

Segregation of rs72647757 With Inherited Vascular Disease

As previously described, the minor allele of rs72647757 was observed in a total of 7/236 probands of families having an inherited form of vascular disease, including TAA288. Each family (TAA171, TAA437, TAA259, TAA115, TAA050, CVL) was then analyzed for segregation of the rare rs72647757 allele with the disease phenotype within the family pedigree (Table 3.5). Complete co-segregation of this allele with aneurysm phenotypes occurred in two of these families: TAA171 and TAA437 (Figure 3.7). Incomplete segregation was observed in TAA050 and CVL where disease-affected members of these families did not carry the rare allele of this variant. In TAA259 and TAA115, this rare allele was observed in unaffected spouses.

Family	Individual Member Status	Altered Genotype	Notes
TAA288 ϕ	Affected: 8 Unknown: 6 Unaffected: 4 Total: 18	8/8 3/6 0/4 11/18	
TAA171 ϕ	Affected: 2 Unknown: 15 Unaffected: 4 Total: 24	2/2 7/15 0/4 9/24	Possibly 3 affected
TAA437 ϕ	Affected: 2 Unknown: 3 Unaffected: 3 Total: 8	2/2 2/3 0/3 4/8	Possibly 3 affected
CVL Ψ	Affected: 5 Unknown: 19 Unaffected: 0 Total: 25	2/4 1/19 0/0 3/25	Two affected individuals without genotype
TAA050 Ψ	Affected: 3 Unknown: 6 Unaffected: 0 Total: 9	2/3 2/6 0/6 4/9	One affected individual without genotype
TAA115 Υ	Affected: 2 Unknown: 26 Unaffected: 5 Total: 33	2/2 9/26 1/5 12/33	Possibly 3 affected individuals
TAA259 Υ	Affected: 4 Unknown: 44 Unaffected: 10 Total: 58	3/4 9/44 1/10 13/58	Possibly 2 more affected Need to re-genotype

ϕ = Segregation With Disease, Absent From Unaffected Members
 Ψ = Not Observed in Both Affected Patients
 Υ = Observed in Unaffected Members

Table 3.5: Occurrence rs72647757 Minor Allele within Pedigrees having Inherited

Vascular Disease. The probands from these families were initially sequenced in an effort to characterize the prevalence of this rare allele in the inherited vascular disease population.

The other members of each family were then sequenced, in order to investigate the segregation of this allele with the disease phenotype within each pedigree.

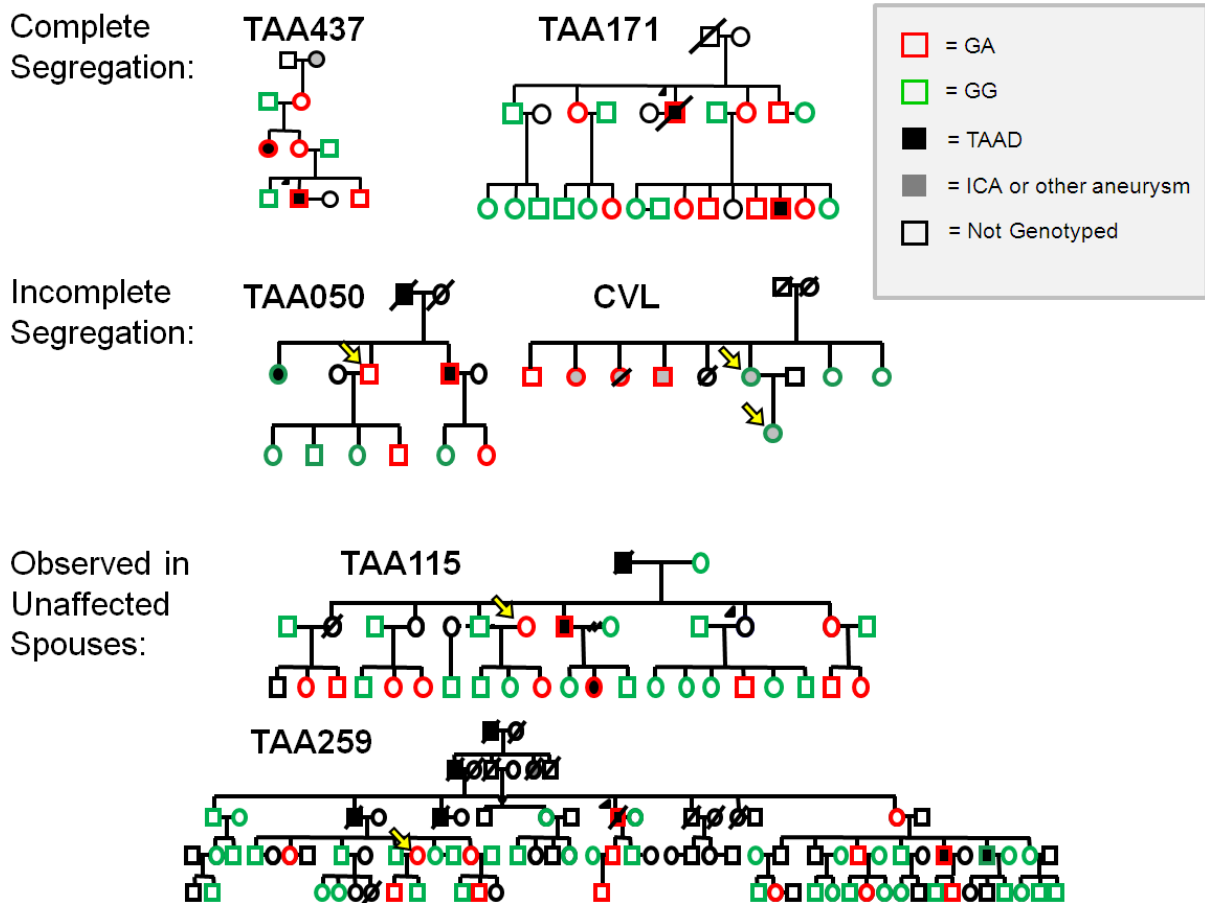


Figure 3.7: Segregation of rs72647757 Minor Allele within Pedigrees having Inherited Vascular Disease. In total, complete segregation of the rs72647757 minor allele was observed in three pedigrees: TAA288 (shown in figure 3.6), TAA437, and TAA171. Incomplete segregation was observed in two pedigrees: TAA050 and CVL. Here, affected members do not carry the minor allele, as indicated with yellow arrows. Finally, unaffected spouses were observed to carry the minor rs72647757 allele in two pedigrees: TAA115 and TAA259.

Other ADAMTS16 Targeted Sequencing

The updated status of rs72647757 as a population variant prompted the sequencing of other conserved regions of ADAMTS16, with the intention of observing a disease causing alteration closely linked to this rare population variant. Introns 12, 13 and 14 of this gene were sequenced due to their physical proximity to rs72647757 but we detected no novel variants in these introns. We are also sequencing the promoter region of ADAMTS16, not yet observing any novel sequence variants within the genomic regions ~1800 bp 5' to exon 1 of this gene.

CNV Detection in TAA288

In addition to DNA sequencing, we sought to identify novel large genomic CNV events which may not be detectable by our sequencing methods, or may reside outside the TAA288 critical interval. Genomic CNV analysis of III:5 on the Illumina 610-quad platform indicated the presence of seven genomic CNVs on six different chromosomes. None of the events were novel, but we investigated a genomic deletion event reported on Chromosome 5 in close proximity to the TAA288 critical interval (Table 3.6). We attempted to verify this deletion by genotyping known population polymorphisms within the alleged deletion interval indicated by this platform: chromosome 5p: 7,230,740-7,246,456 (GRCh37/hg19). For this analysis, we genotyped patients III:5 and III:4 at loci containing known population variation using our bidirectional sequencing methods, and observed heterozygous genotypes in both patients at the marker rs4355490, located at within the alleged deletion on chromosome 5p:

7,235,186 (GRCh37/hg19). Thus, we did not attempt to characterize this genomic deletion event any further.

PennCNV					
Chr	Start	End	Size	Value	Confidence
1	103921620	104091739	170120	3	126
4	162172873	162221357	48485	3	26
5	7230740	7246456	15717	1	16
11	51204244	51219066	14823	3	34
17	20651	31586	10936	3	32
17	31469658	31506122	36465	3	16
19	1088304	1103656	15353	3	20

CNVP					
Chr	Start	End	Size	Value	Confidence
1	103907158	104091739	184581	3	154
4	162164752	162223074	58322	3	100
5	7230740	7246456	15716	1	53
11	51204244	51219066	14822	3	56
17	20651	31497	10846	3	65
17	31469658	31505872	36214	3	73
19	1088823	1202115	113292	3	51

Table: 3.6: CNV Events in TAA288 Detected by Both PennCNV and CNVP

Algorithms. The table above lists all CNV events detected by both the PennCNV (left) and CNVP (right) algorithms. The “value” column describes the number of genomic copies predicted at that interval, with 2 copies being the wildtype. “Confidence” describes the numbers of SNP markers within the CNV event. All of these events are reported in the CHOP reference database.

3.3 Transcript and Protein Level Analysis of ADAMTS16 Results

Detection of ADAMTS16 Protein in Aneurysm Tissues

In order to determine if ADAMTS16 is expressed in aneurysm tissues, we sought to observe the levels of this protein using immunohistochemical detection methods on several paraffin-embedded human aortic tissue samples. Compared to four controls (MG8978, MG8453, MG7751, and MG2954), we observed increased ADAMTS16-positive staining in two patients with TGFBR2 mutations (MG1606, MG2785) and two patients with Marfan Syndrome (MG3631, MG4520) (Figures 3.8, 3.9). We also performed this procedure on an aneurysm patient with a mutation in the *MHY11* gene and a patient with a mutation in *ACTA2*, but we did not observe a similar elevated protein level in these two patient types.

Alternative Splicing of ADAMTS16 Exon 14

The variant rs72647757 was initially ascertained as a novel, disease-segregating genetic alteration, and is located in intron 13 of ADAMTS16 81 bp 5' to the start of exon 14. Several alternative transcripts of ADAMTS16 had been reported at the time of this study, including one lacking exon 14 reported in the hippocampus (ADAMTS16-005 (ENST00000513709)); deletion of this exon results in a downstream frameshift generating an in-frame stop codon "TGA" in the 5th codon downstream of exon 13. Given the proximity of rs72647757 to an alternatively spliced exon, we investigated the potential role of this rare variant in the splicing of *ADAMTS16* exon 14.

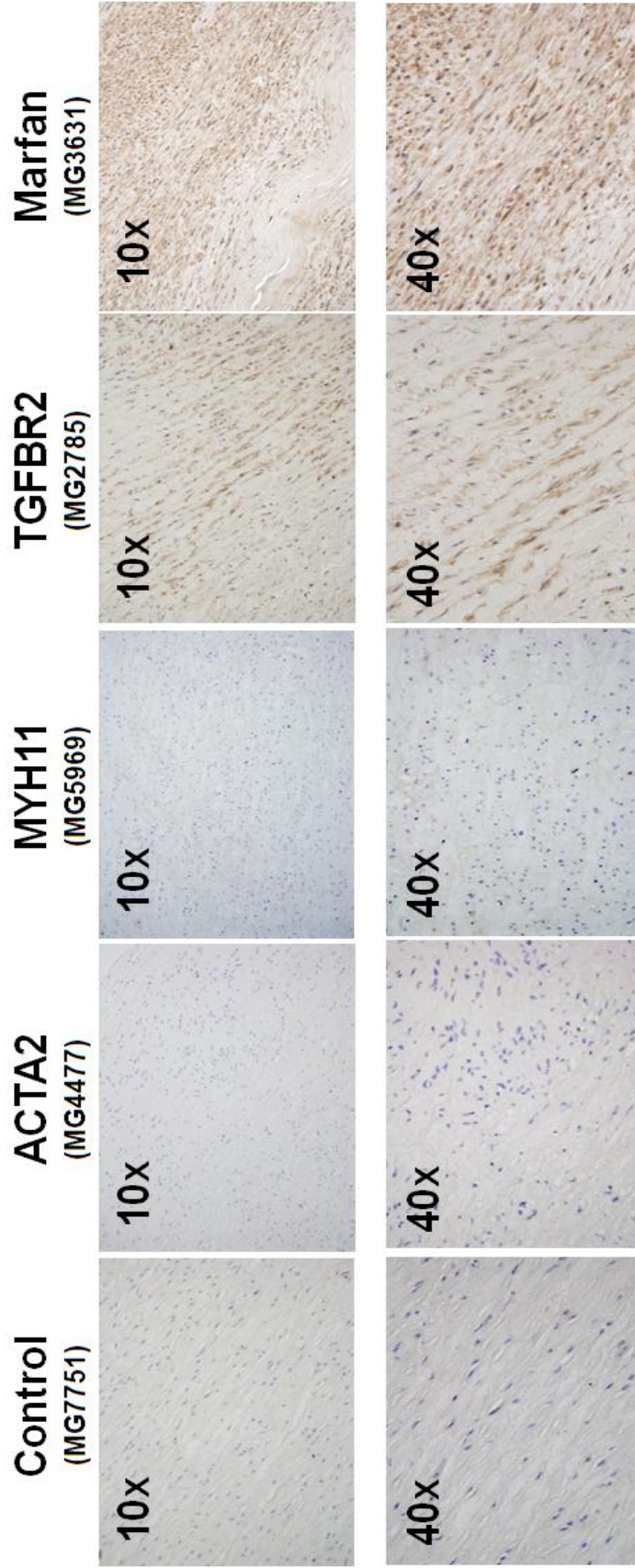


Figure 3.8: Immunohistochemical detection of ADAMTS16 in Aortic Media. Here, we used an antibody raised against a C-terminal epitope fragment of ADAMTS16. A brown color indicates a positive stain, and nuclei are shown in blue. We observed increased levels of what appears to be a cell-specific staining in TGFBR2 mutants and patients with MFS.

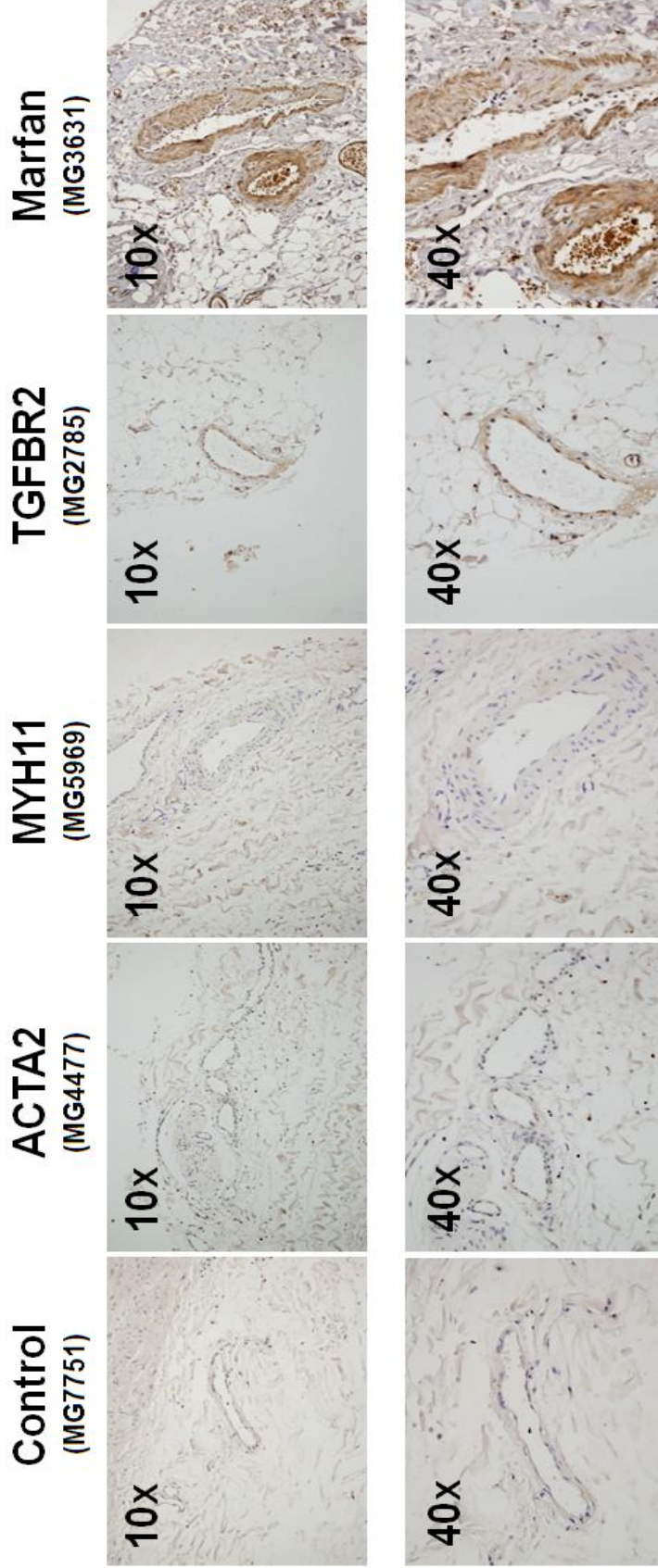


Figure 3.9: Immunohistochemical detection of ADAMTS16 in Aortic Adventitia. Again, we used an antibody raised against a C-terminal epitope fragment of ADAMTS16. A brown color indicates a positive stain, and nuclei are shown in blue. Once again, we observed increased levels of what appears to be a cell-specific staining in TGFBR2 mutants and patients with MFS. In this arterial layer, we were interested in the *vasa vasorum*, which are smaller blood vessels supplying nutrients to the outer portions of the aortic wall. These smaller vessels have similar structure to the cranial arteries which we were not directly available for our studies.

We performed PCR to amplify a fragment of the *ADAMTS16* gene transcript immediately proximal to exon 14. Here, we expected a fragment size of 488 bp from a full-length amplicon, and 357 bp from a fragment with exon 14 deleted. We amplified the *ADAMTS16* transcript from total RNA isolated from two different dermal fibroblast control cell lines (MG3007, MG3002) differentiated into myofibroblasts by TGF- β 1 treatment, as described earlier. In this experiment, two sets of parallel time points were harvested: one receiving TGF- β 1 treatment and the other remaining in media without receiving this cytokine; specific time points were 0 hr, 48 hr \pm TGF- β 1, 72 hr \pm TGF- β 1. After PCR amplification using oligonucleotides annealing exons 12 and 16 of *ADAMTS16*, we observed a band of approximately 488bp in all samples receiving TGF- β 1 treatment (TGF- β 1 +). DNA sequencing also verified that these bands were from the correct region of the *ADAMTS16* transcript (Figure 3.10).

We then cultured fibroblast cells explanted from the TAA288 patient III:5 for a similar analysis. An additional time point was harvested for this experiment 24 hrs after TGF- β 1 treatment. Unlike the control samples, our PCR reaction amplified fragments of approximate size 488 bp and 357 bp at all time points tested regardless of TGF- β 1 treatment from patient III:5 (Figure 3.10). No bands were at the 357 bp length were observed in control samples MG3002 or MG3028.

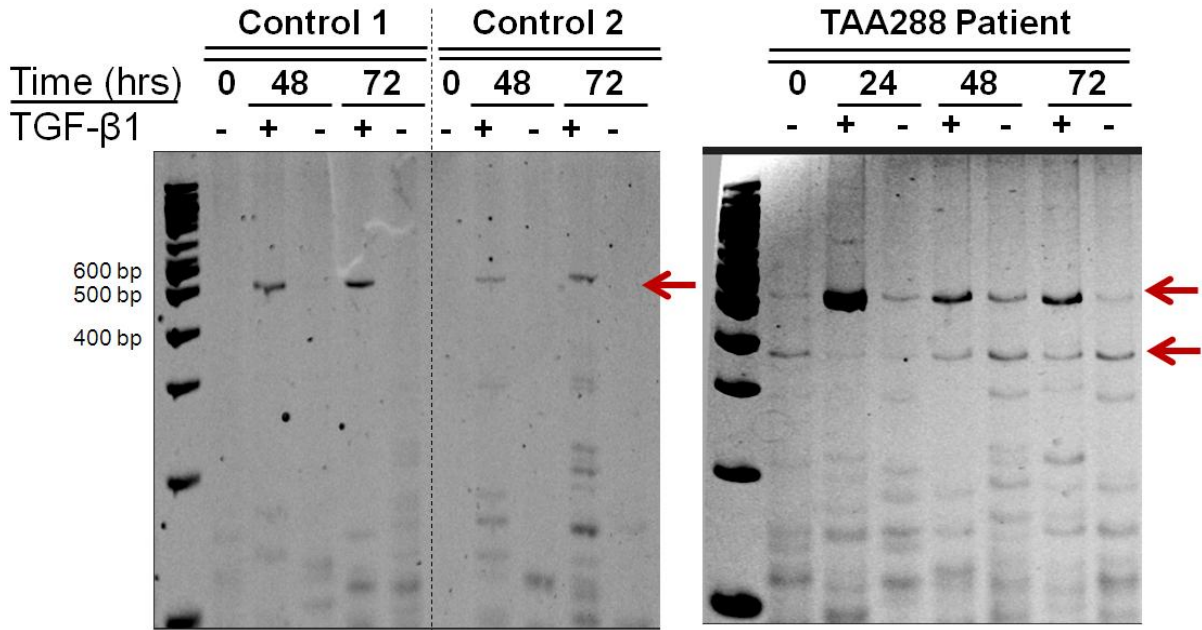


Figure 3.10: Amplification of ADAMTS16 Transcript from Patient and Control Fb Cells. Depicted are polyacrylamide gels visualizing PCR products of ADAMTS16 exon12/16 annealing primers. Here, we expect a fragment 188bp in size from a full length fragment, and 357 bp from a transcript lacking exon 14. On the left, we observed a 488 size fragment in two control samples 1 (MG3002) and 2 (MG3028) in samples treated with TGF- β 1. The gel on the right displays PCR fragments amplified from TAA288 patient III:5. In this patient, we observe a fragment of size 488 and 357 bp in all samples regardless of TGF- β 1 treatment.

qPCR of ADAMTS16 Transcript in Cultured Cells

We performed quantitative real-Time PCR (qPCR) to detect the relative levels of mRNA transcript in fibroblasts receiving TGF- β 1 treatment. As with our analysis of alternative splicing, this analysis was performed on cDNA synthesized from total RNA harvested at specific time points after fibroblasts were exposed to TGF- β 1 in supplemented media. For this analysis, we used a fluorescent probe designed to bind the exon 17-18 junction of the *ADAMTS16* transcript (Taqman probe: Hs01046723) of the *ADAMTS16* transcript.

We used three fibroblast control cell lines for this experiment (MG3000, MG3007, MG3029), which were closely matched to TAA288 patient III:5 by race, gender, and ethnicity. These three control cell lines were grown in parallel with two fibroblast cell lines from TAA288 patients III:5 and IV:1. Cells for this experiment were harvested at five time points (0, 6, 12, 18, 24, and 48 hours) after TGF- β 1 treatment, and all $\Delta\Delta$ CT values were normalized to control MG3000 at 0 hrs. Elevated levels of *ADAMTS16* transcript were observed in all three control cell lines starting 12 hours after TGF- β 1 treatment, and remained significantly elevated compared to their zero hour time point (Figure 3.11).

A statistically significant deviation from the control cell lines was observed in TAA288 patient IV:1 cells at the 12 hr time point ($p=0.0025$) following TGF- β 1 treatment (Figure 3.12). A significant deviation from the controls was observed in sample III:5 at the 18 hr ($p=0.0001$) and 24 hr (0.0023) time points. We performed this experiment several times (data not shown) and consistently observed significantly elevated levels of *ADAMTS16* transcript in the TAA288 patient cell lines treated with TGF- β 1. Though the

specific temporal pattern varied, we consistently observed fibroblasts cultured from affected members of TAA288 to express elevated levels of ADAMTS16 transcript in at least one time point following TGF- β 1 per experiment. Thus we decided to investigate whether this upregulation was also observed in protein harvested from these cells.

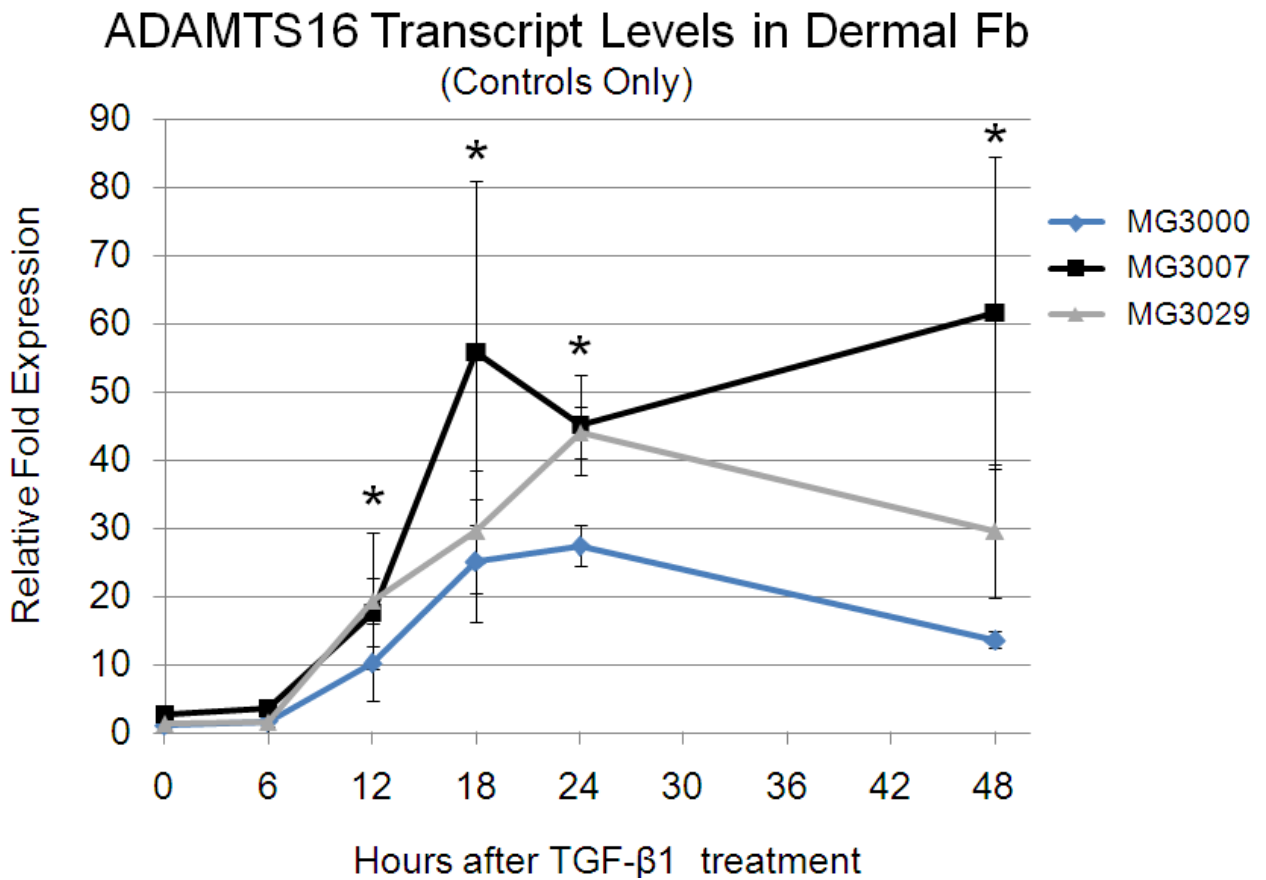


Figure 3.11: ADAMTS16 Transcript Levels in Control Fibroblasts Treated with TGF- β 1. We observed elevated transcript levels on all three controls from 12-48 hours after receiving TGF- β 1 treatment. MG3007 has a slightly different temporal pattern from the other two controls, indicating that some baseline variation of this gene expression exists within control populations.

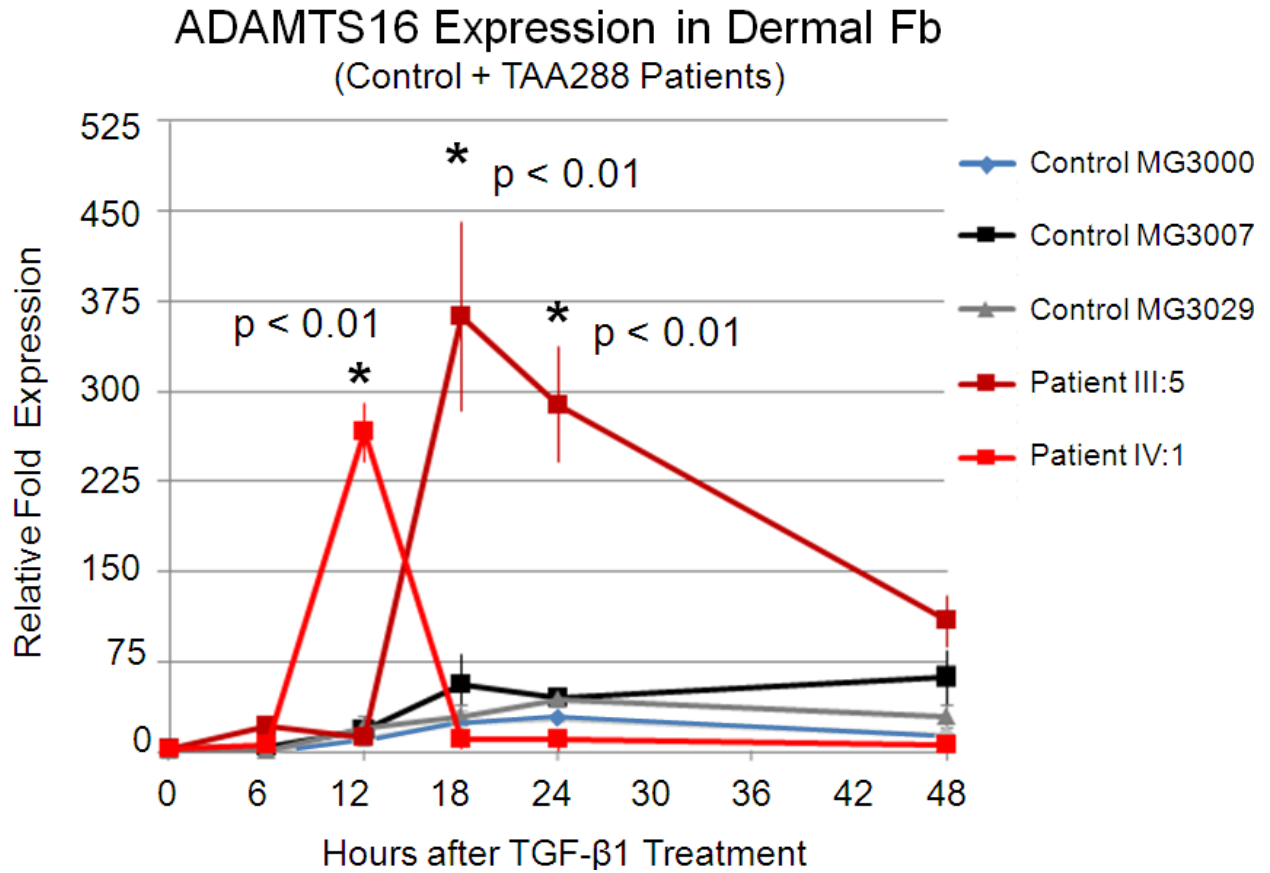


Figure 3.12: ADAMTS16 Transcript Levels in TAA288 Patient and Control

Fibroblasts Treated with TGF-β1. Here, we compare the ADAMTS16 transcript levels between two TAA288 Patients and the same set of three controls in Figure 3.11. These five cell lines were all grown in parallel and subjected to the same TGF-β1 protocol. Elevated levels of ADAMTS16 transcript were observed in patient IV:1 at 12 hrs after treatment, but quickly returned to baseline. Elevated levels of ADAMTS16 transcript were observed in patient III:5 at 18 and 24 hours after treatment compared to all three controls.

Immunoblotting of ADAMTS16 Protein

The expected full-length protein product of ADAMTS16 is 1224 aa, with a predicted mass of 130 kD, not accounting for post-translational modification. For our initial characterization, we used the antibody sc-67440 (Santa Cruz) diluted 1:500 according to the manufacturer's recommendation. Sc-67440 is a rabbit polyclonal antibody raised against an epitope within the range of ADAMTS16 amino acids 986-1060 (exons 19-21) near the C-terminus of ADAMTS-16. As with our analysis of splicing, we first sought to observe the expression of this protein in control samples.

We observed increased mRNA levels of ADAMTS16 in TAA288 patients at time points ranging from 12-48 hours after treatment with TGF- β 1. We expected that protein accumulation would be evident at time points following the observed upregulation of gene transcript. Thus, we harvested protein from TGF- β 1-treated fibroblast lysates at time points 0, 24, 48, and 72 hrs following treatment. For this analysis, we again used MG3002 as a fibroblast control, and VSMC cells from three healthy individuals (MG8131, MG8438, and MG8458) were also used. Our initial immunodetection assay in these controls using antibody sc-67440 revealed a doublet of bands at approximately 130 kD in all samples (Figure 3.13). In the fibroblasts from control MG3002, the relative intensity of the 130 kD band appears to increase slightly at the 24 hr time point following TGF- β 1 treatment.

We also detected a band approximately 150kD in size, which was more prominent in the VSMC lysates. However, when we compared our results to previously published studies of this gene, we observed a similar 150 kD band in their negative control for ADAMTS16 [139]. Therefore, we interpreted our observed 150kD band as nonspecific.

We next observed this protein in fibroblasts cultured from TAA288 patient III:5 in order to make direct comparisons with control MG3007. Here, we harvested samples at additional time points to increase temporal resolution of expression leading up to the first 24 hrs after TGF- β 1 treatment, due to the variable gene expression we previously observed in patient cells (Figure 3.12); we harvested these samples from the 0, 6, 12, 24, 48, and 72 hr time points post TGF- β 1 treatment. Immunostaining with anti-ADAMTS16 antibody sc-67440 detected prominent bands at 130 kD in the patient and control samples. These bands stained more intensely in the patient compared to the control (Figure 3.14). However, we also observed a similarly increased intensity in our immunodetection of the protein GAPDH, which we performed as a protein loading control. This suggests that more total protein was loaded in the TAA288 samples, but we were unable to repeat this experiment due to apparent degradation of our total cell lysates.

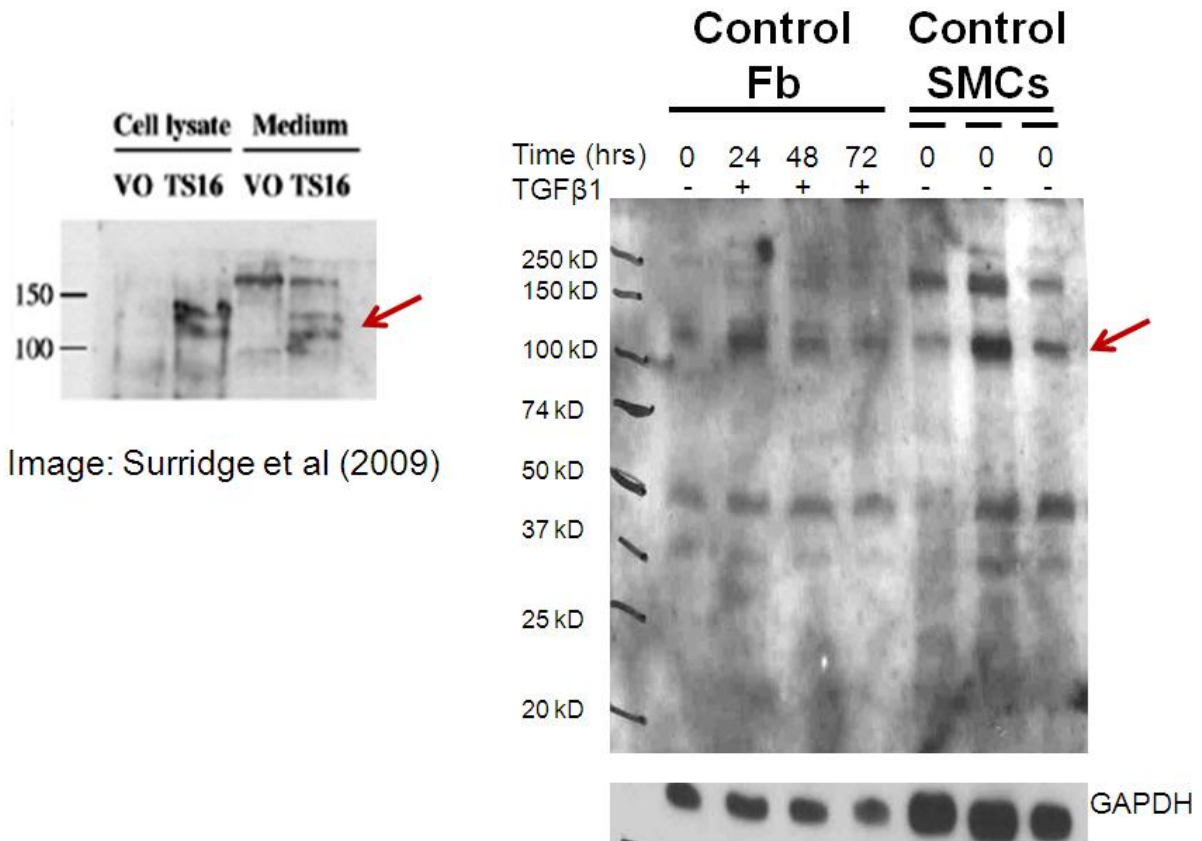


Image: SurrIDGE et al (2009)

Figure 3.13: Immunoblot of Cultured Control Lysates Compared to SurrIDGE et al.

Left image: SurrIDGE et al, α -Flag shown, later verified with α -ADAMTS16 (not shown).

The 130 kD doublet is consistent with the expected size of ADAMTS16. The 150 kD band is not identified, but is present in the media of their vector only (VO) negative control as well as their ADAMTS16 (TS16) over-expressing cell line. Right top image: α -ADAMTS16 (sc-67440), 1:500. Right bottom image: α -GAPDH, 1:20,000 as a loading indicator. The control cell line used for this experiment was MG3002. The three SMC control cell lines are MG8131, MG8438, and MG8458 from left to right.

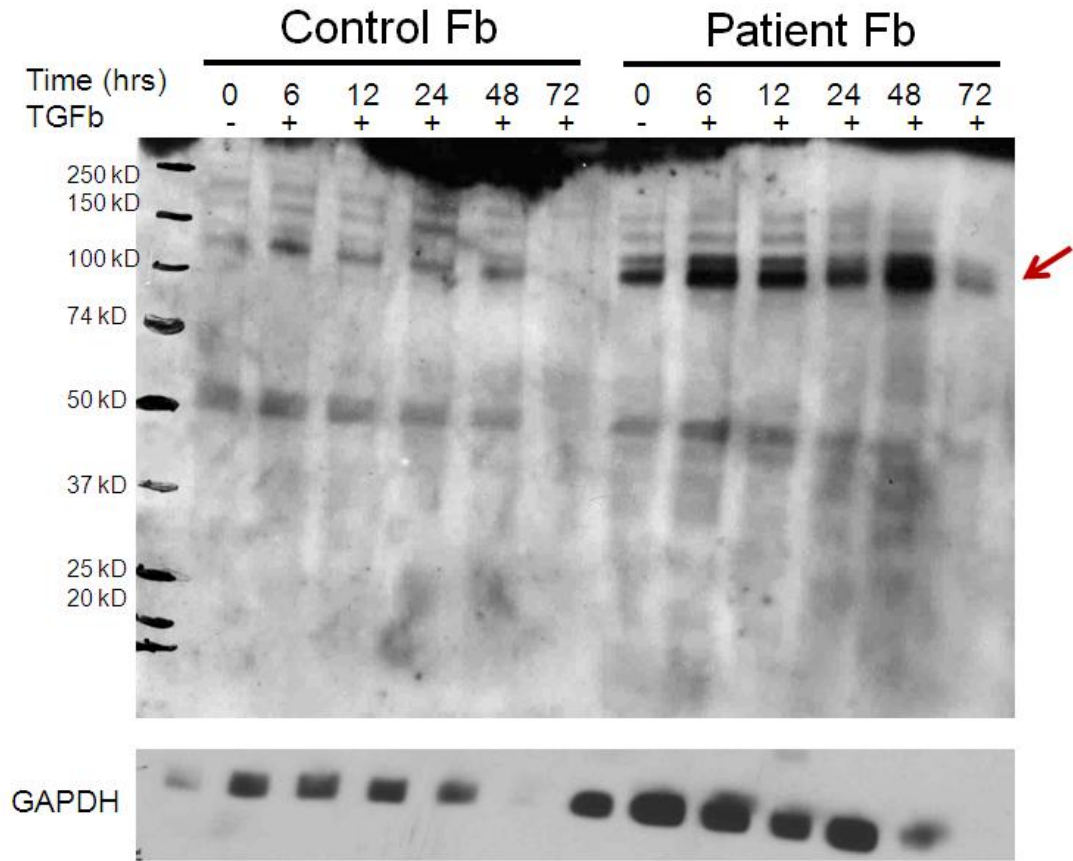


Figure 3.14: Immunoblot of Cultured Control and TAA288 Patient Fb Lysates. Top image: α -ADAMTS16 (sc-67440), 1:500. Bottom image: α -GAPDH, 1:20,000. In this blot, we see increased immune signal at a size consistent with ADAMTS16 full length protein (130kD), though we also see a similar increase in the loading control GAPDH. The patient cell line for this experiment was III:5, and the control cell line was MG3007.

CHAPTER 4: DISCUSSION

4.1 Selection of ADAMTS16 Candidate Gene

Our genome-wide linkage analysis did not reveal any genomic loci with strong evidence of linkage, as denoted by a LOD score of 3.0 or greater. This was surprising, given the size of the pedigree and the number of informative meioses we could infer. However, the 5p15 genomic interval was the most strongly linked genetic interval in this family. We also observed evidence of linkage to this region in two other pedigrees with similar inherited phenotypes (Figure 3.5). Thus, the location of ADAMTS16 within this genomic interval prompted our investigation of this gene as a potential cause of disease in the TAA288 family.

In addition, our initial ascertainment of the *ADAMTS16* rare variant rs72647757 in this family was intriguing given that it was not in any reference databases at the time. It was also not observed in the first 376 Caucasian control chromosomes we sequenced. With these initial observations, and the segregation of this variant with the disease phenotype of TAA288, we initially considered rs72647757 a strong candidate for the disease-causing alteration in this family. However, there were two observations which caused us to redirect our investigation rs72647757: The first was the frequency of this variant in the general population (0.73%, n=1100), and the second was the incomplete segregation of this allele in several pedigrees with inherited aneurysms. Neither of these observations support our initial hypothesis of rs72647757 as the primary disease-causing variant in TAA288, so we shifted our consideration of this variant from disease-causing to a disease-associated variant closely linked to a cryptic causal mutation. In hoping that the causal mutation was closely linked to this variant, we sequenced introns 12, 13 and 14 of ADAMTS16 but did not detect novel disease-segregating alterations within the DNA sequence of these introns.

4.2 ADAMTS16 in Aneurysm Tissues

ADAMTS16 in TGFBR2 Mutation and Marfan Syndrome Tissues

We observed an increase of ADAMTS16 immunosignal in aortic tissues from two patients with MFS and two patients with TGFBR2 mutations (one of each shown). Our observations of ADAMTS16 expression in these particular aneurysm patients were intriguing for two reasons. First, it verified that ADAMTS16 was present in diseased arterial tissues from aneurysms. This upregulation was observed in both the aortic media, and in the smaller *vasa vasorum*, which we used as an approximation to muscular arteries; intracranial artery tissue was not available from these patients for direct immunohistochemical detection. Second, patients with mutations in TGFBR2 and MFS both are thought to have dysregulation of TGF- β signaling [140;141]. Since expression of ADAMTS is induced in fibroblast cells treated with this cytokine, this provided additional evidence that ADAMTS16 may be involved with a pathway already implicated in the development of inherited aneurysms.

We did not observe a similar increase in ADAMTS16 protein levels in aortic tissues from patients with *MHY11* and *ACTA2* mutations. This suggests that ADAMTS16 is not upregulated in all aneurysm tissues; rather it is only increased in patients with mutations affecting the TGF- β signaling pathway.

ADAMTS16 Expression in TAA288 Patient Fibroblast Cells

We had two important observations of ADAMTS16 transcript levels in the TAA288 patient cell lines. The first was an apparent abundance of a gene transcript skipping exon 14 (Figure 3.10). This was especially interesting to us initially, since the rare variant is

rs72647757 is located in intron 13 of *ADAMTS16*, and mutations in intronic sequences can cause skipping of adjacent exons from mRNA transcripts [142]. In addition, this variant is located 81 bp from the 5' start of exon 14, and RNA splicing elements have been observed as far as -273 bp 5' to target exons [143]. However, we decided not to directly explore this possibility after ascertaining the rs72647757 variant in our control population. Thus, we cannot say whether the increased deletion of exon 14 in TAA288 patient cells is directly due to this variant, or an undetected distal mutation.

We next observed increased relative levels of *ADAMTS16* transcript in TGF- β treated cells from TAA288 patients compared to controls (Figure 3.12). Our qPCR detection methods consistently detected a significant difference between the TAA288 patient cell lines and controls, though the specific time point of this difference varied between experiments. However, even our control samples varied with respect to each other, suggesting that there are small baseline fluctuations in the expression of this gene in individuals without aneurysms.

Since we hypothesize that the source of disease in the TAA288 family is due to a common inherited mutation, the increased levels of *ADAMTS16* transcript we observed could result from a mutation leading to either over expression of this gene or from a mutation affecting transcript stability. Since we could not distinguish between these two sources using our qPCR analysis, we decided to consider both options. Thus, we sequenced the ~1800 bp promoter region [144] and the 3' UTR of *ADAMTS16*. We did not detect any novel variants in the promoter region of this gene, but we detected a novel point alteration in the 3'UTR of this gene. However, that alteration was immediately observed in the first unaffected control sample we sequenced, and was not characterized further.

4.3 Possible Function of ADAMTS16

Activation of ADAMTS16 by TGF- β Signaling

The initial binding of TGF- β ligand to the extracellular domain of receptors initiates the canonical Smad-dependant signaling of this cytokine in fibroblast cells. This initial wave of signaling causes the cell to upregulate the expression of matrix proteins and integrins within 12 hours of ligand binding. Two observations indicate that ADAMTS16 is first activated through this canonical Smad signaling pathway. The first is that we first observed a significant upregulation of ADAMTS16 gene transcript at 12 hours after TGF- β treatment in our control fibroblasts. The timing of the ADAMTS16 transcript elevation is consistent with the timing of the upregulation of matrix components by TGF- β treat fibroblasts, such as collagen and fibronectin. Other members of the *ADAMTS* gene family are co-expressed with collagen isoforms, so the secretion of ADAMTS16 at this stage is also plausible [145]. The second observation implicating ADAMTS16 as a downstream Smad target is the presence of Sp1 and Egr1 transcription factor binding motifs in the promoter of this gene [146]. These factors can both bind Smad proteins, and are both implicated in the TGF- β induced upregulation of the ECM protein collagen [147;148].

There is also a “delayed” component of TGF- β signaling that is focal adhesion and integrin dependant. This secondary signal is necessary for the sustained maintenance of the myofibroblast phenotype, and begins 48 hours after initial ligand binding. Given that we observed significantly elevated ADAMTS16 transcript in our control cells from 12-48 hours after exposure, it is possible that this protein is also secreted and plays a role in this secondary wave of adhesion dependent signaling. However, it is difficult to elucidate the specific role of this protein without knowing its target substrate.

Potential ADAMTS16 Gene Functions

Though it is difficult to predict the function of a protease without knowing its substrate, we can predict the role of ADAMTS16 by the timing of its expression in fibroblasts treated with TGF- β . If this protein is initially expressed by Smad-dependent signaling induced by this cytokine, it may be secreted by cells along with collagen, fibronectin, integrins, and other ECM components. It is already known that some members of the ADAMTS gene family can modify ECM precursors into their mature active form [149], and ADAMTS16 may perform a similar function within this context. Appropriate binding of certain integrins to ECM proteins may require prior modification by ADAMTS16 metalloproteinase activity. Thus, ADAMTS16 proteinase activity may have implications in initiating the “outside-in” adhesion-dependant signaling pathway needed to sustain the myofibroblast phenotype.

We can also attempt to infer function from the location of this protein. ADAMTS16 contains several C-terminus thrombospondin type-1 repeats. Thrombospondins are adhesive glycoproteins known to mediate both intercellular and cell-matrix interactions [150]. In addition, thrombospondin-1 can mediate the release of latent TGF- β from the LAP [151]. Presuming that the TSP type-1 repeats on ADAMTS16 localize this metalloproteinase to thrombospondin-1, this would place it in a context to have implications in regulating TGF- β bioavailability. Other members of the ADADMTS gene family may have similar roles in regulating cytokine availability. Researchers have revealed evidence that ADAMTS10 can bind fibrillin, which sequesters the latent TGF- β within the LAP [152]. Given that members of the ADAMTS gene family can share functions [153;154], it is possible that these two proteins both have implications in regulating the bioavailability of this cytokine in the ECM.

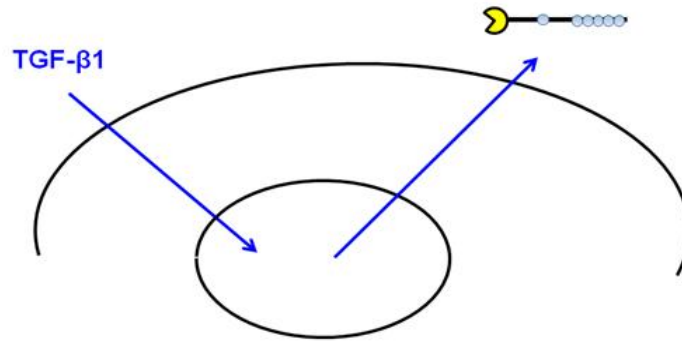
Potential Role of ADAMTS16 in TAA288 Pathology

Using the myofibroblast model system, we observed an increased deletion of exon 14 from *ADAMTS16* in TAA288 patient fibroblasts, independent of TGF- β treatment. We currently do not know if this increase in exon 14 deletion in the TAA288 family is due to the intron 13 variant rs72647757 or another undetected mutation. It is possible that the variant rs72647757 does indeed affect splicing of *ADAMTS16* exon 14 but is not enough to cause disease on its own. This would mean that the hyper-responsiveness of TAA288 cells to TGF- β serves as a “second hit” which only causes disease when coupled with the abnormal splicing we observed.

A protein generated using the shortened transcript (truncated at exon 14) would lack C-terminal motifs, such as the thrombospondin type-1 repeats thought to localize this protein to its target substrate in vivo. The metalloproteinase domains of *ADAMTS16* are located at the N-terminus of this protein and would not be affected by truncation at exon 14. Thus, we hypothesize that this truncated protein isoform could carry out non-specific protease activity within the ECM. This increase in nonspecific protease activity coupled with a hyper-expression of this gene in response to TGF- β leads to the aneurysm phenotype within TAA288 patients. This abnormal protease activity could lead to a dysregulation of latent ECM cytokines, or a disruption of adhesion-dependant outside-in TGF- β signaling requiring proper formation of focal adhesions.

**Normal ADAMTS16
Context:**

- Proper ECM localization
- Targeted degradation of ECM Products
- Normal gene function



TAA288 Family:

- **Increased** total protein
- **Increased** truncated variant
 - **Improper** ECM localization
- **Untargeted** degradation of ECM products
- Increased, unspecific activity → **Aneurysm**

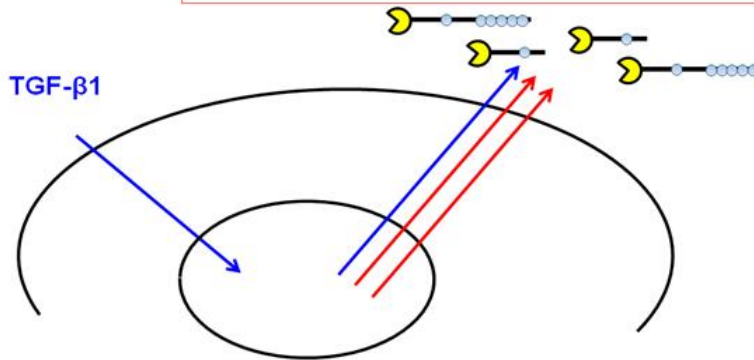


Figure 4.1: Schema of ADAMTS16 Dysregulation in TAA288 Family. The image above depicts our currently hypothesis of aneurysm formation in this family. Here, we believe that an unascertained mutation leads to both a increase in secretion of total and truncated form of ADAMTS16 into the ECM. This increase in nonspecific protease activity within the ECM contributes to the formation of aneurysms in the TAA288 family.

4.4 Future Work

Since the *ADAMTS16* intron 13 point variation rs72647757 was observed as a rare population variant, we do not believe that this variation alone is the causal mutation in the TAA288 family. Therefore, we must continue to search for a novel mutation in the TAA288 family. Potential targets include distal regulatory DNA elements, predicted to influence expression of the *ADAMTS16* gene or other genes in the 5p15 region. Of particular interest are gene silencer and enhancer motifs, as they could directly contribute to the elevated levels of gene transcript we observed. To ascertain such targets, we can utilize bioinformatic tools available on the web, available through: http://molbiol-tools.ca/DNA_Motifs.htm. These free programs can detect candidate sequences based off their species conservation and similarity to known regulatory elements.

We also need to verify our observations in patient cell lines from affected members of TAA288. Repeating the experiments we performed using the myofibroblast model is an effective way to verify that our observations are repeatable and reflect differences in biological processes and are not due to an undetected bias in the initial experiments. For these future experiments, we will also modify our protein isolation methods to better isolate matrix proteins [155]. Importantly, we also need to obtain an effective antibody targeting a C-terminal epitope of *ADAMTS16* in order to detect the isoform of this protein truncated at exon 14 that we hypothesize is contributing to the development of disease in this family.

We can also investigate the myofibroblasts from TAA288 in more detail. If *ADAMTS16* is necessary for the secondary wave of adhesion-dependant TGF- β signaling, the cells from TAA288 should not maintain the myofibroblast phenotype. We can investigate this possibility by repeating our TGF- β treatment protocol and observing the

expression of smooth muscle alpha actin, which is a marker for myofibroblast differentiation. A disruption of this process could help elucidate the role of the ADAMTS16 gene which we can use to refine our hypothesis and elucidate the role of this gene in the development of disease in this family.

Since we observed ADAMTS16 protein at elevated levels in TGFBR2 and MFS patients, it would also be interesting to investigate the role of this protein in these aneurysm types. It is not clear whether ADAMTS16 directly contributes to the development of these aneurysms, or whether the elevated protein levels we observed are merely the byproduct of TGF- β signaling defects in these patients. Other future studies of this protein could investigate the localization of this protein within the ECM, as well as identify the target substrate of this gene *in vivo*. With this knowledge, we can then begin to understand the role of this protein in TGFBR2 and MFS aneurysm tissue.

Our evidence is not complete; many questions remain and some experiments must be repeated and optimized. Despite our observations of elevated levels of ADAMTS16 transcript in fibroblasts from the patient III:5, we have not identified a genetic alteration likely to be responsible. Thus, we intend to continue sequencing the 5p15 region in this family until we uncover a strong candidate mutation. We have also not been able to confirm whether the accumulation of the protein is also increased, and will continue to improve our techniques related to the visualization of this protein on immunoblots. Currently, other members of our group are collaborating with a lab at Stanford University, learning techniques to induce the transformation of dermal fibroblasts into pluripotent stem cells which can then be transformed into VSMCs; such a model would be an improvement to the fibroblast model we have applied in this dissertation. However, we believe the work

presented in this dissertation justifies a continued investigation of the potential role of this gene in the development of the disease phenotype observed in family TAA288.

REFERENCES

- [1] Harrison's Principles of Internal Medicine, ed 17th. McGraw-Hill Companies, 2008.
- [2] Kahn RA, Konstadt S: Thoracic aortic disease: endovascular stents. *Echocardiography* 2002;19:589-597.
- [3] Aydin F: Do human intracranial arteries lack vasa vasorum? A comparative immunohistochemical study of intracranial and systemic arteries. *Acta Neuropathol* 1998;96:22-28.
- [4] Pannu H, Tran-Fadulu V, Milewicz DM: Genetic basis of thoracic aortic aneurysms and aortic dissections. *Am J Med Genet C Semin Med Genet* 11-15-2005;139:10-16.
- [5] Pepin M, Schwarze U, Superti-Furga A, Byers PH: Clinical and genetic features of Ehlers-Danlos syndrome type IV, the vascular type. *N Engl J Med* 3-9-2000;342:673-680.
- [6] Gillum RF: Epidemiology of aortic aneurysm in the United States. *J Clin Epidemiol* 1995;48:1289-1298.
- [7] Rinkel GJ, Djibuti M, Algra A, van GJ: Prevalence and risk of rupture of intracranial aneurysms: a systematic review. *Stroke* 1998;29:251-256.
- [8] Kuzmik GA, Feldman M, Tranquilli M, Rizzo JA, Johnson M, Elefteriades JA: Concurrent intracranial and thoracic aortic aneurysms. *Am J Cardiol* 2-1-2010;105:417-420.
- [9] Bickerstaff LK, Pairolero PC, Hollier LH, Melton LJ, Van Peenen HJ, Cherry KJ, Joyce JW, Lie JT: Thoracic aortic aneurysms: a population-based study. *Surgery* 1982;92:1103-1108.
- [10] Drott C, Arfvidsson B, Ortenwall P, Lundholm K: Age-standardized incidence of ruptured aortic aneurysm in a defined Swedish population between 1952 and 1988: mortality rate and operative results. *Br J Surg* 1992;79:175-179.
- [11] Johansson G, Markstrom U, Swedenborg J: Ruptured thoracic aortic aneurysms: a study of incidence and mortality rates. *J Vasc Surg* 1995;21:985-988.
- [12] Coady MA, Rizzo JA, Hammond GL, Mandapati D, Darr U, Kopf GS, Elefteriades JA: What is the appropriate size criterion for resection of thoracic aortic aneurysms? *J Thorac Cardiovasc Surg* 1997;113:476-491.
- [13] Judge DP, Dietz HC: Marfan's syndrome. *Lancet* 12-3-2005;366:1965-1976.

- [14] Loeys BL, Chen J, Neptune ER, Judge DP, Podowski M, Holm T, Meyers J, Leitch CC, Katsanis N, Sharifi N, Xu FL, Myers LA, Spevak PJ, Cameron DE, De BJ, Hellems J, Chen Y, Davis EC, Webb CL, Kress W, Coucke P, Rifkin DB, De Paepe AM, Dietz HC: A syndrome of altered cardiovascular, craniofacial, neurocognitive and skeletal development caused by mutations in TGFBR1 or TGFBR2. *Nat Genet* 2005;37:275-281.
- [15] Robinson PN, Booms P: The molecular pathogenesis of the Marfan syndrome. *Cell Mol Life Sci* 2001;58:1698-1707.
- [16] Biddinger A, Rocklin M, Coselli J, Milewicz DM: Familial thoracic aortic dilatations and dissections: a case control study. *J Vasc Surg* 1997;25:506-511.
- [17] Linn FH, Rinkel GJ, Algra A, van GJ: Incidence of subarachnoid hemorrhage: role of region, year, and rate of computed tomography: a meta-analysis. *Stroke* 1996;27:625-629.
- [18] Juvela S: Risk factors for multiple intracranial aneurysms. *Stroke* 2000;31:392-397.
- [19] Lall RR, Eddleman CS, Bendok BR, Batjer HH: Unruptured intracranial aneurysms and the assessment of rupture risk based on anatomical and morphological factors: sifting through the sands of data. *Neurosurg Focus* 2009;26:E2.
- [20] Huang J, van Gelder JM: The probability of sudden death from rupture of intracranial aneurysms: a meta-analysis. *Neurosurgery* 2002;51:1101-1105.
- [21] Nahed BV, Bydon M, Ozturk AK, Bilguvar K, Bayrakli F, Gunel M: Genetics of intracranial aneurysms. *Neurosurgery* 2007;60:213-225.
- [22] Kissela BM, Sauerbeck L, Woo D, Khoury J, Carrozzella J, Pancioli A, Jauch E, Moomaw CJ, Shukla R, Gebel J, Fontaine R, Broderick J: Subarachnoid hemorrhage: a preventable disease with a heritable component. *Stroke* 2002;33:1321-1326.
- [23] Wang PS, Longstreth WT, Jr., Koepsell TD: Subarachnoid hemorrhage and family history. A population-based case-control study. *Arch Neurol* 1995;52:202-204.
- [24] Ruijgrok YM, Rinkel GJ, Wijmenga C, van GJ: Anticipation and phenotype in familial intracranial aneurysms. *J Neurol Neurosurg Psychiatry* 2004;75:1436-1442.
- [25] Bromberg JE, Rinkel GJ, Algra A, Greebe P, van Duyn CM, Hasan D, Limburg M, ter Berg HW, Wijdicks EF, van GJ: Subarachnoid haemorrhage in first and second degree relatives of patients with subarachnoid haemorrhage. *BMJ* 7-29-1995;311:288-289.
- [26] Milewicz DM, Chen H, Park ES, Petty EM, Zaghi H, Shashidhar G, Willing M, Patel V: Reduced penetrance and variable expressivity of familial thoracic aortic aneurysms/dissections. *Am J Cardiol* 8-15-1998;82:474-479.

- [27] Guo D, Hasham S, Kuang SQ, Vaughan CJ, Boerwinkle E, Chen H, Abuelo D, Dietz HC, Basson CT, Shete SS, Milewicz DM: Familial thoracic aortic aneurysms and dissections: genetic heterogeneity with a major locus mapping to 5q13-14. *Circulation* 5-22-2001;103:2461-2468.
- [28] Hasham SN, Willing MC, Guo DC, Muilenburg A, He R, Tran VT, Scherer SE, Shete SS, Milewicz DM: Mapping a locus for familial thoracic aortic aneurysms and dissections (TAAD2) to 3p24-25. *Circulation* 7-1-2003;107:3184-3190.
- [29] Vaughan CJ, Casey M, He J, Veugelers M, Henderson K, Guo D, Campagna R, Roman MJ, Milewicz DM, Devereux RB, Basson CT: Identification of a chromosome 11q23.2-q24 locus for familial aortic aneurysm disease, a genetically heterogeneous disorder. *Circulation* 5-22-2001;103:2469-2475.
- [30] Khau VK, Wolf JE, Mathieu F, Zhu L, Salve N, Lalande A, Bonnet C, Lesca G, Plauchu H, Dellinger A, Nivelon-Chevallier A, Brunotte F, Jeunemaitre X: Familial thoracic aortic aneurysm/dissection with patent ductus arteriosus: genetic arguments for a particular pathophysiological entity. *Eur J Hum Genet* 2004;12:173-180.
- [31] Zhu L, Vranckx R, Khau Van KP, Lalande A, Boisset N, Mathieu F, Wegman M, Glancy L, Gasc JM, Brunotte F, Bruneval P, Wolf JE, Michel JB, Jeunemaitre X: Mutations in myosin heavy chain 11 cause a syndrome associating thoracic aortic aneurysm/aortic dissection and patent ductus arteriosus. *Nat Genet* 2006;38:343-349.
- [32] Guo DC, Pannu H, Papke CL, Yu RK, Avidan N, Bourgeois S, Estrera AL, Safi HJ, Sparks E, Amor D, Ades L, McConnell V, Willoughby CE, Abuelo D, Willing M, Lewis RA, Kim DH, Scherer S, Tung PP, Ahn C., Buja LM, Raman CS, Shete S, Milewicz DM: Mutations in smooth muscle alpha-actin (*ACTA2*) lead to thoracic aortic aneurysms and dissections. *Nat Genet* 2007;39:1488-1493.
- [33] Milewicz DM, Michael K, Fisher N, Coselli JS, Markello T, Biddinger A: Fibrillin-1 (*FBN1*) mutations in patients with thoracic aortic aneurysms. *Circulation* 12-1-1996;94:2708-2711.
- [34] Pannu H, Fadulu V, Chang J, Lafont A, Hasham SN, Sparks E, Giampietro PF, Zaleski C, Estrera AL, Safi HJ, Shete S, Willing MC, Raman CS, Milewicz DM: Mutations in transforming growth factor-beta receptor type II cause familial thoracic aortic aneurysms and dissections. *Circulation* 7-26-2005;112:513-520.
- [35] Kainulainen K, Karttunen L, Puhakka L, Sakai L, Peltonen L: Mutations in the fibrillin gene responsible for dominant ectopia lentis and neonatal Marfan syndrome. *Nat Genet* 1994;6:64-69.
- [36] Ades LC, Sullivan K, Biggin A, Haan EA, Brett M, Holman KJ, Dixon J, Robertson S, Holmes AD, Rogers J, Bennetts B: *FBN1*, *TGFBR1*, and the Marfan-

craniosynostosis/mental retardation disorders revisited. *Am J Med Genet A* 4-4-2006;140A:1047-1058.

- [37] Loeys BL, Chen J, Neptune ER, Judge DP, Podowski M, Holm T, Meyers J, Leitch CC, Katsanis N, Sharifi N, Xu FL, Myers LA, Spevak PJ, Cameron DE, Backer JD, Hellemans J, Chen Y, Davis EC, Webb CL, Kress W, Coucke P, Rifkin DB, De Paepe AM, Dietz HC: A syndrome of altered cardiovascular, craniofacial, neurocognitive and skeletal development caused by mutations in TGFBR1 or TGFBR2. *Nat Genet* 1-30-2005.
- [38] ten DP, Arthur HM: Extracellular control of TGFbeta signalling in vascular development and disease. *Nat Rev Mol Cell Biol* 2007;8:857-869.
- [39] Loeys BL, Chen J, Neptune ER, Judge DP, Podowski M, Holm T, Meyers J, Leitch CC, Katsanis N, Sharifi N, Xu FL, Myers LA, Spevak PJ, Cameron DE, Backer JD, Hellemans J, Chen Y, Davis EC, Webb CL, Kress W, Coucke P, Rifkin DB, De Paepe AM, Dietz HC: A syndrome of altered cardiovascular, craniofacial, neurocognitive and skeletal development caused by mutations in TGFBR1 or TGFBR2. *Nat Genet* 1-30-2005.
- [40] Milewicz DM, Kwartler CS, Papke CL, Regalado ES, Cao J, Reid AJ: Genetic variants promoting smooth muscle cell proliferation can result in diffuse and diverse vascular diseases: evidence for a hyperplastic vasculomyopathy. *Genet Med* 2010;12:196-203.
- [41] Guo DC, Pannu H, Papke CL, Yu RK, Avidan N, Bourgeois S, Estrera AL, Safi HJ, Sparks E, Amor D, Ades L, McConnell V, Willoughby CE, Abuelo D, Willing M, Lewis RA, Kim DH, Scherer S, Tung PP, Ahn C., Buja LM, Raman CS, Shete S, Milewicz DM: Mutations in smooth muscle alpha-actin (*ACTA2*) lead to thoracic aortic aneurysms and dissections. *Nat Genet* 2007;39:1488-1493.
- [42] Guo DC, Papke CL, Tran-Fadulu V, Regalado ES, Avidan N, Johnson RJ, Kim DH, Pannu H, Willing MC, Sparks E, Pyeritz RE, Singh MN, Dalman RL, Grotta JC, Marian AJ, Boerwinkle EA, Frazier LQ, LeMaire SA, Coselli JS, Estrera AL, Safi HJ, Veeraraghavan S, Muzny DM, Wheeler DA, Willerson JT, Yu RK, Shete SS, Scherer SE, Raman CS, Buja LM, Milewicz DM: Mutations in smooth muscle alpha-actin (*ACTA2*) cause coronary artery disease, stroke, and moyamoya disease, along with thoracic aortic disease. *Am J Hum Genet* 2009;84:617-627.
- [43] Zhu L, Vranckx R, Khau Van KP, Lalande A, Boisset N, Mathieu F, Wegman M, Glancy L, Gasc JM, Brunotte F, Bruneval P, Wolf JE, Michel JB, Jeunemaitre X: Mutations in myosin heavy chain 11 cause a syndrome associating thoracic aortic aneurysm/aortic dissection and patent ductus arteriosus. *Nat Genet* 2006;38:343-349.
- [44] Ruigrok YM, Wijmenga C, Rinkel GJ, van't SR, Baas F, Wolfs M, Westerveld A, Roos YB: Genomewide linkage in a large Dutch family with intracranial

- aneurysms: replication of 2 loci for intracranial aneurysms to chromosome 1p36.11-p36.13 and Xp22.2-p22.32. *Stroke* 2008;39:1096-1102.
- [45] Nahed BV, Seker A, Guclu B, Ozturk AK, Finberg K, Hawkins AA, DiLuna ML, State M, Lifton RP, Gunel M: Mapping a Mendelian form of intracranial aneurysm to 1p34.3-p36.13. *Am J Hum Genet* 2005;76:172-179.
- [46] Verlaan DJ, Dube MP, St-Onge J, Noreau A, Roussel J, Satge N, Wallace MC, Rouleau GA: A new locus for autosomal dominant intracranial aneurysm, ANIB4, maps to chromosome 5p15.2-14.3. *J Med Genet* 2006;43:e31.
- [47] Onda H, Kasuya H, Yoneyama T, Takakura K, Hori T, Takeda J, Nakajima T, Inoue I: Genomewide-linkage and haplotype-association studies map intracranial aneurysm to chromosome 7q11. *Am J Hum Genet* 2001;69:804-819.
- [48] Olson JM, Vongpunsawad S, Kuivaniemi H, Ronkainen A, Hernesniemi J, Ryyanen M, Kim LL, Tromp G: Search for intracranial aneurysm susceptibility gene(s) using Finnish families. *BMC Med Genet* 8-1-2002;3:7.
- [49] Yamada S, Utsunomiya M, Inoue K, Nozaki K, Inoue S, Takenaka K, Hashimoto N, Koizumi A: Genome-wide scan for Japanese familial intracranial aneurysms: linkage to several chromosomal regions. *Circulation* 12-14-2004;110:3727-3733.
- [50] Ruigrok YM, Rinkel GJ, Wijmenga C, van GJ: Anticipation and phenotype in familial intracranial aneurysms. *J Neurol Neurosurg Psychiatry* 2004;75:1436-1442.
- [51] Yamada S, Utsunomiya M, Inoue K, Nozaki K, Inoue S, Takenaka K, Hashimoto N, Koizumi A: Genome-wide scan for Japanese familial intracranial aneurysms: linkage to several chromosomal regions. *Circulation* 12-14-2004;110:3727-3733.
- [52] Ruigrok YM, Rinkel GJ: Genetics of intracranial aneurysms. *Stroke* 2008;39:1049-1055.
- [53] Schievink WI, Parisi JE, Piepgras DG, Michels VV: Intracranial aneurysms in Marfan's syndrome: an autopsy study. *Neurosurgery* 1997;41:866-870.
- [54] Conway JE, Hutchins GM, Tamargo RJ: Marfan syndrome is not associated with intracranial aneurysms. *Stroke* 1999;30:1632-1636.
- [55] Yoneyama T, Kasuya H, Onda H, Akagawa H, Hashiguchi K, Nakajima T, Hori T, Inoue I: Collagen type I alpha2 (COL1A2) is the susceptible gene for intracranial aneurysms. *Stroke* 2004;35:443-448.
- [56] Hashikata H, Liu W, Inoue K, Mineharu Y, Yamada S, Nanayakkara S, Matsuura N, Hitomi T, Takagi Y, Hashimoto N, Miyamoto S, Koizumi A: Confirmation of an association of single-nucleotide polymorphism rs1333040 on 9p21 with familial and sporadic intracranial aneurysms in Japanese patients. *Stroke* 2010;41:1138-1144.

- [57] Helgadottir A, Thorleifsson G, Magnusson KP, Gretarsdottir S, Steinthorsdottir V, Manolescu A, Jones GT, Rinkel GJ, Blankensteijn JD, Ronkainen A, Jaaskelainen JE, Kyo Y, Lenk GM, Sakalihasan N, Kostulas K, Gottsater A, Flex A, Stefansson H, Hansen T, Andersen G, Weinsheimer S, Borch-Johnsen K, Jorgensen T, Shah SH, Quyyumi AA, Granger CB, Reilly MP, Austin H, Levey AI, Vaccarino V, Palsdottir E, Walters GB, Jonsdottir T, Snorraddottir S, Magnusdottir D, Gudmundsson G, Ferrell RE, Sveinbjornsdottir S, Hernesniemi J, Niemela M, Limet R, Andersen K, Sigurdsson G, Benediktsson R, Verhoeven EL, Teijink JA, Grobbee DE, Rader DJ, Collier DA, Pedersen O, Pola R, Hillert J, Lindblad B, Valdimarsson EM, Magnadottir HB, Wijmenga C, Tromp G, Baas AF, Ruigrok YM, Van Rij AM, Kuivaniemi H, Powell JT, Matthiasson SE, Gulcher JR, Thorgeirsson G, Kong A, Thorsteinsdottir U, Stefansson K: The same sequence variant on 9p21 associates with myocardial infarction, abdominal aortic aneurysm and intracranial aneurysm. *Nat Genet* 2008;40:217-224.
- [58] Ruigrok YM, Rinkel GJ: Genetics of intracranial aneurysms. *Stroke* 2008;39:1049-1055.
- [59] Santiago-Sim T, Mathew-Joseph S, Pannu H, Milewicz DM, Seidman CE, Seidman JG, Kim DH: Sequencing of TGF-beta pathway genes in familial cases of intracranial aneurysm. *Stroke* 2009;40:1604-1611.
- [60] Klima T, Spjut HJ, Coelho A, Gray AG, Wukasch DC, Reul GJ, Jr., Cooley DA: The morphology of ascending aortic aneurysms. *Hum Pathol* 1983;14:810-817.
- [61] Klima T, Spjut HJ, Coelho A, Gray AG, Wukasch DC, Reul GJ, Jr., Cooley DA: The morphology of ascending aortic aneurysms. *Hum Pathol* 1983;14:810-817.
- [62] He R, Guo DC, Estrera AL, Safi HJ, Huynh TT, Yin Z, Cao SN, Lin J, Kurian T, Buja LM, Geng YJ, Milewicz DM: Characterization of the inflammatory and apoptotic cells in the aortas of patients with ascending thoracic aortic aneurysms and dissections. *J Thorac Cardiovasc Surg* 2006;131:671-678.
- [63] Ishihara S, Mawad ME, Ogata K, Suzuki C, Tsuzuki N, Katoh H, Ohnuki A, Miyazawa T, Nawashiro H, Kaji T, Shima K: Histopathologic findings in human cerebral aneurysms embolized with platinum coils: report of two cases and review of the literature. *AJNR Am J Neuroradiol* 2002;23:970-974.
- [64] Frosen J, Piippo A, Paetau A, Kangasniemi M, Niemela M, Hernesniemi J, Jaaskelainen J: Remodeling of saccular cerebral artery aneurysm wall is associated with rupture: histological analysis of 24 unruptured and 42 ruptured cases. *Stroke* 2004;35:2287-2293.
- [65] Kim SC, Singh M, Huang J, Prestigiacomo CJ, Winfree CJ, Solomon RA, Connolly ES, Jr.: Matrix metalloproteinase-9 in cerebral aneurysms. *Neurosurgery* 1997;41:642-666.

- [66] Chung AW, Au YK, Sandor GG, Judge DP, Dietz HC, van BC: Loss of elastic fiber integrity and reduction of vascular smooth muscle contraction resulting from the upregulated activities of matrix metalloproteinase-2 and -9 in the thoracic aortic aneurysm in Marfan syndrome. *Circ Res* 8-31-2007;101:512-522.
- [67] LeMaire SA, Wang X, Wilks JA, Carter SA, Wen S, Won T, Leonardelli D, Anand G, Conklin LD, Wang XL, Thompson RW, Coselli JS: Matrix metalloproteinases in ascending aortic aneurysms: bicuspid versus trileaflet aortic valves. *J Surg Res* 2005;123:40-48.
- [68] Koullias GJ, Ravichandran P, Korkolis DP, Rimm DL, Elefteriades JA: Increased tissue microarray matrix metalloproteinase expression favors proteolysis in thoracic aortic aneurysms and dissections. *Ann Thorac Surg* 2004;78:2106-2110.
- [69] Guo DC, Papke CL, He R, Milewicz DM: Pathogenesis of thoracic and abdominal aortic aneurysms. *Ann N Y Acad Sci* 2006;1085:339-352.
- [70] Pannu H, Kim DH, Guo D, King TM, Van GG, Chin T, Chang K, Qi Y, Shete S, Milewicz DM: The role of MMP-2 and MMP-9 polymorphisms in sporadic intracranial aneurysms. *J Neurosurg* 2006;105:418-423.
- [71] Apte SS: A disintegrin-like and metalloprotease (reprolysin-type) with thrombospondin type 1 motif (ADAMTS) superfamily: functions and mechanisms. *J Biol Chem* 11-13-2009;284:31493-31497.
- [72] Kuno K, Kanada N, Nakashima E, Fujiki F, Ichimura F, Matsushima K: Molecular cloning of a gene encoding a new type of metalloproteinase-disintegrin family protein with thrombospondin motifs as an inflammation associated gene. *J Biol Chem* 1-3-1997;272:556-562.
- [73] Koo BH, Longpre JM, Somerville RP, Alexander JP, Leduc R, Apte SS: Regulation of ADAMTS9 secretion and enzymatic activity by its propeptide. *J Biol Chem* 6-1-2007;282:16146-16154.
- [74] Hofsteenge J, Huwiler KG, Macek B, Hess D, Lawler J, Mosher DF, Peter-Katalinic J: C-mannosylation and O-fucosylation of the thrombospondin type 1 module. *J Biol Chem* 3-2-2001;276:6485-6498.
- [75] Ricketts LM, Dlugosz M, Luther KB, Haltiwanger RS, Majerus EM: O-fucosylation is required for ADAMTS13 secretion. *J Biol Chem* 6-8-2007;282:17014-17023.
- [76] Ricketts LM, Dlugosz M, Luther KB, Haltiwanger RS, Majerus EM: O-fucosylation is required for ADAMTS13 secretion. *J Biol Chem* 6-8-2007;282:17014-17023.

- [77] Wang LW, Leonhard-Melief C, Haltiwanger RS, Apte SS: Post-translational modification of thrombospondin type-1 repeats in ADAMTS-like 1/punctin-1 by C-mannosylation of tryptophan. *J Biol Chem* 10-30-2009;284:30004-30015.
- [78] Rodriguez-Manzaneque JC, Milchanowski AB, Dufour EK, Leduc R, Iruela-Arispe ML: Characterization of METH-1/ADAMTS1 processing reveals two distinct active forms. *J Biol Chem* 10-27-2000;275:33471-33479.
- [79] Somerville RP, Longpre JM, Apel ED, Lewis RM, Wang LW, Sanes JR, Leduc R, Apte SS: ADAMTS7B, the full-length product of the ADAMTS7 gene, is a chondroitin sulfate proteoglycan containing a mucin domain. *J Biol Chem* 8-20-2004;279:35159-35175.
- [80] Koo BH, Longpre JM, Somerville RP, Alexander JP, Leduc R, Apte SS: Cell-surface processing of pro-ADAMTS9 by furin. *J Biol Chem* 5-5-2006;281:12485-12494.
- [81] Somerville RP, Jungers KA, Apte SS: Discovery and characterization of a novel, widely expressed metalloprotease, ADAMTS10, and its proteolytic activation. *J Biol Chem* 12-3-2004;279:51208-51217.
- [82] Cal S, Arguelles JM, Fernandez PL, Lopez-Otin C: Identification, characterization, and intracellular processing of ADAM-TS12, a novel human disintegrin with a complex structural organization involving multiple thrombospondin-1 repeats. *J Biol Chem* 5-25-2001;276:17932-17940.
- [83] Koo BH, Longpre JM, Somerville RP, Alexander JP, Leduc R, Apte SS: Regulation of ADAMTS9 secretion and enzymatic activity by its propeptide. *J Biol Chem* 6-1-2007;282:16146-16154.
- [84] Gao G, Westling J, Thompson VP, Howell TD, Gottschall PE, Sandy JD: Activation of the proteolytic activity of ADAMTS4 (aggrecanase-1) by C-terminal truncation. *J Biol Chem* 3-29-2002;277:11034-11041.
- [85] Kashiwagi M, Enghild JJ, Gendron C, Hughes C, Caterson B, Itoh Y, Nagase H: Altered proteolytic activities of ADAMTS-4 expressed by C-terminal processing. *J Biol Chem* 3-12-2004;279:10109-10119.
- [86] Rodriguez-Manzaneque JC, Milchanowski AB, Dufour EK, Leduc R, Iruela-Arispe ML: Characterization of METH-1/ADAMTS1 processing reveals two distinct active forms. *J Biol Chem* 10-27-2000;275:33471-33479.
- [87] Cal S, Arguelles JM, Fernandez PL, Lopez-Otin C: Identification, characterization, and intracellular processing of ADAM-TS12, a novel human disintegrin with a complex structural organization involving multiple thrombospondin-1 repeats. *J Biol Chem* 5-25-2001;276:17932-17940.

- [88] Somerville RP, Longpre JM, Jungers KA, Engle JM, Ross M, Evanko S, Wight TN, Leduc R, Apte SS: Characterization of ADAMTS-9 and ADAMTS-20 as a distinct ADAMTS subfamily related to *Caenorhabditis elegans* GON-1. *J Biol Chem* 3-14-2003;278:9503-9513.
- [89] Levy GG, Nichols WC, Lian EC, Foroud T, McClintick JN, McGee BM, Yang AY, Siemieniak DR, Stark KR, Gruppo R, Sarode R, Shurin SB, Chandrasekaran V, Stabler SP, Sabio H, Bouhassira EE, Upshaw JD, Jr., Ginsburg D, Tsai HM: Mutations in a member of the ADAMTS gene family cause thrombotic thrombocytopenic purpura. *Nature* 10-4-2001;413:488-494.
- [90] Colige A, Sieron AL, Li SW, Schwarze U, Petty E, Wertelecki W, Wilcox W, Krakow D, Cohn DH, Reardon W, Byers PH, Lapiere CM, Prockop DJ, Nusgens BV: Human Ehlers-Danlos syndrome type VII C and bovine dermatosparaxis are caused by mutations in the procollagen I N-proteinase gene. *Am J Hum Genet* 1999;65:308-317.
- [91] Bevitt DJ, Li Z, Lindrop JL, Barker MD, Clarke MP, McKie N: Analysis of full length ADAMTS6 transcript reveals alternative splicing and a role for the 5' untranslated region in translational control. *Gene* 10-10-2005;359:99-110.
- [92] Levy GG, Nichols WC, Lian EC, Foroud T, McClintick JN, McGee BM, Yang AY, Siemieniak DR, Stark KR, Gruppo R, Sarode R, Shurin SB, Chandrasekaran V, Stabler SP, Sabio H, Bouhassira EE, Upshaw JD, Jr., Ginsburg D, Tsai HM: Mutations in a member of the ADAMTS gene family cause thrombotic thrombocytopenic purpura. *Nature* 10-4-2001;413:488-494.
- [93] Zheng X, Chung D, Takayama TK, Majerus EM, Sadler JE, Fujikawa K: Structure of von Willebrand factor-cleaving protease (ADAMTS13), a metalloprotease involved in thrombotic thrombocytopenic purpura. *J Biol Chem* 11-2-2001;276:41059-41063.
- [94] Colige A, Sieron AL, Li SW, Schwarze U, Petty E, Wertelecki W, Wilcox W, Krakow D, Cohn DH, Reardon W, Byers PH, Lapiere CM, Prockop DJ, Nusgens BV: Human Ehlers-Danlos syndrome type VII C and bovine dermatosparaxis are caused by mutations in the procollagen I N-proteinase gene. *Am J Hum Genet* 1999;65:308-317.
- [95] Dagoneau N, oist-Lasselín C, Huber C, Faivre L, Megarbane A, Alswaid A, Dollfus H, Alembik Y, Munnich A, Legeai-Mallet L, Cormier-Daire V: ADAMTS10 mutations in autosomal recessive Weill-Marchesani syndrome. *Am J Hum Genet* 2004;75:801-806.
- [96] Morales J, Al-Sharif L, Khalil DS, Shinwari JM, Bavi P, Al-Mahrouqi RA, Al-Rajhi A, Alkuraya FS, Meyer BF, Al TN: Homozygous mutations in ADAMTS10 and ADAMTS17 cause lenticular myopia, ectopia lentis, glaucoma, spherophakia, and short stature. *Am J Hum Genet* 2009;85:558-568.

- [97] Morales J, Al-Sharif L, Khalil DS, Shinwari JM, Bavi P, Al-Mahrouqi RA, Al-Rajhi A, Alkuraya FS, Meyer BF, Al TN: Homozygous mutations in ADAMTS10 and ADAMTS17 cause lenticular myopia, ectopia lentis, glaucoma, spherophakia, and short stature. *Am J Hum Genet* 2009;85:558-568.
- [98] Jonsson-Rylander AC, Nilsson T, Fritsche-Danielson R, Hammarstrom A, Behrendt M, Andersson JO, Lindgren K, Andersson AK, Wallbrandt P, Rosengren B, Brodin P, Thelin A, Westin A, Hurt-Camejo E, Lee-Sogaard CH: Role of ADAMTS-1 in atherosclerosis: remodeling of carotid artery, immunohistochemistry, and proteolysis of versican. *Arterioscler Thromb Vasc Biol* 2005;25:180-185.
- [99] Wang L, Zheng J, Bai X, Liu B, Liu CJ, Xu Q, Zhu Y, Wang N, Kong W, Wang X: ADAMTS-7 mediates vascular smooth muscle cell migration and neointima formation in balloon-injured rat arteries. *Circ Res* 3-13-2009;104:688-698.
- [100] Kenagy RD, Min SK, Clowes AW, Sandy JD: Cell death-associated ADAMTS4 and versican degradation in vascular tissue. *J Histochem Cytochem* 2009;57:889-897.
- [101] Apte SS: A disintegrin-like and metalloprotease (reprolysin-type) with thrombospondin type 1 motif (ADAMTS) superfamily: functions and mechanisms. *J Biol Chem* 11-13-2009;284:31493-31497.
- [102] Cal S, Obaya AJ, Llamazares M, Garabaya C, Quesada V, Lopez-Otin C: Cloning, expression analysis, and structural characterization of seven novel human ADAMTSs, a family of metalloproteinases with disintegrin and thrombospondin-1 domains. *Gene* 1-23-2002;283:49-62.
- [103] Gao S, De GC, Kossowska K, Zhang H: FSH stimulates the expression of the ADAMTS-16 protease in mature human ovarian follicles. *Mol Hum Reprod* 2007;13:465-471.
- [104] Zeng W, Corcoran C, Collins-Racie LA, Lavallie ER, Morris EA, Flannery CR: Glycosaminoglycan-binding properties and aggrecanase activities of truncated ADAMTSs: comparative analyses with ADAMTS-5, -9, -16 and -18. *Biochim Biophys Acta* 2006;1760:517-524.
- [105] Cal S, Obaya AJ, Llamazares M, Garabaya C, Quesada V, Lopez-Otin C: Cloning, expression analysis, and structural characterization of seven novel human ADAMTSs, a family of metalloproteinases with disintegrin and thrombospondin-1 domains. *Gene* 1-23-2002;283:49-62.
- [106] Joe B, Saad Y, Lee NH, Frank BC, Achinike OH, Luu TV, Gopalakrishnan K, Toland EJ, Farms P, Yerga-Woolwine S, Manickavasagam E, Rapp JP, Garrett MR, Coe D, Apte SS, Rankinen T, Perusse L, Ehret GB, Ganesh SK, Cooper RS, O'Connor A, Rice T, Weder AB, Chakravarti A, Rao DC, Bouchard C: Positional

- identification of variants of Adamts16 linked to inherited hypertension. *Hum Mol Genet* 8-1-2009;18:2825-2838.
- [107] SurrIDGE AK, Rodgers UR, Swingler TE, Davidson RK, Kevorkian L, Norton R, Waters JG, Goldring MB, Parker AE, Clark IM: Characterization and regulation of ADAMTS-16. *Matrix Biol* 2009;28:416-424.
- [108] Chambers RC, Leoni P, Kaminski N, Laurent GJ, Heller RA: Global expression profiling of fibroblast responses to transforming growth factor-beta1 reveals the induction of inhibitor of differentiation-1 and provides evidence of smooth muscle cell phenotypic switching. *Am J Pathol* 2003;162:533-546.
- [109] Hinz B, Phan SH, Thannickal VJ, Galli A, Bochaton-Piallat ML, Gabbiani G: The myofibroblast: one function, multiple origins. *Am J Pathol* 2007;170:1807-1816.
- [110] Desmouliere A, Geinoz A, Gabbiani F, Gabbiani G: Transforming growth factor-beta 1 induces alpha-smooth muscle actin expression in granulation tissue myofibroblasts and in quiescent and growing cultured fibroblasts. *J Cell Biol* 1993;122:103-111.
- [111] Tomasek JJ, Gabbiani G, Hinz B, Chaponnier C, Brown RA: Myofibroblasts and mechano-regulation of connective tissue remodelling. *Nat Rev Mol Cell Biol* 2002;3:349-363.
- [112] Arora PD, Narani N, McCulloch CA: The compliance of collagen gels regulates transforming growth factor-beta induction of alpha-smooth muscle actin in fibroblasts. *Am J Pathol* 1999;154:871-882.
- [113] Thannickal VJ, Lee DY, White ES, Cui Z, Larios JM, Chacon R, Horowitz JC, Day RM, Thomas PE: Myofibroblast differentiation by transforming growth factor-beta1 is dependent on cell adhesion and integrin signaling via focal adhesion kinase. *J Biol Chem* 4-4-2003;278:12384-12389.
- [114] Igotz RA, Massague J: Transforming growth factor-beta stimulates the expression of fibronectin and collagen and their incorporation into the extracellular matrix. *J Biol Chem* 3-25-1986;261:4337-4345.
- [115] Chambers RC, Leoni P, Kaminski N, Laurent GJ, Heller RA: Global expression profiling of fibroblast responses to transforming growth factor-beta1 reveals the induction of inhibitor of differentiation-1 and provides evidence of smooth muscle cell phenotypic switching. *Am J Pathol* 2003;162:533-546.
- [116] Guo DC, Pannu H, Papke CL, Yu RK, Avidan N, Bourgeois S, Estrera AL, Safi HJ, Sparks E, Amor D, Ades L, McConnell V, Willoughby CE, Abuelo D, Willing M, Lewis RA, Kim DH, Scherer S, Tung PP, Ahn C., Buja LM, Raman CS, Shete S, Milewicz DM: Mutations in smooth muscle alpha-actin (*ACTA2*) lead to thoracic aortic aneurysms and dissections. *Nat Genet* 2007;39:1488-1493.

- [117] Guo DC, Papke CL, Tran-Fadulu V, Regalado ES, Avidan N, Johnson RJ, Kim DH, Pannu H, Willing MC, Sparks E, Pyeritz RE, Singh MN, Dalman RL, Grotta JC, Marian AJ, Boerwinkle EA, Frazier LQ, LeMaire SA, Coselli JS, Estrera AL, Safi HJ, Veeraraghavan S, Muzny DM, Wheeler DA, Willerson JT, Yu RK, Shete SS, Scherer SE, Raman CS, Buja LM, Milewicz DM: Mutations in smooth muscle alpha-actin (ACTA2) cause coronary artery disease, stroke, and moyamoya disease, along with thoracic aortic disease. *Am J Hum Genet* 2009;84:617-627.
- [118] Schievink WI, Parisi JE, Piepgras DG, Michels VV: Intracranial aneurysms in Marfan's syndrome: an autopsy study. *Neurosurgery* 1997;41:866-870.
- [119] Kong X, Matisse TC: MAP-O-MAT: internet-based linkage mapping. *Bioinformatics* 2-15-2005;21:557-559.
- [120] Guo DC, Milewicz DM: Methodology for using a universal primer to label amplified DNA segments for molecular analysis. *Biotechnol Lett* 2003;25:2079-2083.
- [121] O'Connell JR, Weeks DE: PedCheck: a program for identification of genotype incompatibilities in linkage analysis. *Am J Hum Genet* 1998;63:259-266.
- [122] Weeks DE, Lange K: The affected-pedigree-member method of linkage analysis. *Am J Hum Genet* 1988;42:315-326.
- [123] Cottingham RW, Jr., Idury RM, Schaffer AA: Faster sequential genetic linkage computations. *Am J Hum Genet* 1993;53:252-263.
- [124] Lathrop GM, Lalouel JM, Julier C, Ott J: Multilocus linkage analysis in humans: detection of linkage and estimation of recombination. *Am J Hum Genet* 1985;37:482-498.
- [125] Guo D, Hasham S, Kuang SQ, Vaughan CJ, Boerwinkle E, Chen H, Abuelo D, Dietz HC, Basson CT, Shete SS, Milewicz DM: Familial thoracic aortic aneurysms and dissections: genetic heterogeneity with a major locus mapping to 5q13-14. *Circulation* 5-22-2001;103:2461-2468.
- [126] Hasham SN, Willing MC, Guo DC, Muilenburg A, He RM, Tran VT, Scherer SE, Shete SS, Milewicz DM: Mapping a locus for familial thoracic aortic aneurysms and dissections (TAAD2) to 3p24-25. *Circulation* 7-1-2003;107:3184-3190.
- [127] Wang K, Li M, Hadley D, Liu R, Glessner J, Grant SF, Hakonarson H, Bucan M: PennCNV: an integrated hidden Markov model designed for high-resolution copy number variation detection in whole-genome SNP genotyping data. *Genome Res* 2007;17:1665-1674.
- [128] Arora PD, McCulloch CA: The deletion of transforming growth factor-beta-induced myofibroblasts depends on growth conditions and actin organization. *Am J Pathol* 1999;155:2087-2099.

- [129] Verlaan DJ, Dube MP, St-Onge J, Noreau A, Roussel J, Satge N, Wallace MC, Rouleau GA: A new locus for autosomal dominant intracranial aneurysm, ANIB4, maps to chromosome 5p15.2-14.3. *J Med Genet* 2006;43:e31.
- [130] Gomez-Skarmeta JL, Modolell J: Iroquois genes: genomic organization and function in vertebrate neural development. *Curr Opin Genet Dev* 2002;12:403-408.
- [131] Bao ZZ, Bruneau BG, Seidman JG, Seidman CE, Cepko CL: Regulation of chamber-specific gene expression in the developing heart by *Irx4*. *Science* 2-19-1999;283:1161-1164.
- [132] Bruneau BG, Bao ZZ, Fatkin D, Xavier-Neto J, Georgakopoulos D, Maguire CT, Berul CI, Kass DA, Kuroski-de Bold ML, de Bold AJ, Conner DA, Rosenthal N, Cepko CL, Seidman CE, Seidman JG: Cardiomyopathy in *Irx4*-deficient mice is preceded by abnormal ventricular gene expression. *Mol Cell Biol* 2001;21:1730-1736.
- [133] Guo X, Liu W, Pan Y, Ni P, Ji J, Guo L, Zhang J, Wu J, Jiang J, Chen X, Cai Q, Li J, Zhang J, Gu Q, Liu B, Zhu Z, Yu Y: Homeobox gene *IRX1* is a tumor suppressor gene in gastric carcinoma. *Oncogene* 7-8-2010;29:3908-3920.
- [134] Le GC, Somerville RP, Kesteloot F, Powell K, Birk DE, Colige AC, Apte SS: Regulation of procollagen amino-propeptide processing during mouse embryogenesis by specialization of homologous ADAMTS proteases: insights on collagen biosynthesis and dermatosparaxis. *Development* 2006;133:1587-1596.
- [135] Colige A, Sieron AL, Li SW, Schwarze U, Petty E, Wertelecki W, Wilcox W, Krakow D, Cohn DH, Reardon W, Byers PH, Lapiere CM, Prockop DJ, Nusgens BV: Human Ehlers-Danlos syndrome type VII C and bovine dermatosparaxis are caused by mutations in the procollagen I N-proteinase gene. *Am J Hum Genet* 1999;65:308-317.
- [136] Le GC, Somerville RP, Kesteloot F, Powell K, Birk DE, Colige AC, Apte SS: Regulation of procollagen amino-propeptide processing during mouse embryogenesis by specialization of homologous ADAMTS proteases: insights on collagen biosynthesis and dermatosparaxis. *Development* 2006;133:1587-1596.
- [137] Fiore R, Rahim B, Christoffels VM, Moorman AF, Puschel AW: Inactivation of the *Sema5a* gene results in embryonic lethality and defective remodeling of the cranial vascular system. *Mol Cell Biol* 2005;25:2310-2319.
- [138] Hoj BR, la Cour JM, Mollerup J, Berchtold MW: ALG-2 knockdown in HeLa cells results in G2/M cell cycle phase accumulation and cell death. *Biochem Biophys Res Commun* 1-2-2009;378:145-148.
- [139] Surridge AK, Rodgers UR, Swingler TE, Davidson RK, Kevorkian L, Norton R, Waters JG, Goldring MB, Parker AE, Clark IM: Characterization and regulation of ADAMTS-16. *Matrix Biol* 2009;28:416-424.

- [140] ten DP, Arthur HM: Extracellular control of TGFbeta signalling in vascular development and disease. *Nat Rev Mol Cell Biol* 2007;8:857-869.
- [141] Loeys BL, Chen J, Neptune ER, Judge DP, Podowski M, Holm T, Meyers J, Leitch CC, Katsanis N, Sharifi N, Xu FL, Myers LA, Spevak PJ, Cameron DE, Backer JD, Hellemans J, Chen Y, Davis EC, Webb CL, Kress W, Coucke P, Rifkin DB, De Paepe AM, Dietz HC: A syndrome of altered cardiovascular, craniofacial, neurocognitive and skeletal development caused by mutations in TGFBR1 or TGFBR2. *Nat Genet* 1-30-2005.
- [142] Scholl R, Marquis J, Meyer K, Schumperli D: Spinal muscular atrophy: position and functional importance of the branch site preceding SMN exon 7. *RNA Biol* 2007;4:34-37.
- [143] Hallegger M, Sobala A, Smith CW: Four exons of the serotonin receptor 4 gene are associated with multiple distant branch points. *RNA* 2010;16:839-851.
- [144] SurrIDGE AK, Rodgers UR, Swingler TE, Davidson RK, Kevorkian L, Norton R, Waters JG, Goldring MB, Parker AE, Clark IM: Characterization and regulation of ADAMTS-16. *Matrix Biol* 2009;28:416-424.
- [145] Le GC, Somerville RP, Kesteloot F, Powell K, Birk DE, Colige AC, Apte SS: Regulation of procollagen amino-propeptide processing during mouse embryogenesis by specialization of homologous ADAMTS proteases: insights on collagen biosynthesis and dermatosparaxis. *Development* 2006;133:1587-1596.
- [146] SurrIDGE AK, Rodgers UR, Swingler TE, Davidson RK, Kevorkian L, Norton R, Waters JG, Goldring MB, Parker AE, Clark IM: Characterization and regulation of ADAMTS-16. *Matrix Biol* 2009;28:416-424.
- [147] Chen SJ, Ning H, Ishida W, Sodin-Semrl S, Takagawa S, Mori Y, Varga J: The early-immediate gene EGR-1 is induced by transforming growth factor-beta and mediates stimulation of collagen gene expression. *J Biol Chem* 7-28-2006;281:21183-21197.
- [148] Sysa P, Potter JJ, Liu X, Mezey E: Transforming growth factor-beta1 up-regulation of human alpha(1)(I) collagen is mediated by Sp1 and Smad2 transacting factors. *DNA Cell Biol* 2009;28:425-434.
- [149] Le GC, Somerville RP, Kesteloot F, Powell K, Birk DE, Colige AC, Apte SS: Regulation of procollagen amino-propeptide processing during mouse embryogenesis by specialization of homologous ADAMTS proteases: insights on collagen biosynthesis and dermatosparaxis. *Development* 2006;133:1587-1596.
- [150] Stenina OI, Topol EJ, Plow EF: Thrombospondins, their polymorphisms, and cardiovascular disease. *Arterioscler Thromb Vasc Biol* 2007;27:1886-1894.

- [151] Tan K, Lawler J: The interaction of Thrombospondins with extracellular matrix proteins. *J Cell Commun Signal* 2009;3:177-187.
- [152] Apte SS: A disintegrin-like and metalloprotease (reprolysin-type) with thrombospondin type 1 motif (ADAMTS) superfamily: functions and mechanisms. *J Biol Chem* 11-13-2009;284:31493-31497.
- [153] Le GC, Somerville RP, Kesteloot F, Powell K, Birk DE, Colige AC, Apte SS: Regulation of procollagen amino-propeptide processing during mouse embryogenesis by specialization of homologous ADAMTS proteases: insights on collagen biosynthesis and dermatosparaxis. *Development* 2006;133:1587-1596.
- [154] McCulloch DR, Nelson CM, Dixon LJ, Silver DL, Wylie JD, Lindner V, Sasaki T, Cooley MA, Argraves WS, Apte SS: ADAMTS metalloproteases generate active versican fragments that regulate interdigital web regression. *Dev Cell* 2009;17:687-698.
- [155] Rodgers UR, Kevorkian L, SurrIDGE AK, Waters JG, Swingler TE, Culley K, Illman S, Lohi J, Parker AE, Clark IM: Expression and function of matrix metalloproteinase (MMP)-28. *Matrix Biol* 2009;28:263-272.

VITA

Alexander Hung Li was born in Houston, Texas on February 6, 1983, the son of Beverly Li and Joseph Li. After completing his work at Clear Lake High School in Houston, Texas in 2001, he entered the University of Rochester in Rochester, NY. He received the degree of Bachelor of Science with a major in Ecology and Evolutionary Biology from the University of Rochester in May, 2005. In May of 2008 he entered The University of Texas Health Science Center at Houston Graduate School of Biomedical Sciences. He will graduate with his Masters of Science in August of 2010.

Permanent address:

16203 Brookford Ct

Houston, Texas 77059